

Editor-in-Chief B.E.Paton

Editorial board:

Yu.S.Borisov	V.F.Khorunov
A.Ya.Ishchenko	I.V.Krivtsun
B.V.Khitrovskaya	L.M.Lobanov
V.I.Kyrian	A.A.Mazur
S.I.Kuchuk-Yatsenko	
Yu.N.Lankin	I.K.Pokhodnya
V.N.Lipodaev	V.D.Poznyakov
V.I.Makhnenko	K.A.Yushchenko
O.K.Nazarenko	A.T.Zelnichenko
I.A.Ryabtsev	

International editorial council:

N.P.Alyoshin	(Russia)
U.Diltey	(Germany)
Guan Qiao	(China)
D. von Hofe	(Germany)
V.I.Lysak	(Russia)
N.I.Nikiforov	(Russia)
B.E.Paton	(Ukraine)
Ya.Pilarczyk	(Poland)
G.A.Turichin	(Russia)
Zhang Yanmin	(China)
A.S.Zubchenko	(Russia)

Promotion group:

V.N.Lipodaev, V.I.Lokteva
A.T.Zelnichenko (exec. director)

Translators:

A.A.Fomin, O.S.Kurochko,
I.N.Kutianova, T.K.Vasilenko

Editor:

N.A.Dmitrieva
Electron gallery:
D.I.Sereda, T.Yu.Snegiryova

Address:

E.O. Paton Electric Welding Institute,
International Association «Welding»,
11, Bozhenko str., 03680, Kyiv, Ukraine
Tel.: (38044) 200 82 77
Fax: (38044) 200 81 45
E-mail: journal@paton.kiev.ua
http://www.nas.gov.ua/pwj
State Registration Certificate
KV 4790 of 09.01.2001

Subscriptions:

\$324, 12 issues per year,
postage and packaging included.
Back issues available.

All rights reserved.
This publication and each of the articles
contained herein are protected by copyright.
Permission to reproduce material contained in
this journal must be obtained in writing from
the Publisher.
Copies of individual articles may be obtained
from the Publisher.

CONTENTS

SCIENTIFIC AND TECHNICAL

<i>Goncharov I.A., Galinich V.I., Mishchenko D.D., Shevchenko M.A. and Sudavtsova V.S.</i> Prediction of thermodynamic properties of melts of MgO-Al ₂ O ₃ -SiO ₂ -CaF ₂ system	2
<i>Poklyatsky A.G.</i> Resistance of welds on thin-sheet aluminium alloys to initiation and propagation of service cracks	5
<i>Kostin V.A., Golovko V.V. and Grigorenko G.M.</i> Methods for assessment of strengthening of HSLA steel weld metal	9
<i>Kuskov Yu.M., Novikova D.P. and Bogajchuk I.L.</i> Role of non-metallic inclusions in cracking during arc cladding	14
<i>Ryabtsev I.A., Babinets A.A. and Ryabtsev I.I.</i> Effect of ductile sub-layer on heat resistance of multilayer deposited metal	18
<i>Wielage B., Rupprecht C. and Pokhmurska H.</i> Peculiarities of thermal spraying of coatings using flux-cored wire (Review)	21

INDUSTRIAL

<i>Shlepakov V.N.</i> Current consumables and methods of fusion arc welding (Review)	26
<i>Nesterenkov V.M. and Kravchuk L.A.</i> Electron beam welding of measuring chamber of magnetic pneumatic gas analyser	29
<i>Nazarenko O.K. and Matvejchuk V.A.</i> Limitation of overvoltages in high-voltage circuits after discharges in welding gun	32
<i>Knysh V.V., Solovej S.A. and Kuzmenko A.Z.</i> Influence of preliminary cyclic loading on effectiveness of welded joint strengthening by high-frequency peening	36
<i>Rymar S.V., Zhernosekov A.M. and Sydorets V.N.</i> Influence of welding power sources on three-phase mains	40

NEWS

First Meeting of Council of Chinese-Ukrainian E.O. Paton Welding Institute	46
News	47



PREDICTION OF THERMODYNAMIC PROPERTIES OF MELTS OF MgO–Al₂O₃–SiO₂–CaF₂ SYSTEM

I.A. GONCHAROV¹, V.I. GALINICH¹, D.D. MISHCHENKO¹, M.A. SHEVCHENKO² and V.S. SUDAVTSOVA²

¹E.O. Paton Electric Welding Institute, NASU, Kiev, Ukraine

²Taras Shevchenko National University of Kiev, Ukraine

The calculation procedure is proposed for prediction of thermodynamic properties of simple slag melts, allowing for liquidus coordinates of constitutional diagrams. Excess integral functions calculated for more complex systems are given. The possibility of controlling the thermodynamic activity of SiO₂ in slag and, hence, silicon reduction process is shown.

Keywords: arc welding, high-strength steels, fused flux, slag melts, thermodynamic properties, SiO₂ activity

Step-by-step implementation of new high-strength steels has been taking place in the recent years. High requirements are made to toughness and strength of welded joints manufactured from these steels. For their fulfillment it is necessary to have a possibility for control of a content of oxygen and sulfur in weld metal, processes of microalloying, formation of non-metallic inclusions and structure in a process of solidification and cooling of a weld.

Silicon oxide are to be included in a flux for providing the necessary welding-technological properties (for pipes, for example, defect-free formation of the welds in multiarc welding with speed higher than 100 m/h are to be provided). However, presence of the latter in the flux during welding of modern steels results in silicon reduction in the weld metal and formation of non-metallic silicate inclusions, which is the reason of deterioration of mechanical properties of the weld metal. A slag system and flux composition, providing combination of optimum technological and metallurgical indices, are, in particular, the aim of our investigations.

Thermodynamic properties of welding consumables are to be known for prediction of metallurgical and technological characteristics. The experimental investigations of oxide melts are complex due to their aggressive behavior and refractoriness. Therefore, the calculation methods for prediction of thermodynamic properties of such melts are widely used in the recent years using similar data for solid compounds and phase equilibria [1–3]. Present paper proposes a procedure for prediction of thermodynamic properties of melts by liquidus coordinates of constitutional diagrams in area of solid component–solution equilibria which being described by the following equations:

$$(\mu_1^1)_{T_{eq}} = (\mu_1^{So})_{T_{eq}}, \quad (1)$$

$$\mu_1^1 + RT_{eq} \ln a_1^1 = (\mu_1^{So})_{T_{eq}}, \quad (2)$$

$$RT_{eq} \ln \gamma_1^1 = (-\Delta G_{melt})_{1, T_{eq}} - RT_{eq} \ln x_1^1, \quad (3)$$

$$\bar{\Delta H}_1 - T\bar{\Delta S}_1^{ex} = -\Delta G_{melt, 1} - RT \ln x_1^1, \quad (4)$$

where μ is the chemical potential of component; T_{eq} is the temperature at which solid component–solution equilibrium is considered; ΔS^{ex} is the excess entropy of solution mixing.

Investigations of thermodynamic properties were carried out applicable to MgO–Al₂O₃–SiO₂–CaF₂ slag system. These equations were used, however, areas of indicated equilibria for double oxide and oxide-fluoride melts MgO–Al₂O₃, MgO–SiO₂, MgO–CaF₂, Al₂O₃–SiO₂, Al₂O₃–CaF₂, SiO₂–CaF₂ are not large. Partial molar Gibbs energies of the components from constitutional diagrams in area of pure component–liquid solution equilibrium in MgO–Al₂O₃, MgO–SiO₂, MgO–CaF₂, Al₂O₃–SiO₂, Al₂O₃–CaF₂, SiO₂–CaF₂ binary boundary systems were calculated by equation, obtained from formulae (3) and (4):

$$\bar{\Delta G}_i = \Delta S_{melt}(T_L - T_{melt}),$$

where $\bar{\Delta G}_i$ is the partial molar Gibbs energy of component; ΔS_{melt} is the entropy of melting of pure component; T_{melt} is the temperature of pure component melting; T_L is the liquidus temperature.

Activities of the second component can be found through integration of Gibbs–Dugem equation

$$x_A d \ln(a_A) + x_Y d \ln(a_Y) = 0.$$

Hauffe–Wagner equation was used for area of solid quasibinary compound (Mg₂Al₂O₄, Mg₂SiO₄, Al₆Si₂O₁₃)–liquid solution equilibrium:

$$\Delta\mu_1(T, x_2) = \Delta S_{melt} \left\{ -\frac{x_2}{x_2 - y_2} \Delta T - y_2 \int_{y_2}^{x_2} \frac{\Delta T}{(x_2 - y_2)^2} dx_2 \right\},$$

where $\Delta\mu_1(T, x_2)$ is the measurement of chemical potential of the component 1 at temperature T and concentration of the component 2 in x_2 melt (standard condition – component in quasibinary compound); ΔS_{melt} is the entropy of compound melting; y_2 is the mole fraction of component 2 in quasibinary compound; $\Delta T = T_{melt} - T_L$.



For MgO–SiO₂, MgO–CaF₂, SiO₂–CaF₂ systems, which have areas of delamination of melts on constitutional diagram, used a relation

$$a_i(x_1) = a_i(x_2),$$

where x_1, x_2 are the mole fractions of the component i in the solutions which being in equilibrium to each other as well as $da_i/dx_i = 0, d^2a_i/dx_i^2 = 0$ for critical point of delamination.

$\Delta\bar{G}_i^{\text{ex}}$ can be found for binary boundary systems in all concentration interval knowing that $\Delta\bar{G}_i^{\text{ex}} + RTx_i \ln x_i = \Delta\bar{G}_i = RT \ln a_i$, and from them the integral excessive Gibbs energies are determined as $\Delta\bar{G}^{\text{ex}} = \Delta\bar{G}_i^{\text{ex}} x_i$.

Figure 1 shows obtained integral Gibbs energies of mixing recalculated for 1800 K temperature.

It can be seen from the Figure that significant negative values (on absolute value) of Gibbs energy of mixing are character for MgO–Al₂O₃ and MgO–SiO₂ systems in accordance to our calculations, that is proved by formation of stable compounds in these systems. Difference of thermodynamic properties of the solutions from ideal ones is sufficiently small for other systems. Comparison of the predicted Gibbs energies of mixing of melts of Al₂O₃–SiO₂ and MgO–SiO₂ binary systems with that which were determined by method of mass spectrometry in works [4, 5] showed that they have good agreement.

Study of thermodynamic properties of three- and four-component systems is more complex problem than of binary ones, however, they often have wide application. Therefore, the methods allowing calculation of thermodynamic properties of three-component melts using data similar for binary boundary sub-systems (method of Bonnier–Caboz, Toop, Li, Colinet, Kohler, Muggianu and etc.) [6] are developed in the last decades. Analysis of these methods showed that Kohler method has no need in additional data on the boundary sub-systems thought not always provide the maximum accuracy. Therefore, the following method was chosen for calculation of excess integral functions in the melts of three- and four-component systems among used by us boundary binary systems:

$$\Delta G^{\text{ex}} = \sum_A \sum_{B \neq A} (\Delta\bar{G}^{\text{ex}} AB)_{x_A/x_B} (x_A + x_B)^2,$$

where A, B are all components of three- or four-component system.

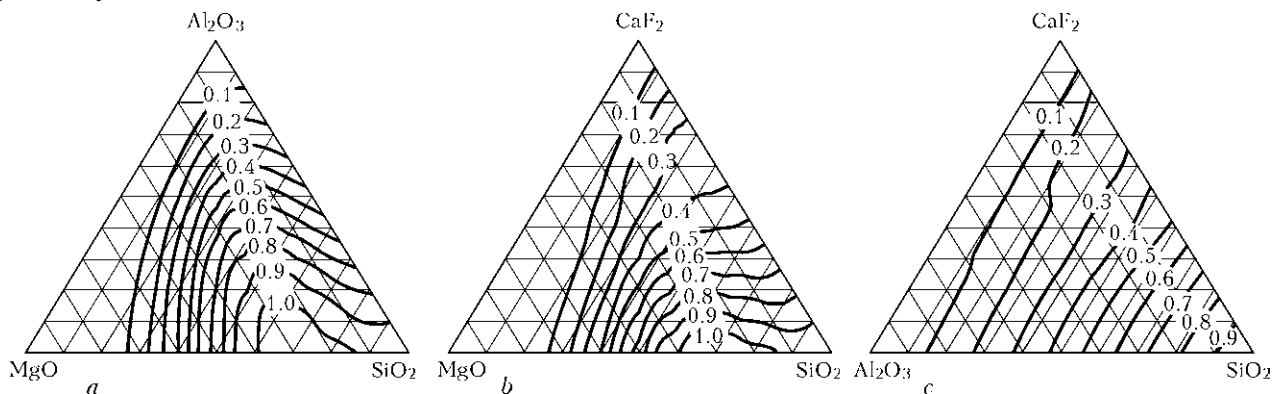


Figure 2. Isoactivities of SiO₂ in MgO–Al₂O₃–SiO₂ (a), MgO–CaF₂–SiO₂ (b) and Al₂O₃–CaF₂–SiO₂ (c) melts at 1800 K

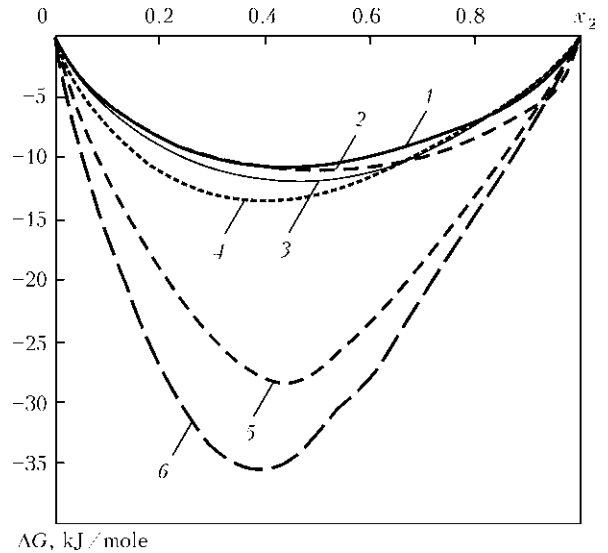


Figure 1. Gibbs energies of mixing of melts of binary systems at 1800 K: 1 – SiO₂–CaF₂; 2 – Al₂O₃–SiO₂; 3 – Al₂O₃–CaF₂; 4 – MgO–CaF₂; 5 – MgO–Al₂O₃; 6 – MgO–SiO₂

Partial excessive Gibbs energies of the components are taken from integral ones through differentiation on formula

$$\bar{\Delta G}_i^{\text{ex}} = \Delta G^{\text{ex}} - x_i \frac{d\Delta G^{\text{ex}}}{dx_i}.$$

Calculation was performed on a special program drawing isolines of excessive Gibbs energies or activities of components over concentration triangular diagrams of the ternary system or section with constant concentration of fourth component for the tetrad system.

Thus, Figure 2 shows calculated isoactivities of SiO₂ in three systems among considered ternary systems.

Delamination in area $0.60 < X_{\text{SiO}_2} < 0.99$ is character for melts of MgO–SiO₂ system. In this connection isoactivities of SiO₂ calculated in this and close to it areas have complex appearance and calculation accuracy is not high. However, reduction of SiO₂ concentration promotes negative deviations from Raoult's law.

Isoactivities of SiO₂ for section $C_{(\text{CaF}_2)} = 0.25$ of tetrad system MgO–Al₂O₃–SiO₂–CaF₂ are given in Figure 3. Data calculated were compared with given in literature [7]. Thus, calculation (lines) and experimental (points) of SiO₂ activity in MgO–Al₂O₃–SiO₂ melts at different operating temperatures [7] are given in Figure 4.

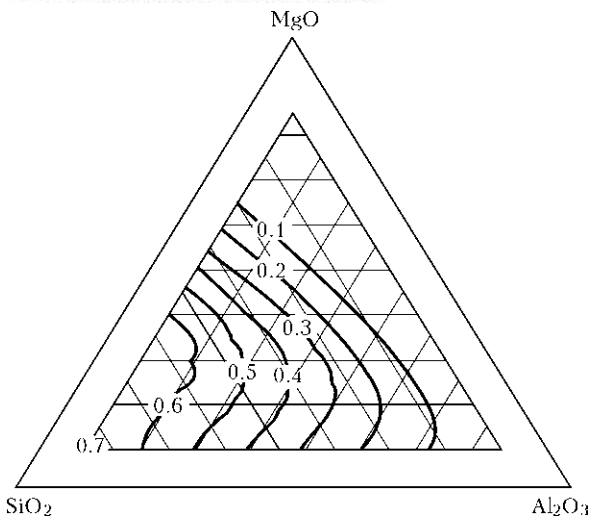


Figure 3. Isoactivities of SiO_2 in $\text{MgO}-\text{Al}_2\text{O}_3-\text{SiO}_2-\text{CaF}_2$ melt at 1800 K for $C_{(\text{CaF}_2)} = 0.25$

It was determined that these data as a whole agree with calculated by us. Thus, predicted alternating deviations from ideal melts for $\text{MgO}-\text{SiO}_2$ system as well as concentration dependence of SiO_2 activity in $\text{Al}_2\text{O}_3-\text{SiO}_2$ system are proved.

It can be seen from Figures 2, *a*, *b* and 3 that increase of magnesium oxide content in $\text{MgO}-\text{Al}_2\text{O}_3-\text{SiO}_2$, $\text{MgO}-\text{CaF}_2-\text{SiO}_2$, $\text{MgO}-\text{Al}_2\text{O}_3-\text{SiO}_2-\text{CaF}_2$ melts results in reduction of thermodynamic activity of SiO_2 in the melt. Therefore, it is possible to suppress processes of silicon reduction and formation of non-metallic silicate inclusions unnecessary from point of view of metallurgy of welding of low-alloyed high-strength steels and preserve, at that, melt structure and its physical-chemical properties favorable from point of view of providing of necessary technological properties of welding fluxes.

CONCLUSIONS

1. The procedure is proposed for prediction of thermodynamic properties of slag melts by liquidus coordinates of constitutional diagrams in area of solid component-solution equilibrium.

2. Thermodynamic properties of $\text{MgO}-\text{Al}_2\text{O}_3$, $\text{MgO}-\text{SiO}_2$, $\text{MgO}-\text{CaF}_2$, $\text{Al}_2\text{O}_3-\text{SiO}_2$, $\text{Al}_2\text{O}_3-\text{CaF}_2$, $\text{SiO}_2-\text{CaF}_2$ binary oxide and oxide-fluoride melts were calculated. Significant negative values of Gibbs energies of mixing for $\text{MgO}-\text{Al}_2\text{O}_3$ and $\text{MgO}-\text{SiO}_2$ systems were found that is proved by formation of stable compounds in these systems. The difference of thermodynamic properties of solutions from ideal ones is sufficiently small for other systems.

3. Calculation of excess integral functions from binary boundary systems was made using Kohler method in the melts of three- and four-component systems. Special program was developed for drawing isolines of excessive Gibbs energies or activities of components on concentration triangular diagram of the ternary system or section with constant concentration of fourth component for the tetrad system.

4. It is determined that increase of magnesium oxide content in $\text{MgO}-\text{Al}_2\text{O}_3-\text{SiO}_2$, $\text{MgO}-\text{CaF}_2-\text{SiO}_2$,

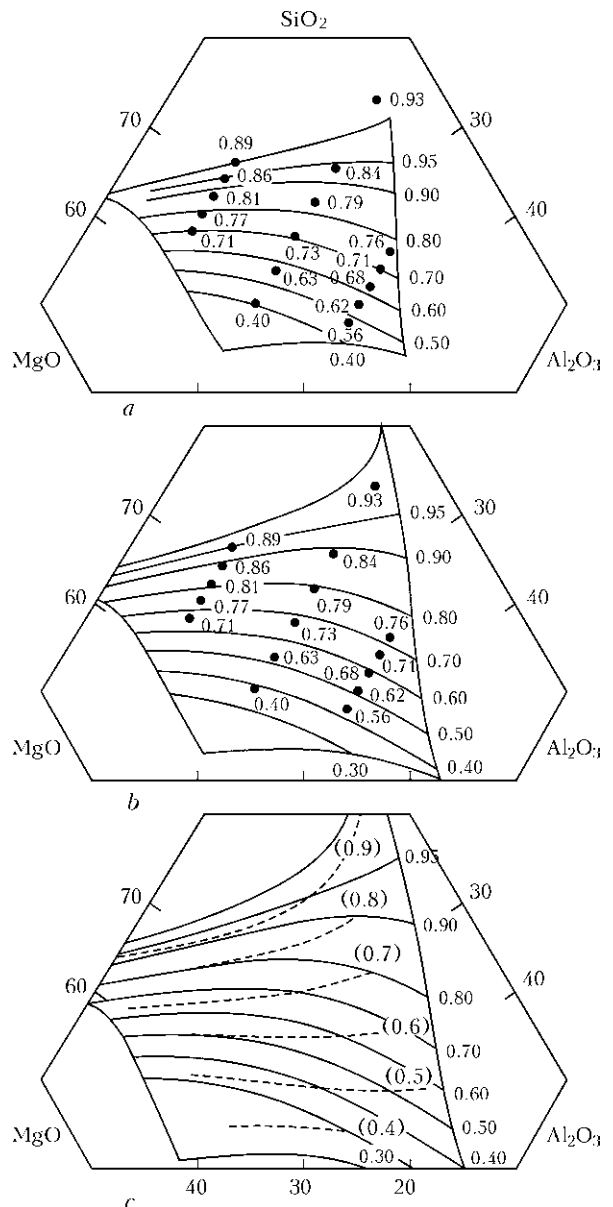


Figure 4. SiO_2 activities at temperature 1500 (*a*), 1550 (*b*) and 1600 (*c*) °C

$\text{MgO}-\text{Al}_2\text{O}_3-\text{SiO}_2-\text{CaF}_2$ melts results in reduction of thermodynamic activity of SiO_2 in the melt that allows controlling the processes of silicon reduction and formation of silicate non-metallic inclusions.

1. Fabrichnaya, O. (2000) Thermodynamic modelling of melting in the system $\text{FeO}-\text{MgO}-\text{SiO}_2-\text{O}_2$ at pressure of 1 bar. *CALPHAD*, 24(6), 113-131.
2. Wang, Ch., Zinkevich, M., Aldinger, F. (2004) On the thermodynamic modelling of the $\text{Zr}-\text{O}$ system. *Ibid.*, 28, 281-292.
3. Chen, M., Hallstedt, B., Gauckler, L.J. (2004) Thermodynamic modelling of the $\text{ZrO}_2-\text{YO}_{1.5}$ system. *Solid State Ionics*, 170, 255-274.
4. Shornikov, S.I. (2006) Thermodynamic properties of melts of system $\text{MgO}-\text{SiO}_2$. *Vestnik Otd. Nauk o Zemle RAN*, 1(22), 1-3.
5. Shornikov, S.I. (2004) Thermodynamic properties of melts of system $\text{Al}_2\text{O}_3-\text{SiO}_2$. *Ibid.*, 1, 1-3.
6. Muggianu, Y.O., Gambino, N.N., Bros, J.P. (2001) Enthalpic formation of liquid alloys bismuth-gallium-tin at 223 °C. *J. Alloys and Compounds*, 321(1), 183-200.
7. Jung, I.-H., Decterov, S.A., Peunov, A.D. (2004) Critical thermodynamic evaluation and optimization of the $\text{MgO}-\text{Al}_2\text{O}_3-\text{SiO}_2$ systems. *J. Phase Equilibria Diffusion*, 25(4), 329-345.



RESISTANCE OF WELDS ON THIN-SHEET ALUMINIUM ALLOYS TO INITIATION AND PROPAGATION OF SERVICE CRACKS

A.G. POKLYATSKY

E.O. Paton Electric Welding Institute, NASU, Kiev, Ukraine

Resistance friction stir and TIG welds on ductile low aluminium alloys and high-strength multi-component aluminium alloys 1.8 mm thick to initiation and propagation of cracks was determined by subjecting specimens comprising stress raisers to tension. It was shown that the welds made without metal melting have a higher resistance to service cracks.

Keywords: friction stir welding, TIG welding, thin-sheet aluminium alloys, service cracks

Ductile low aluminium alloys and high-strength multi-component aluminium alloys are widely used for fabrication of various-application welded structures. Different fusion welding methods are applied in the majority of cases to produce permanent joints. The welds in this case are formed as a result of melting of a certain volume of the materials joined and filler wire in a common weld pool, as well as their subsequent solidification in a shielding inert gas. The resulting welds have a cast dendritic coarse-crystalline structure, this making them inferior to the base material in mechanical properties [1, 2].

Melting of metal within the weld formation zone can be avoided and properties of base materials can be maintained in weldments by using solid-state friction stir welding (FCW) [3, 4]. The finely dispersed structure is formed in such a weld as a result of heating of an aluminium alloy due to friction within the welding zone to the plastic state, intensive stirring, deformation in a limited volume and compression by the working surfaces of a tool, and the base material in the HAZ weakens less than in fusion welding. This leads to increase in tensile strength of such joints in uniaxial tension of specimens [5–7], their fatigue strength under cyclic loading [8, 9] and resistance to corrosion in aggressive environments [10, 11], as well as to decrease in levels of residual stresses and strains [12, 13]. However, of high importance for estimation of performance of welded structures is resistance of the welds to initiation and propagation of cracks during operation. The purpose of this study was to evaluate resistance of the TIG and friction stir welds on thin-sheet aluminium alloys to initiation and propagation of cracks.

Ductile low aluminium alloys (AMtsN and AMg2M) and high-strength multi-component aluminium alloys (AMg6M, 1201, 1420 and 1460) used for fabrication of various welded structures were studied. Sheets 1.8 mm thick were welded by automatic

TIG welding in argon atmosphere at a speed of 20 m/h using machine MW-450 (Fronius, Austria). The welding process was carried out at currents of 130–145 A by using strips of matching alloys (for alloys AMtsN and AMg2M), or welding wires SvAMg6, SvAMg63 (for alloys AMg6M and 1420) and Sv1201 (for alloys 1201 and 1460). The FSW process was performed with a laboratory unit designed by the E.O. Paton Electric Welding Institute.

Butt welded joints were made by using a special tool with a tapered tip and a shoulder 12 mm in diameter. The speed of rotation of the tool was 1420 rpm, and the linear speed of its movement along the joint was 18–14 m/h.

Characteristics of resistance of the base metal and welds of the welded joints to fracture were determined on Kahn specimens [14] with a sharp ($R = 0.1$ mm) notch 11 mm long (Figure 1), providing initiation of crack at a relatively low energy level using versatile testing machine RU-5. The notch was arranged so that its apex coincided with the weld axis. The cross section area of the specimens was 44.75 mm². Tensile strength at off-centre tension and specific crack propagation energy (SCPE) for each specimen were determined by means of the load–strain diagrams plotted during the tests.

As shown by the studies, alloy AMtsN was characterised by the highest ductility. Even the presence of a stress raiser in the form of the sharp with $R = 0.1$ mm notch did not always lead to initiation of crack near its apex, and a specimen during tension might fracture outside the critical zone where this notch was located (Figure 2, *a*).

If a crack nevertheless initiated at the stress raiser apex, in tension of a specimen it propagated very slowly (Figure 3, *a*). The value of tensile strength in tension of such specimens of the AMtsN base metal was at a level of 261 MPa.

Tests of specimens of the TIG welded joints showed that the cracks forming near the stress raiser propagated in the weld metal (Figure 2, *b*). The cracks initiated and propagated in such specimens during tension much faster than in the base metal (Figure 3).

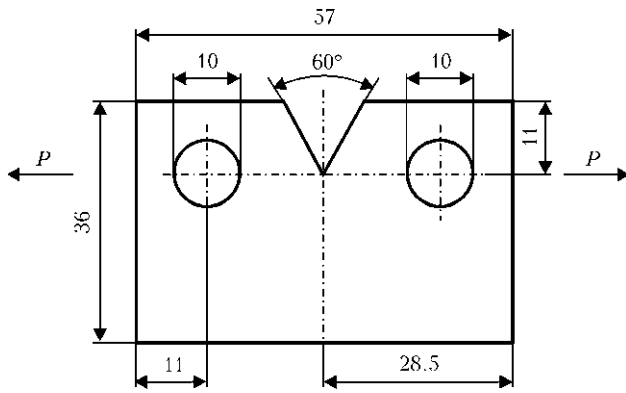


Figure 1. Schematic of Kahn specimen for evaluation of tensile strength of metal and SCPE under tension and bending conditions

The value of tensile strength of the weld metal was at a level of 191 MPa, which is substantially lower than that of the base metal.

The cracks that initiated at the stress raiser apex in specimens produced by the solid-state FSW method shifted to the thermomechanically affected zone (Figure 2, *c*). Tensile strength of metal in this zone was approximately identical to that of the fusion weld metal and equalled 192 MPa, and the diagram describing the character of initiation and propagation of the cracks was very similar to that plotted in tests of the specimens made by the TIG welding (Figure 3, *a*).

Initiation of cracks in the weld metal occurred easier than in the base metal, but resistance of the welds to propagation of the cracks that initiated at the stress raiser apex was higher compared to the base metal. This is evidenced by the SCPE values, which for the FS- and TIG-welded specimens were 7.0 and 6.9 J/cm², respectively, whereas for the base metal this value was only 4.5 J/cm².

Low aluminium alloy AMg2M was also characterised by a sufficiently high ductility. Therefore, a stress raiser in the form of the sharp notch did not cause instantaneous initiation and propagation of cracks (Figure 3, *b*). The value of tensile strength of such specimens was at a level of 256 MPa.

In specimens produced by the TIG welding method the cracks propagated in the weld metal, while their tensile strength was 214 MPa. In tests of the FSW specimens the cracks propagated from the central part of the weld to a zone where it interfaced the base metal. The value of tensile strength of such welds was at a level of 270 MPa.

Initiation and propagation of cracks in tension of specimens occurred easier in the TIG welds. For in-

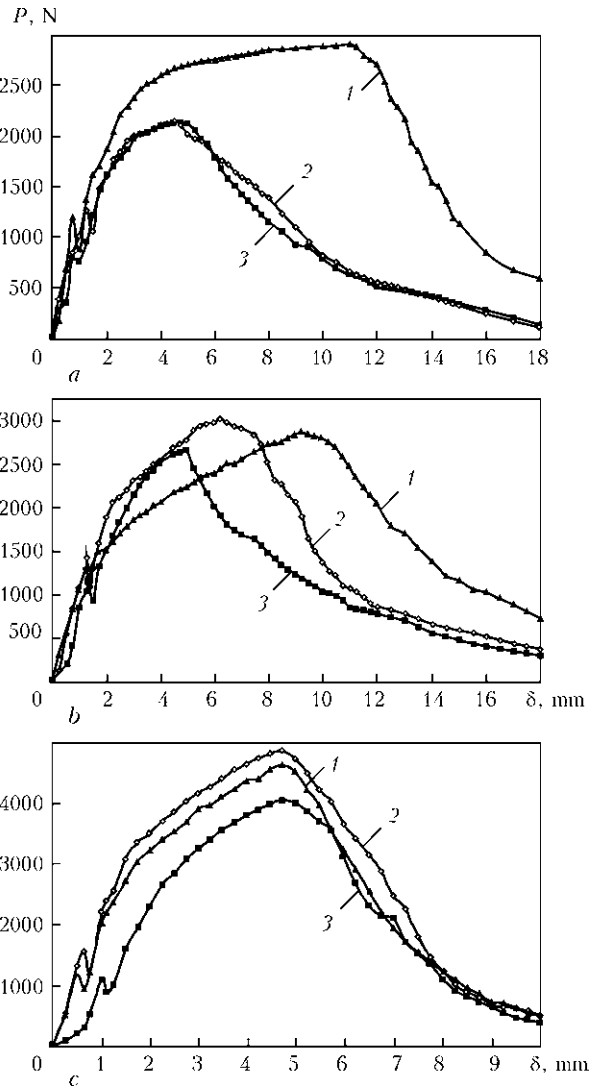


Figure 3. Load-strain diagram plotted during tests of the base metal (1) and metal of the FS- (2) and TIG- (3) welded joints on alloys AMtsN (*a*), AMg2M (*b*) and AMg6M (*c*)

stance, the value of SCPE in tests of such specimens amounted to 4.9 J/cm², which is 68 % of the corresponding value of the FSW specimens, although the base metal of alloy AMg2M had a higher resistance to initiation and propagation of cracks compared to the weld metal.

Alloy AMg6M was also characterised by a sufficiently high ductility. The process of initiation of a crack at the stress raiser apex occurred smoothly, but it propagated much faster than in low alloys (Figure 3, *c*). Tensile strength of specimens of this alloy base metal was at a level of 415 MPa.

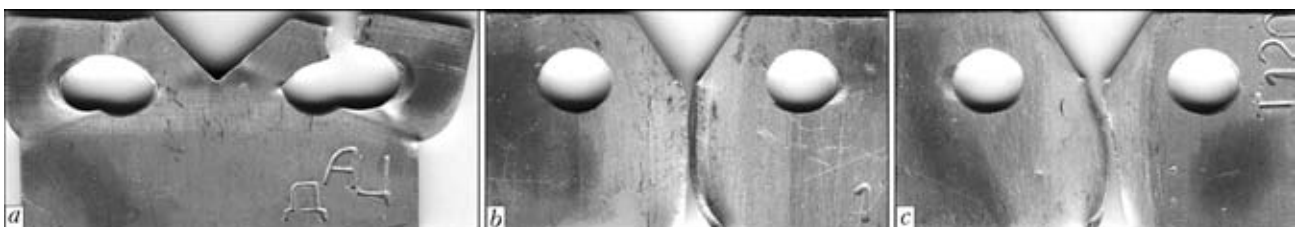


Figure 2. Appearances of fractured specimens of base metal (*a*) and TIG- (*b*) and FS- (*c*) welded joints on alloy AMtsN

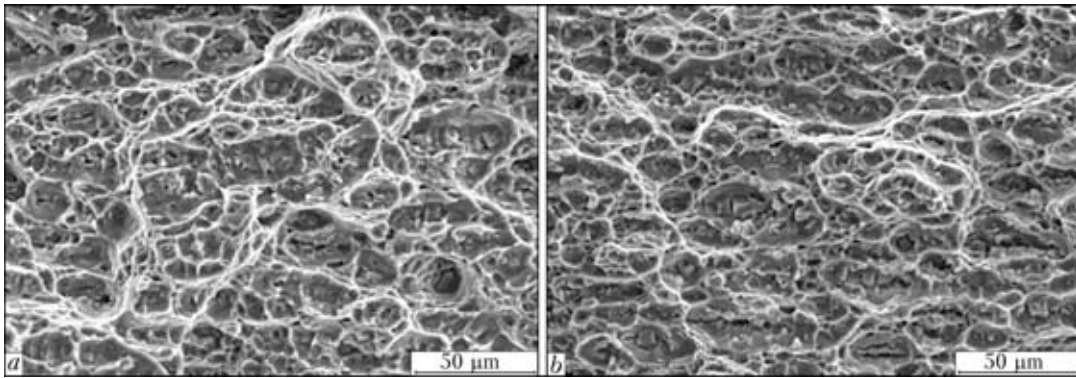


Figure 4. Fractography patterns ($\times 500$) of fracture surfaces of the weld (*a*) and weld to base metal interface zone (*b*) obtained in tests of FSW specimens on alloy AMg6M

The cracks that initiated at the sharp notch apex in specimens produced by the TIG welding method propagated in the weld metal. Tensile strength of metal of such welds was lower compared to the base metal and equalled 361 MPa. In tension of the FSW specimens the cracks shifted to the weld to base metal interface zone, and their tensile strength value was at a level of 436 MPa.

The cracks in the FSW specimens propagated during tension even slower than in the base metal. For example, the SCPE value of the weld metal in such specimens was at a level of 8.8 J/cm^2 , whereas for alloy AMg6M this value was 5.7 J/cm^2 , and for the fusion weld metal it was 4.7 J/cm^2 .

Fractography of fracture surfaces of specimens of the FS-welded joints indicated to a tough character of fracture of the welds (Figure 4). Shallow pits with

thin ridges can be clearly seen in the central part of the weld near the apex of a stress raiser in the form of the sharp notch. Fine structure of the welds provided a large total length of the grain boundaries, which hampered an abrupt increase of stress concentration and suppressed propagation of an avalanche crack in the weld metal.

Values of fracture resistance of Kahn tensile test specimens of aluminium alloys and their FS- and TIG-welded joints

Alloy welded	Welding method	Filler metal	σ_t , MPa	SCPE, J/cm^2
AMtsN	–	–	261	4.5
	FSW	–	192	7.0
	TIG	AMtsN	191	6.9
AMg2M	–	–	256	9.5
	FSW	–	270	7.2
	TIG	AMg2M	214	4.9
AMg6M	–	–	415	5.7
	FSW	–	436	8.8
	TIG	SvAMg6	361	4.7
1201	–	–	479	2.7
	FSW	–	449	3.8
	TIG	Sv1201	335	3.7
1420	–	–	458	2.6
	FSW	–	385	4.3
	TIG	SvAMg63	421	5.3
1460	–	–	571	8.5
	FSW	–	410	4.5
	TIG	Sv1201	366	2.7

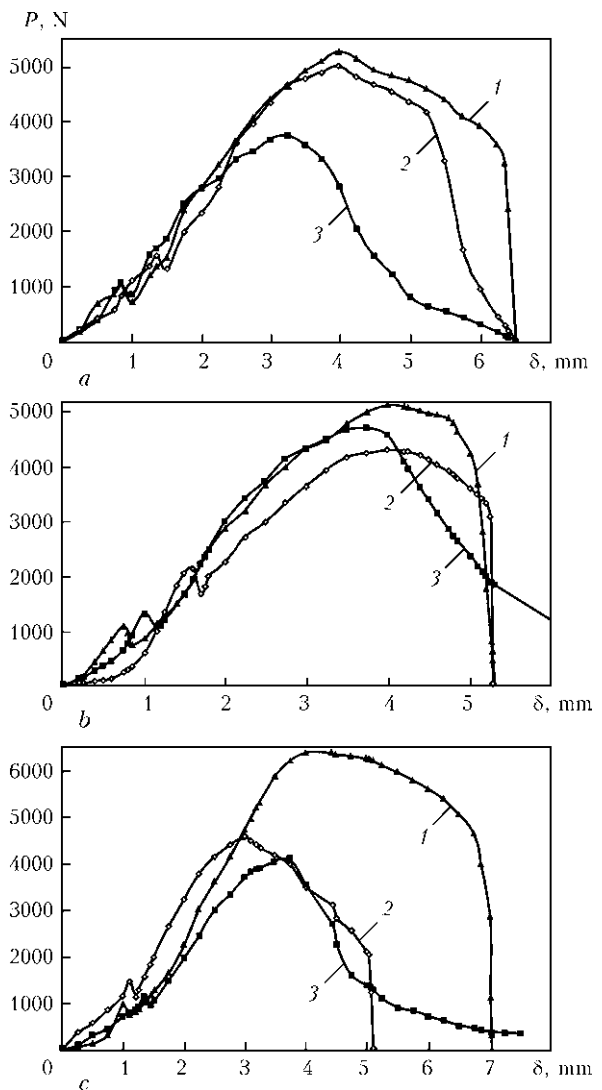


Figure 5. Load–strain diagram plotted in tests of specimens of the base metal (1) and FS- (2) and TIG- (3) welded joints on alloys 1201 (*a*), 1420 (*b*) and 1460 (*c*)

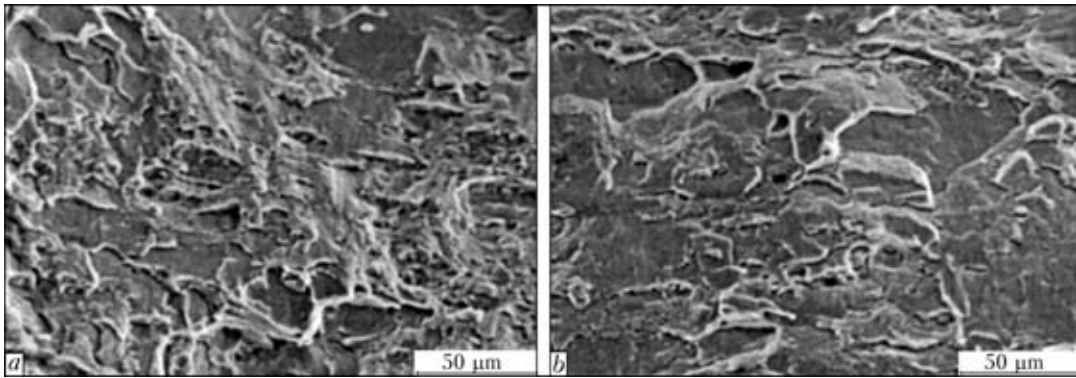


Figure 6. Fractography patterns ($\times 500$) of fracture surfaces of the weld (a) and weld to base metal interface zone (b) obtained in tests of FSW specimens on alloy 1460

Tension of such specimens of alloy 1201 with a stress raiser in the form of the sharp notch led to a quick initiation and propagation of cracks in them (Figure 5, a). Tensile strength of the base metal was about 479 MPa.

In specimens of the TIG-welded joints on alloy 1201 the crack that initiated at the sharp notch apex propagated in the weld metal. Tensile strength of the weld metal was approximately 335 MPa. In tests of the FSW specimens the crack shifted to the weld to base metal interface zone. Tensile strength of metal in this zone amounted to 449 MPa. The minimal value of SCPE in the base metal (2.7 J/cm^2) is indicative of the fact that the crack propagation process in it occurred easier than in metal of the solid-state and fusion welds.

High-strength aluminium-lithium alloy 1420 is more brittle than alloy AMg6M. Hence, a crack initiated at the sharp notch apex much quicker in the base metal (Figure 5, b), and it propagated almost instantaneously. The value of tensile strength of the base metal was at a level of 458 MPa.

The crack that initiated at the sharp notch apex in the fusion welded specimens propagated in the base metal, whereas in the FS-welded specimens it shifted to the weld to base metal interface zone. Tensile strength of such specimens was 421 and 385 MPa, respectively. The character of initiation and propagation of cracks in the solid-state weld metal was almost identical to that in the base metal (Figure 5, b).

The crack that initiated at the sharp notch apex propagated most easily in the base metal having a minimal SCPE value equal to 2.6 J/cm^2 . For the welds produced both by the solid-state and fusion methods this value was considerably higher, i.e. 5.3 and 4.3 J/cm^2 , respectively.

Alloy 1460 is characterised by a low ductility. Hence, initiation of cracks in tension of the base metal specimens occurred almost as quickly as in tension of alloy 1420, while propagation of cracks was a bit slower, approximately like in alloy 1201 (Figure 5, c). The tensile strength value of specimens of the 1460 base metal was about 571 MPa.

The cracks in the fusion welded specimens propagated in the base metal, while tensile strength of metal of such welds was approximately 366 MPa. In the FSW specimens the crack shifted to the weld to base metal interface zone, the tensile strength value of this metal being 410 MPa.

Propagation of the cracks that initiated at the notch apex occurred easier in the TIG weld metal, whose SCPE value was only 2.7 J/cm^2 . This value of the solid-state weld metal was much higher (4.5 J/cm^2) and constituted 53 % of the base metal level.

Fractography of fracture surfaces of the welds made on alloy 1460 by the FSW method (Figure 6) showed that they had the form typical of ductile materials, which are characterised by a high energy-consuming fracture by the tough mechanism. The groove-type relief formed as a result of plastic displacement of material in tension of the specimens. The weld to base metal interface zone featured a substantial increase in length of plane relief regions, which are indicative of a higher brittleness of the material with such a structure. Therefore, the crack initiated by the sharp notch in the central part of the weld shifted in tension of the specimen to the weld to base metal interface zone, where it propagated at lower levels of stress concentration and required much lower energy consumption.

Therefore, fracture resistance of the solid-state FS welds on aluminium alloys AMg2M, AMg6M, 1201 and 1460 was higher than that of the fusion welds. This confirms their higher resistance to initiation and propagation of cracks. The welds on low alloy AMtsN characterised by a super high ductility, made both by the solid-state and fusion welding methods, had identical values of tensile strength and SCPE. The higher values of fracture resistance of the welds on alloy 1420 were provided in fusion welding using filler metal than in friction stir welding.

1. Rabkin, D.M., Lozovskaya, A.V., Sklabinskaya, I.E. (1992) *Metals science of welding of aluminium and its alloys*. Ed. by V.N. Zamkov. Kiev: Naukova Dumka.
2. Mashin, V.S., Poklyatsky, A.G., Fedorchuk, V.E. (2005) Mechanical properties of aluminium alloys in consumable and nonconsumable electrode arc welding. *The Paton Welding J.*, **9**, 39–45.



3. Klimentko, Yu.V. *Method of friction welding of metals*. USSR author's cert. 195846. Int. Cl. 23 B k 35/02. Publ. 04.05.67.
4. Thomas, W.M., Nicholas, E.D., Needham, J.C. *Friction stir butt welding*. Int. Pat. Appl. PCT/GB 92/02203. Publ. 1991.
5. Pietras, A., Zadroga, L. (2003) Rozwoj metody zdrzewiania tarcowego z mieszaniami materialu zgrzeiny (FSW) i mozliwosci jej zastosowania. *Byuletyn Instytutu Spawalnictwa w Gliwicach*, **5**, 148–154.
6. Tsumura, T., Komazaki, T., Nakata, K. (2006) Structure and mechanical properties of ADC12 and A5083 dissimilar friction stir welded joints. *Transact. of JWRI*, **1**, 53–56.
7. Polovtsev, V.A., Shtrikman, M.M., Shilo, G.V. et al. (2005) Service characteristics of 1201 and AMg6 aluminium alloy joints made by friction welding. *Svarochn. Proizvodstvo*, **2**, 8–14.
8. Kluken, A., Raney, M. (1995) Aluminium bridge constructions — welding technology and fatigue properties. *Svetsaren*, **3**, 13–15.
9. Ericsson, M., Sandstrom, R. (2003) Influence of melting speed on the fatigue of friction stir welds, and comparison with MIG and TIG. *Int. J. Fatigue*, **25**, 1379–1387.
10. Enomoto, M. (2003) Friction stir welding: research and industrial applications. *Welding Int.*, **5**, 341–345.
11. Shtrikman, M.M., Polovtsev, V.A., Shilo, G.V. et al. (2004) Friction welding of sheet structures of aluminium alloys 1201 and AMg6. *Svarochn. Proizvodstvo*, **4**, 41–47.
12. Lanciotti, A., Vitali, F. (2003) Characterization of friction welded joints in aluminium alloy 6082-T6 plates. *Welding Int.*, **8**, 624–630.
13. Jata, K.V., Sankaran, K.K., Ruschau, J.J. (2000) Friction stir welding effects on microstructure and fatigue of aluminium alloy 7050-T7451. *Metallurg. Transact. A*, **31**, 2181–2192.
14. Kachanov, L.M. (1974) *Principles of fracture mechanics*. Moscow: Nauka.

METHODS FOR ASSESSMENT OF STRENGTHENING OF HSLA STEEL WELD METAL

V.A. KOSTIN, V.V. GOLOVKO and G.M. GRIGORENKO

E.O. Paton Electric Welding Institute, NASU, Kiev, Ukraine

Possibilities of application of strengthening mechanisms and structural approach to evaluation of strengthening of weld metal of high-strength low-alloyed (HSLA) steels were analyzed. It is shown that brittle fracture resistance of welds is mainly influenced by solid solution and grain-boundary strengthening.

Keywords: arc welding, HSLA steels, weld metal, strengthening mechanisms, structure, forecasting mechanical properties

At present HSLA steels are one of the most promising materials in welded structure fabrication. Starting from 1970s a lot of attention was given to investigations of the problems of metallurgy and technology of welding these steels. The accumulated extensive material on the properties of welded structures from this steel class allows forecasting the ways and the background technologies of further improvement of the entire set of mechanical properties of welds on HSLA steels. Analysis and generalization of the data of various researchers allowed defining several postulates aimed at producing reliable welded joints of HSLA steels with a high level of service properties [1, 2]. In particular, it is believed that in order to ensure an optimum combination of the values of strength, toughness and ductility of the metal of welds, made on HSLA with up to 560 MPa yield point, it is necessary to form welds with a high content of acicular ferrite structure [3, 4]. Investigations performed recently [5, 6] showed that an increased content of acicular ferrite in the weld structure in itself does not guarantee producing metal with high strength and toughness values. The process of brittle fracture, on the one hand, is influenced by solid solution alloying, and on the other hand — by the characteristics of non-metallic inclusions.

At evaluation of the influence of alloying on solid solution strengthening many authors used three main approaches: by metal composition, strengthening mechanisms and content of microstructural components.

In the first case, regression equations are used, which are based on the results of experiments on determination of metal mechanical properties, depending on the change of its alloying element content within certain limits. Such dependencies are valid only for that part of the compositions, for which they were established. So, the results of investigation of weldability of HSLA steels with C–Mn–Si alloying system [7] generalized in the equations

$$\sigma_t = 268 + 450[C + 0.33Si + Mn(1.6C - 0.145)], \quad (1)$$

$$a_T^{+20} = 144 - 387C + 330C^2 \quad (2)$$

cannot be used for low-alloyed steels with C–Mn–Si–Mo–Ni–Ti alloying system.

In the second case proceeding from the physical processes influencing the weld metal strengthening, an evaluation is proposed which is based on analysis of strengthening mechanisms, in keeping with which it is necessary to take into account the mechanism of solid solution, dislocation, dispersion and grain-boundary strengthening [8]. For instance, yield point $\Delta\sigma_y^F$ and temperature of transition from the brittle to tough fracture mode of ferritic-pearlitic steel T_{br}^{FP} can be determined as



$$\sigma_y^{FP} = \sigma_0 + \Delta\sigma_{s,s}^F + \Delta\sigma_{disl}^F + \Delta\sigma_P + \Delta\sigma_{d,stri}^F + \Delta\sigma_{gr}^F + \Delta\sigma_{sub}^F, \quad (3)$$

$$T_{br}^{FP} = T_0 + (0.4-0.6)\Delta\sigma_{s,s}^F + 0.4\Delta\sigma_{disl}^F + 0.3\Delta\sigma_{d,stri}^F - 0.7\Delta\sigma_{gr}^F, \quad (4)$$

where σ_0 , T_0 are the initial strength and transition temperature of an iron single-crystal ($\sigma_0 = 2 \cdot 10^{-4} G \sim 30$ MPa); $\Delta\sigma_{s,s}^F$ is the solid solution strengthening at the expense of ferrite alloying; $\Delta\sigma_{disl}^F$ is the contribution of dislocation strengthening at the expense of dislocation density in ferrite; $\Delta\sigma_P$ is the pearlite strengthening at the expense of pearlite grain formation; $\Delta\sigma_{d,stri}^F$ is the dispersion strengthening at the expense of disperse inclusions of carbides and nitrides in ferrite; $\Delta\sigma_{gr}^F$, $\Delta\sigma_{sub}^F$ is the grain boundary strengthening at the expense of the change of ferrite grain and subgrain size, respectively.

Contribution of various strengthening mechanisms can be given by the following system of equations:

$$\Delta\sigma_{s,s} = 4670[C] + 33[Mn] + 86[Si] + 82[Ti] + 30[Ni] + 11[Mo], \quad (5)$$

$$\Delta\sigma_{disl} = \alpha G b \rho^{1/2}, \quad (6)$$

$$\Delta\sigma_{gr} = \frac{k_y}{\sqrt{d}}, \quad \Delta\sigma_{sub} = \frac{k_y}{d}, \quad (7)$$

$$\Delta\sigma_{d,stri} = (9.8 \cdot 10^3 / \lambda) \ln 2\lambda, \quad (8)$$

$$\Delta\sigma_P = 2.4P, \quad (9)$$

where $\alpha = 0.5$, $k_y = 0.63 \text{ MPa}\sqrt{\text{m}}$ are the coefficients for steel; $G = 84,000$ MPa for steel; $b = 2.5 \cdot 10^{-7}$ mm is the Burgers vector for steel; d is the average size of the ferrite grain or subgrain, μm ; λ is the interparticle spacing having a strengthening effect on the solid solution; P is the pearlite fraction, %.

Development of the concepts of the mechanism of microstructural feature influence on solid solution strengthening and mechanical properties of the weld metal allowed defining one more method of assessment of the values of strength and ductility of welds, proceeding from the data on the number of microstructural components and their individual properties [9]. HSLA steels can be regarded as a polyphase mixture, the composition of which includes ferrite (F), pearlite (P), bainite (B) and martensite (M), secondary phases in the form of carbides and carbonitrides of microalloying elements, non-metallic inclusions (oxides, sulphides). If steel is to be considered as a natural composite of the above phases, then its strength properties (σ_y , σ_t) can be presented as a sum of strength properties of each component, multiplied by its volume fraction in the weld:

$$\sigma_y = \sigma_F V_F + \sigma_P V_P + \sigma_B V_B + \sigma_M V_M + \sum \sigma_{d,stri} V_{d,stri}, \quad (10)$$

where σ_F , σ_P , σ_B , σ_M are the volume fractions of ferrite, pearlite, bainite and martensite, allowing for their volume fractions V_F , V_P , V_B , V_M ; $\sigma_{d,stri}$, $V_{d,stri}$ are the strength and fraction of secondary phase component in the weld metal.

The properties of each structural component, included into formula (1), are determined by the composition, morphology and dispersity of the structure. Strength of ferrite component σ_F is presented as a sum of three addends

$$\sigma_F = \Delta\sigma_{s,s}^F + \Delta\sigma_{disl}^F + \Delta\sigma_{gr}^F, \quad (11)$$

which are found by formulas (5)–(7), and pearlite strength σ_P – by expression (9).

Influence of the bainite component of the structure can be assessed using a linear dependence of strength in the range from the temperature of the start of bainite transformation B_s up to the temperature of martensite formation M_s :

$$\sigma_B = \frac{(\sigma_F V_F + \sigma_P V_P)}{(V_F + V_P)} + \left[\frac{1}{V_M} \sum \frac{(B_s - T_i)}{(B_s - M_s)} \frac{\sigma_M - (\sigma_F V_F + \sigma_P V_P)}{(V_F + V_P) \Delta V_{B_i}} \right], \quad (12)$$

where T_i is the temperature of bainite transformation at i -th moment of time; ΔV_{B_i} is the increment of bainite volume during i -th time interval [10].

The main factor determining the strength properties of martensite is carbon content in martensite. The contribution of martensite component can be assessed by the formula from work [11]:

$$\sigma_M = A_M + B_M \sqrt{C}, \quad (13)$$

where A_M , B_M are the empirical components; C is the carbon content in martensite (MAC-phase).

According to Marder and Krauss, martensite strength is related to the dimensions of martensite packs, d_p , by a relationship of Hall–Petch type $\sigma_M = 449 + 60 d_p^{-1/2}$, where σ_M is expressed in megapascals, d_p in micrometers.

Dispersion strengthening $\sigma_{d,stri}$ depends on the volume fraction and dispersity of secondary phases (carbide, carbonitride and non-metallic inclusions) and is given by the formula in (8).

Thus, knowing the composition of weld metal, volume fractions of primary (ferrite, pearlite, bainite and martensite) and secondary phases (carbide, carbonitride phases and non-metallic inclusions), dispersity and morphology of the structure, it is possible to reliably predict the mechanical properties of metal of HSLA steel welds.

Welded joints of HSLA steel were made in order to analyze the possibilities of application of strengthening mechanisms and structural approach to weld metal strengthening. Composition of base metal, welding wire and welds is given in [12].



Table 1. Quantity of microstructural constituents (%) and average size of ferrite grain d_f of weld metal alloyed by manganese

Weld designation	Acicular ferrite	Polygonal ferrite	Lamellar ferrite		Polyherdral ferrite	Side Widmanstaetten ferrite	$d_f, \mu\text{m}$
			With unordered second phase	With ordered second phase			
GA13G	49.5	2.0	17.0	5.0	26.5	0	360
GA09G	48.0	9.5	9.0	3.5	30.0	0	250
GA19G	61.5	13.5	3.0	0	22.0	0	150
GA13G2	55.0	7.5	17.5	2.5	15.5	1	300
GA09G2	64.5	8.0	0	0	25.0	2	250
GA19G2	85.0	4.0	0	0	8.0	3	170

Table 2. Quantity of microstructural coconstituents (%) and average size of ferrite grain d_f of the metal of welds alloyed by titanium

Weld designation	Acicular ferrite	Polygonal ferrite	Lamellar ferrite		Polyherdral ferrite	Side Widmanstaetten ferrite	$d_f, \mu\text{m}$
			With unordered second phase	With ordered second phase			
GA13T	23.5	10.5	21.5	7.5	29	8	150
GA09T	10.0	20.0	–	20.0	50	–	120
GA19T	6.0	3.7	55.0	33.0	2.3	–	70
GA13T2	7.0	9.0	41.0	9.0	–	–	100
GA09T2	–	5.7	36.7	57.6	34	–	70
GA19T2	–	2.0	25.3	71.7	1	–	50

During metallographic investigations the fraction of individual components of weld metal microstructure, elemental composition and distribution of non-metallic inclusions by size were determined. The microstructure was studied by the method of optical and electron metallography using light microscope «Neophot-32» and JEOL scanning electron microscope JSM-840, fitted with MicroCapture card for image capturing with subsequent recording of the image on the computer screen. Quantitative determination of microstructural components was conducted in keeping with IIW procedure.

Results of determination of microstructural composition of the metal of welds and average size of ferrite grain, obtained when studying ground samples in 4 % solution of nitric acid in ethanol, are given in Tables 1 and 2.

Analysis of the data on the quantity, volume fraction and size distribution of non-metallic inclusions, obtained at metallographic investigations of unetched sections, showed the existence of certain differences in the morphology of inclusions of different sizes. Finely-dispersed inclusions of up to 1.0 μm size have a nugget, consisting of aluminium and titanium oxides, and external fringe of a cubic shape with a high content of titanium nitrides (Figure 1, *a*). Larger inclusions consist of oxides of a complex composition, which have manganese sulphide precipitates on their surface (Figure 1, *b*).

Strengthening effect of the inclusion on the surrounding matrix is determined by the difference in the coefficients of thermal expansion of the inclusion and matrix. The contribution of secondary nitride or carbonitride phases to dispersion strengthening $\sigma_{d.str. i}$

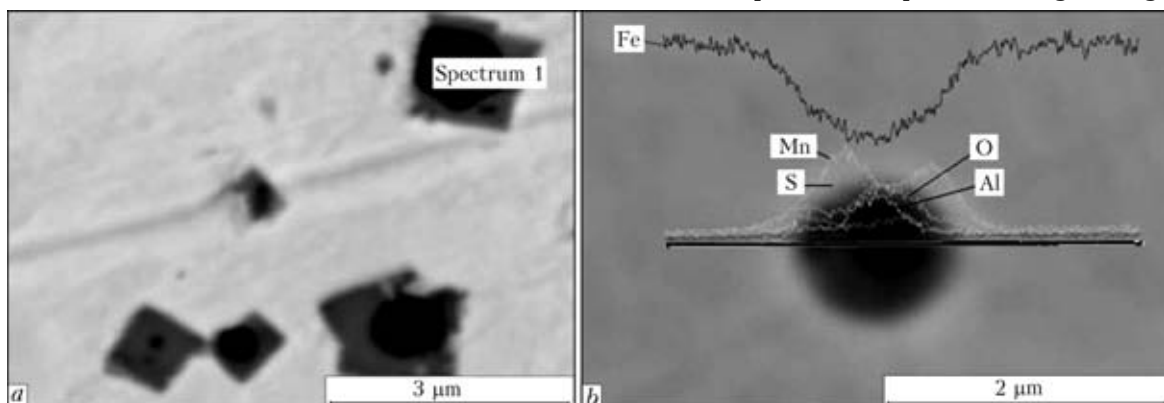


Figure 1. Morphology of non-metallic inclusions of less than 1.0 (*a*) and more than 1.5 (*b*) μm size



Table 3. Volume fraction of non-metallic inclusions, their size distribution and results of calculation of particle spacing λ by formula (8)

Weld designation	Volume fraction of inclusions, %	Content (%) /quantity (pcs) of inclusions in the dimensional range, μm					λ , μm
		< 0.3	0.5–1.0	1.25–2.0	2.25–3.0	> 3.0	
GA13G	0.83	32/761	45/1050	18/422	3/74	2/43	3.21
GA09G	0.24	37/558	49/735	11/169	1.5/22	1/16	3.09
GA19G	0.09	31/274	62/547	6.5/57	0.1/1	0/0	2.69
GA13G2	0.79	35/665	43/827	18/340	3/54	2/33	2.89
GA09G2	0.25	37/513	52/718	10/138	1/16	0.3/4	2.71
GA19G2	0.14	46/423	45/416	7/60	1/9	0.7/6	2.16
GA13T	0.40	25/243	51/490	17/159	5/45	3/26	3.96
GA09T	0.24	53/647	37/458	8/94	2/21	0.25/3	2.99
GA19T	0.12	33/233	52/360	11/79	3/21	0.6/4	1.89
GA13T2	0.65	53/408	33/258	10/75	3/21	1.5/12	1.89
GA09T2	0.35	56/315	35/197	2/10	1.5/8	1.5/8	1.80
GA19T2	0.23	62/386	30/189	6/36	2/11	0.16/1	1.61

is considerable, so that the matrix develops compressive forces around such inclusions, whereas for sulphides this value is significantly lower that promotes formation of ruptures on the inclusion-matrix interphase and practically complete absence of the influence of inclusions on weld metal properties [13].

During analysis and processing of metallographic images the fraction of non-metallic inclusions of not more than 1.0 μm size was calculated. Obtained data were used to calculate the values of interinclusion distances, λ , given in Table 3.

Based on the results of metallographic investigations (see Tables 1 and 2), calculations were performed by formulas (5)–(8) to determine the contribution of individual components to solid solution strengthening of weld metal. Pearlite influence on strengthening was not calculated in view of its absence in the weld structure. Proceeding from the reasons given in [14, 15], the contribution of dislocation strengthening (about 150–180 MPa) was taken to be constant, and

it change during alloying by manganese and titanium was not considered.

Results of testing weld metal samples to GOST 6996 are given in Table 4, Figures 2 and 3 show the results of calculation of the contribution of solid solution, dispersion and grain-boundary mechanisms into strengthening of the studied weld metal and its comparison with the yield point and tensile strength.

Analysis of the obtained results shows that the greatest contribution to strengthening is made by grain-boundary and solid solution strengthening. Comparison of the calculated (Figure 3) and experimental data on tensile strength and yield point of weld metal (Figure 4) shows their reasonably good agreement. On the other hand, the observed deviations from the calculated and experimental results (in welds alloyed with large quantities of titanium) are due to the fact that titanium being a strong carbide-forming element starts interacting with carbon and nitrogen forming finely-dispersed carbides and carbonitrides, which, similar to oxide inclusions, have a strengthen-

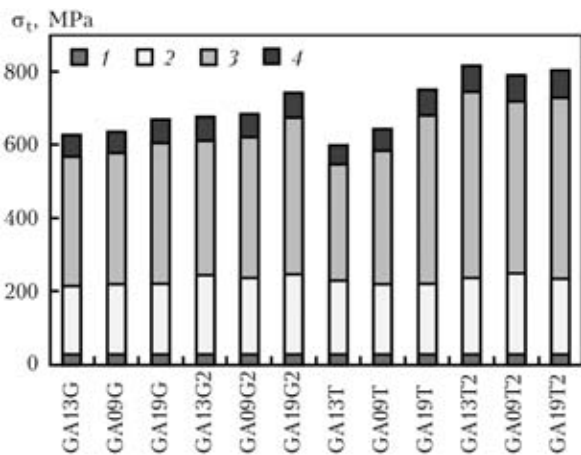


Figure 2. Calculated contribution of various strengthening mechanisms into the strength of the metal of welds alloyed by manganese and titanium: 1 – lattice friction; 2 – solid solution 3 – grain-boundary; 4 – dispersion strengthening,

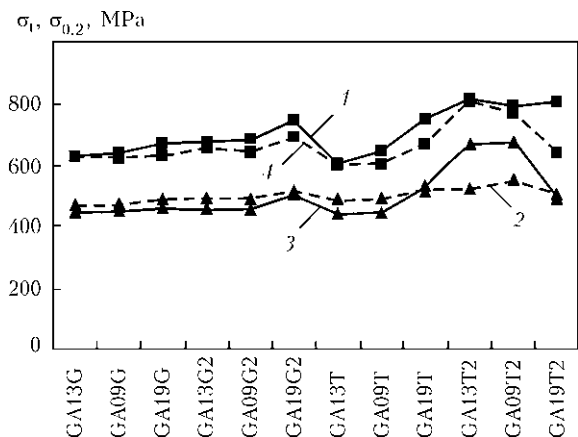


Figure 3. Comparison of calculated values (1, 2) of tensile strength (σ_t) and yield point ($\sigma_{0.2}$) with their experimental (3, 4) values obtained for the studied welds

**Table 4.** Mechanical properties of the metal of welds alloyed by manganese and titanium

Weld designation	$\sigma_{0.2}$, MPa	σ_t , MPa	δ_5 , %	ψ , %	KCV, J/cm ² , at T, °C		
					20	0	-20
GA13G	446.4	626.2	21.0	59.9	47.3	31.9	20.8
GA09G	444.4	621.1	23.4	65.0	126.2	94.6	66.8
GA19G	458.8	627.9	22.3	67.9	144.1	107.7	94.2
GA13G2	453.8	652.8	21.2	57.5	58.0	41.4	29.9
GA09G2	455.2	638.9	23.4	64.0	98.4	78.0	60.1
GA19G2	501.0	686.7	21.8	64.8	103.9	69.4	53.5
GA13T	437.7	597.5	23.1	58.8	62.4	42.9	23.7
GA09T	443.4	603.5	23.5	67.7	64.3	40.8	19.0
GA19T	527.2	665.9	18.8	66.9	43.3	20.9	13.8
GA13T2	664.2	807.3	17.6	66.0	22.2	16.7	13.0
GA09T2	673.3	769.0	17.5	63.9	28.5	13.8	16.0
GA19T2	488.9	634.0	20.6	59.8	49.6	18.3	13.9

ing impact on the solid solution. Unfortunately, determination of the composition, size, distribution and spacing of carbides (8) requires performance of additional transmission electron microscopy investigations and X-ray spectral analysis.

Increase of weld metal alloying by manganese causes a lowering of the temperature range of ferrite transformations [12] and promotes formation of ferritic structure with grain size in the range of 170–260 μm (see Table 1). Non-metallic inclusions in welds in this case have predominant dimensions of up to 1.0 μm , and fraction of inclusions of 0.5–1.0 μm size is from 30 up to 45 % (see Table 3).

Lowering of the temperature of the start of $\gamma \rightarrow \alpha$ transformation suppresses the growth of grain-boundary ferrite and leads to reduction of the content of its allomorphous morphology in the weld metal. Formation of relatively large ferrite grains in combination with a high content of disperse (up to 1.0 μm) inclusions and lower temperature of the end of bainite transformation, promote intragranular nucleation of bainitic ferrite and formation of up to 85 % of ferritic structure of acicular morphology (see Table 1). It should be noted that with lowering of temperature interval of bainite transformation the width of ferrite needles increases from 80 up to 160 μm . The structure of wider needles shows twinning boundaries that causes an increase of acicular ferrite hardness and lowering of weld metal impact toughness, despite an increased content of this constituent in the structure [12].

Weld metal alloying by titanium does not influence the temperatures of the start of ferrite and bainite transformation, but raises the temperature of the end of the latter [12], thus leading to an essential refinement of ferrite grain size (see Table 2). Volume fraction of non-metallic inclusions in the weld metal decreases, but content of inclusions of not more than 0.3 μm size with a high content of carbonitride phase,

increases (see Table 3). Increase of the content of finely-dispersed carbide phase in the metal of welds alloyed by titanium led to growth of the centers of α -phase nucleation, on the one hand, and increase of the fraction of dispersion strengthening in formation of mechanical properties of weld metal, on the other. At increase of the density of intergranular boundaries distribution, they become more probable sites of ferrite structure growth in terms of energy, while the high contamination of the boundaries by non-metallic inclusions larger than 1.5 μm , promotes the start of these transformations in the high temperature region, resulting in formation of a structure of Widmanstaetten ferrite type. Increase of ferrite content in the metal of titanium-alloyed weld series, with second phase precipitations in the form of thin plates, is accompanied by increase of its structure microhardness and lowering of brittle fracture resistance [12].

Thus, brittle fracture resistance of HSLA steel weld metal is mainly affected by solid solution and grain-boundary strengthening. While in samples of titanium-alloyed series the adverse influence of solid solution strengthening was compensated by refinement of the grain structure from 200 to 100 μm , in samples of titanium-alloyed series the extremely high contribution of solid solution strengthening could not be neutralized even at the expense of grain refinement to 50 μm .

Increase of the content of finely-dispersed carbide phase in the metal of titanium-alloyed welds led to enhancement of the role of dispersion strengthening in formation of mechanical properties of weld metal. Apparently, such carbides promote formation of a dispersed structure in the region of high-temperature austenite decomposition. However, in the case of formation of high-temperature morphological forms of bainitic ferrite the welds have a low level of toughness. To increase weld metal toughness, it is necessary to



attempt to achieve formation of an increased content of low-temperature bainitic ferrite forms in their structure through alloying by elements increasing the austenite stability.

CONCLUSIONS

1. Application of the method of strengthening evaluation, which allows for the strengthening mechanisms, enables an adequate prediction of strength properties of HSLA steel weld metal.

2. At simulation of the composition of HSLA steel weld metal, in order to achieve high values of strength, ductility and toughness of welded joints, it is necessary to achieve an increase of the contribution of $\Delta\sigma_{d, str}$ and $\Delta\sigma_{gr}$ at limitation of $\Delta\sigma_{s, s}$. The structure of weld metal in this case will develop morphological forms of bainitic ferrite, while the presence of a dispersed carbide phase will promote formation of a fine-grained secondary structure.

1. Pokhodnya, I.K. (2008) Metallurgy of arc welding of structural steels and welding consumables. *The Paton Welding J.*, **11**, 54–64.
2. Fujita, Y., Nakanishi, Y., Yurioka, N. (2008) Advanced welding technologies in recent industries in Japan (Review). *Ibid.*, **11**, 40–45.
3. Lyakishev, N.P., Nikolaev, A.V. (2003) Metallurgy of steel: specifics of production in the XX century, problems and prediction of future development. *Ibid.*, **10/11**, 38–45.

4. Olson, D.L., Metzbower, E., Liu, S. et al. (2003) Developments in property predictions for weld metal. *Ibid.*, **10/11**, 31–37.
5. Grabin, V.F., Golovko, V.V. (2007) Effect of distribution of manganese in structural components on properties of low-alloy weld metal. *Ibid.*, **12**, 19–22.
6. Golovko, V.V., Grabin, V.F. (2008) Effect of alloying of high-strength weld metal with titanium on its structure and properties. *Ibid.*, **1**, 13–17.
7. Frantov, I.I., Stolyarov, V.I., Nazarov, A.V. et al. (1987) Optimization of composition of low-alloy welded steels. *Metallovedenie i Term. Obrab. Metallov*, **11**, 37–42.
8. Goldshtejn, M.I. (1987) Ways of increase in strength and cold resistance of structural steels. *Ibid.*, **11**, 6–11.
9. Young, C.H., Bhadeshia, H.K.D.H. (1994) Strength of mixtures of bainite and martensite. *Material Sci. and Technology*, **10(3)**, 209–214.
10. Mazur, V.L., Nogovitsin, A.V. (2010) *Theory and technology of sheet rolling (numerical analysis and technical appendixes)*. Dnepropetrovsk: Dnipro-VAL.
11. Liska, S., Wozniak, J. (1981) Matematiský model pro analýz v technologických podmínek valcování oceli za tepla. *Hutn. Actual*, **22(9)**, 1–49.
12. Golovko, V.V., Kostin, V.A., Zhukov, V.N. et al. (2010) Effect of alloying with manganese and titanium on peculiarities of decomposition of austenite in low-alloy weld metal. *Vesnik ChGTU*, **45**, 125–133.
13. Gubenko, S.I., Parusov, V.V., Derevyanchenko, I.V. (2005) *Non-metallic inclusions in steel*. Donetsk: Art-Press.
14. Vysotsky, V.M., Motovilina, G.D., Khlusova, E.I. (2004) Theoretical and experimental evaluation of strengthening and embrittlement of low-alloy ferritic-pearlitic steels. *Voprosy Materialovedeniya*, **4**, 5–13.
15. Schastlivtsev, V.M., Yakovleva, I.L. (2009) Principal structural factors of strengthening of low-alloy low-carbon pipe steels after controlled rolling. *Metallovedenie i Term. Obrab. Metallov*, **1**, 41–45.

ROLE OF NON-METALLIC INCLUSIONS IN CRACKING DURING ARC CLADDING

Yu.M. KUSKOV, D.P. NOVIKOVA and I.L. BOGAJCHUK

E.O. Paton Electric Welding Institute, NASU, Kiev, Ukraine

The effect of non-metallic inclusions in the base metal on initiation and propagation of cracks in the deposited metal is considered. It is shown that, in addition to the non-metallic inclusions, the propagation of cracks in the deposited metal is also promoted by the hardening phases present in its structure, as well as by the polygonisation boundaries. However, the latter are not the initiating factors of cracking.

Keywords: base and deposited metals, non-metallic inclusions, cracks, hardening phases, polygonisation boundaries

The optimal composition of a wear-resistant deposited metal is chosen experimentally or by mathematical modelling. The second variant is a better choice, as it is more cost-effective. However, as shown by practice, in many cases, especially in cladding of high-carbon steels, at a stage of verification of workability of a chosen cladding consumable the calculated «optimal» composition should be corrected to avoid cracks in the deposited metal. The use of this twofaced method of assessment of the investigation data results in formation of the final composition of the deposited

metal. In this case, the technological part of the investigations is usually limited to studies of the processes taking place only in the deposited metal. Moreover, in view of some economical difficulties with purchasing of metal, the use is made of the «available» steels, although the provisions are made for conducting a high-quality chemical analysis of this metal.

This study is dedicated to investigation of the effect of quality of the base metal on the results of cladding, and in particular on the initiation of cracks in the deposited metal.*

Cladding was performed on specimens cut by the gas cutting method from the «available» rolled steel

*The study was carried out with participation of Dr. I.I. Ryabtsev.

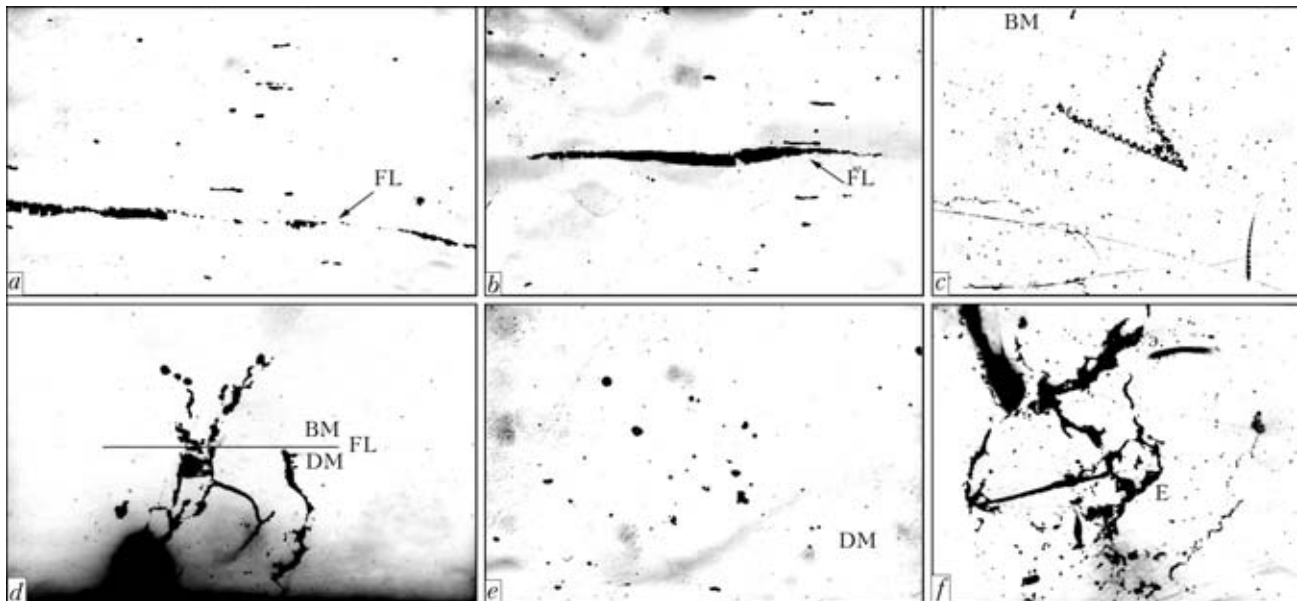


Figure 1. Non-metallic inclusions, dislocations and cracks in base (BM) and deposited (DM) metals: *a* – stringers of alumina, inclusions of aluminosilicates and oxysulphides of the base metal ($\times 400$); *b* – stringers of iron-manganese sulphides, inclusions of aluminosilicates and oxysulphides of the base metal ($\times 400$); *c* – dislocation stringers located near cracks in the base metal ($\times 200$); *d* – cracks propagating from globular inclusions of the base metal ($\times 250$); *e* – globular inclusions in the deposited metal ($\times 400$); *f* – cracks propagating through eutectic (E) ($\times 25$)

corresponding in chemical composition to steel St3. Self-shielding flux-cored wires providing the high-carbon ($C = 1\%$) deposited metal served as a deposited metal. Cladding was performed in four layers.

Cracks were revealed in the deposited metal after cladding. Because of small (through thickness) sizes of the cracks, they could not be visually detected after deposition of each layer. Therefore, it was difficult to locate the site of initiation of a crack. It could be done only on metallographic sections.

The clad specimens were prepared by the conventional procedure in the form of transverse sections for metallographic examinations, which were conducted both on polished surfaces and on surfaces after electrolytic etching in 20 % aqueous solution of chromic acid.

Examinations of polished surfaces of sections.

A large number of non-metallic inclusions were fixed in the base metal. They were arranged in the form of stringers of different thicknesses and lengths, or in the form of isolated inclusions of various shapes and sizes. Supposedly, dark-gray stringers elongated in the rolling direction were inclusions of alumina Al_2O_3 (Figure 1, *a*). Although, being relatively brittle components, they most often fractured in rolling into isolated particles. Iron-manganese sulphides $FeS \cdot MnS$ of the light-gray colour had an identical direction of the arrangement (Figure 1, *b*).

Isolated inclusions were presented by aluminosilicates $3Al_2O_3 \cdot SiO_2$ and $Al_2O_3 \cdot SiO_2 \cdot FeO$, and by oxysulphides (Figure 1, *a, b*). This quantity of various non-metallic inclusions formed the zones of weakness in the base metal, which might act as centres of probable initiation of cracks in them. Heterogeneity of metal and imperfection of its structure led to the fact

that dislocation stringers were detected near some of the cracks (Figure 1, *c*).

Despite that the acute-angled non-metallic inclusions of the type of alumina, silica etc. are most dangerous in terms of initiation of cracks [1], in fact a crack may initiate in a zone with the most stressed state (Figure 1, *d*).

Moreover, in the case of small non-metallic inclusions (in the form of isolated inclusions or stringers in the base metal) the welding arc affecting them may cause their crushing and spheroidisation. Further on these rounded particles will transfer step-by-step from the base metal to the deposited layers (Figure 1, *e*). Floating of non-metallic inclusions and their forwarding to each of the next deposited layers were detected. Further propagation of cracks takes place along various hardening phases of structure, in particular along locations of eutectic (Figure 1, *f*). As a result, the crack may have a developed zigzag (Figure 2, *a*) or straight-line shape (Figure 2, *b*).

Examination of surfaces of sections after etching. Examination of microstructure after etching allows a more detailed evaluation and checking of the sequence of stages of propagation of a crack: from the moment of its initiation to the final stage. The zone of fusion of the base metal and first layer of the deposited metal with globular non-metallic inclusions located in the base metal is shown in Figure 3, *a*. The site of initiation of the crack near one of the non-metallic inclusions in the base metal is clearly proved in Figure 3, *b*. Transfer of non-metallic inclusions from the first layer to a boundary of the second and third deposited layers is shown in Figure 3, *c*.

The earlier conclusion on propagation of cracks in the deposited metal along the zones of location of the

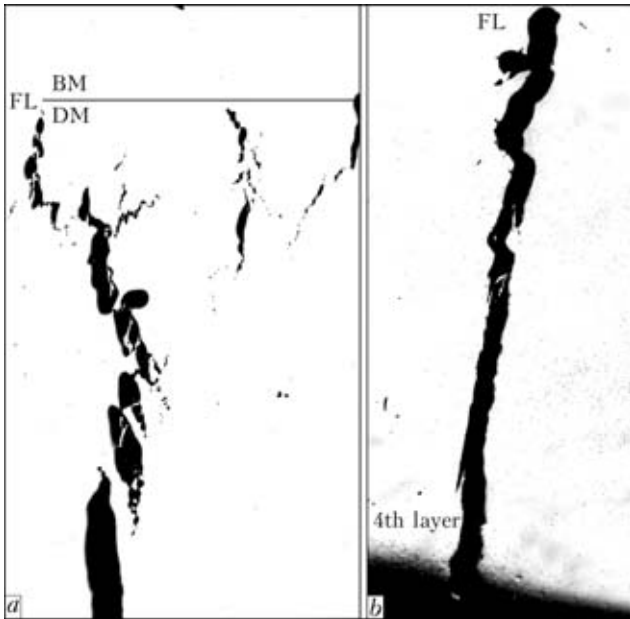


Figure 2. Propagation of zigzag (a) and straight-line (b) cracks in four layers of the deposited metal (x25)

hardening phases, i.e. martensite and eutectic, is proved in Figure 4.

However, the new information was generated. It was found that the ways of propagation of cracks in the deposited metal are not only the hardening phases but also the polygonisation boundaries, which are manifestations of physical microheterogeneity of the deposited metal [2]. Propagation of cracks in a zone of location of martensite and polygonisation boundaries (going along the polygonisation boundary) is shown in Figure 5. To check correctness of this mechanism of initiation and propagation of cracks, small ingots were melted in a copper mould 20 mm in diameter and 50 mm long. This allowed elimination of the probability of the effect of non-metallic inclusions, which is characteristic of the base metal.

No cracks were detected in the deposited metal. The lower part of an ingot consisted of martensite in the austenitic matrix and a developed network of the polygonisation boundaries. Hardness of martensite was HV0.5-5090 MPa, and microhardness of austenite was HV0.5-2710-3030 MPa. Eutectic was located along the polygonisation boundaries (Figure 6). The

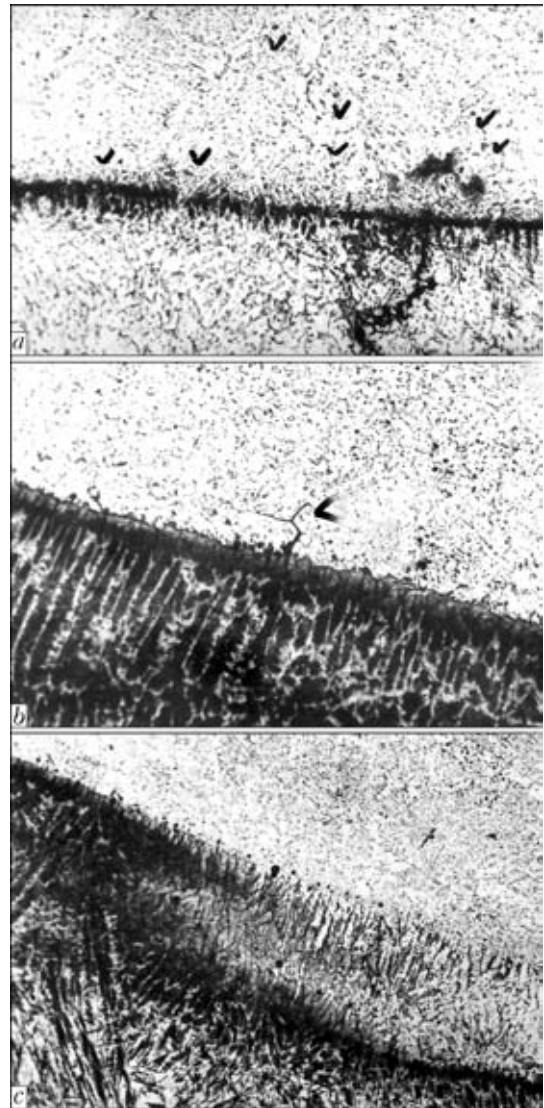


Figure 3. Globular non-metallic inclusions in base and deposited metals (x320): a – globular non-metallic inclusions of the base metal located near the fusion line; b – initiation of cracks near the base metal; c – non-metallic inclusions that transferred («floated») from the 1st deposited layer to the 2nd one

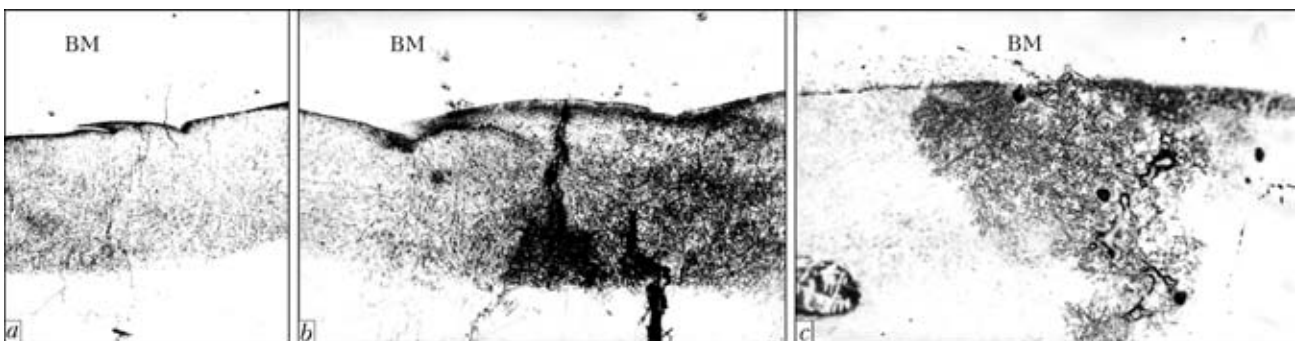


Figure 4. Cracks in base and deposited metals (x50): a – crack propagating from the base metal to martensite component of structure of the deposited metal; b – cracks in martensite component of the 1st and 2nd deposited layers; c – cracks in eutectic component of structure of the 1st and 2nd deposited layers

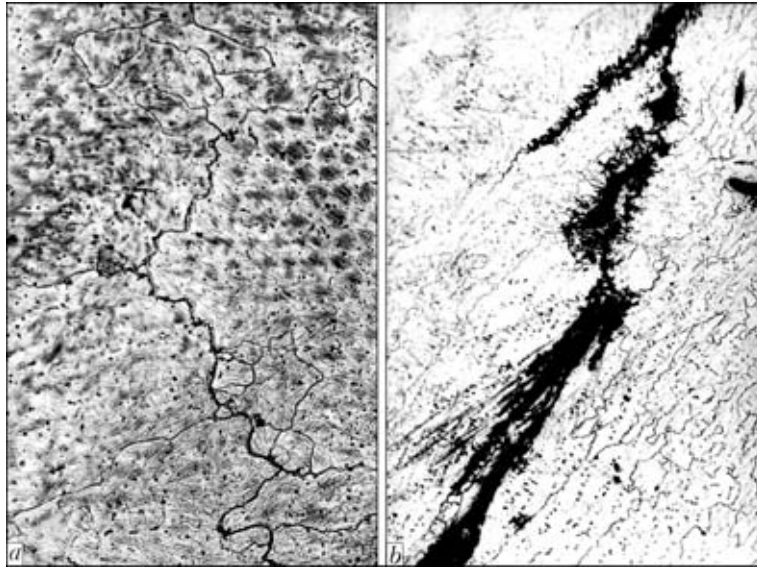


Figure 5. Propagation of crack in martensite component of structure along polygonisation boundaries in the 1st layer of the deposited metal (*a* – $\times 200$; *b* – $\times 400$)

presence of the hardening phases in the form of martensite and eutectic is not a cause of initiation of cracks in the deposited metal.

CONCLUSIONS

1. In cladding of steels, especially those that are susceptible to cracking, special consideration should be given to the quality of the base metal in terms of its purity from non-metallic inclusions.

2. Non-metallic inclusions in the base metal may not only initiate cracks but also affect their further propagation in the deposited metal due to the effect of «floating» from layer to layer of the deposited metal.

3. The cracks initiated in the base metal propagate in the deposited metal not only along the non-metallic inclusions and hardening phases of structure, but also along the polygonisation boundaries.

4. The hardening phases in structure of the deposited metal and polygonisation boundaries are not always the sources of initiation of cracks in it.

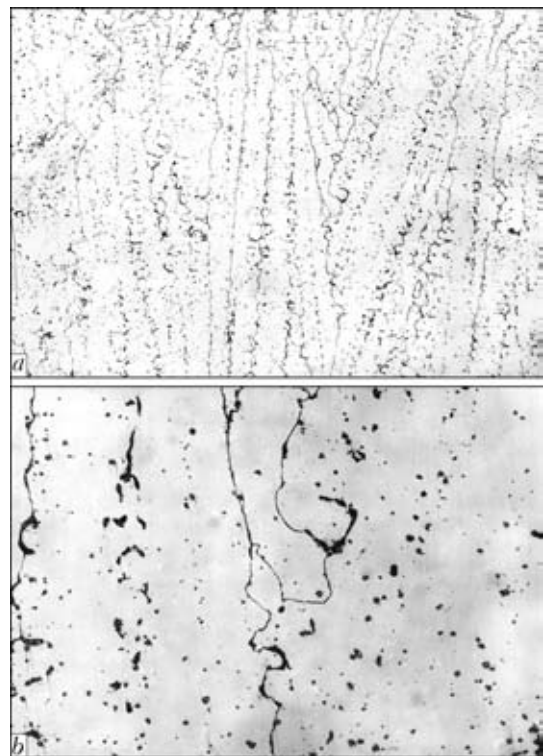


Figure 6. Polygonisation boundaries with eutectic component of structure of the cast metal (*a* – $\times 100$; *b* – $\times 400$)

1. Kuslitsky, A.B. (1976) *Non-metallic inclusions and fatigue of steel*. Kiev: Tekhnika.
2. Movchan, B.A. (1962) *Microscopic heterogeneity in cast alloys*. Kiev: Gostekhizdat UkrSSR.



EFFECT OF DUCTILE SUB-LAYER ON HEAT RESISTANCE OF MULTILAYER DEPOSITED METAL

I.A. RYABTSEV, A.A. BABINETS and I.I. RYABTSEV

E.O. Paton Electric Welding Institute, NASU, Kiev, Ukraine

Effect of deposition of a ductile sub-layer on heat resistance of deposited metal 25Kh5FMS was studied. It was established that deposition of the ductile sub-layer with wire Sv-08A provides an approximately 20 % increase in heat resistance of the 40Kh steel specimens deposited with flux-cored wire PP-Np-25Kh5FMS.

Keywords: arc cladding, deposited metal, multilayer cladding, ductile sub-layer, heat resistance

Thermal fatigue is a characteristic type of damage of the tools used for hot deformation of metals, such as forming rolls, hot shaping dies, hot cutting knives, and many others that are subjected to the effect of thermal cycling [1, 2].

Thermal fatigue cracks initiate on the surfaces of such tools after a certain quantity of thermal cycles. The process of their formation depends on the properties of tool materials and a number of parameters that characterise service conditions. Even before initiation of cracks the material experiences irreversible structural changes, which may affect its mechanical properties, shape and size of parts [3–10]. Normally, the quantity of heating–cooling cycles to formation of the fire crack network serves as a characteristic of resistance of materials to thermal fatigue.

Surface layers of a forming roll (die) heat up in contact with a billet whose temperature amounts to 1200 °C, and dramatically cool down after this contact is terminated. Hence, each heating–cooling cycle will cause a change in volume and stress-strain state of these layers (Figure 1).

Surface layers expand in heating, but colder internal layers prevent it, this causing elastic compression

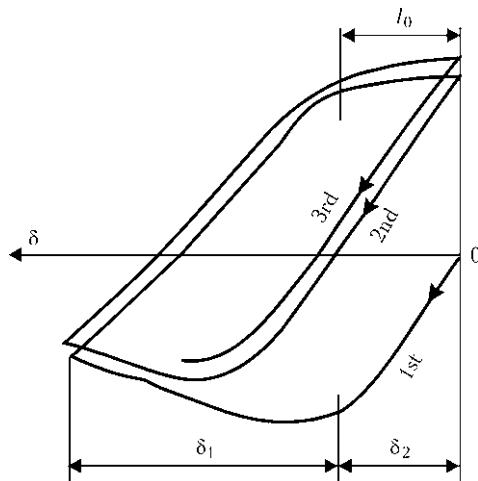


Figure 1. Residual plastic δ_1 and elastic δ_2 strains causing thermal fatigue [8]: 1–3 – heating-cooling cycles; l_0 – elongation

of the external layers. If a temperature gradient from the surface deep into a part is high, the values of compressive stresses may amount to the yield stress value. In rapid cooling the surface layer will gradually compress, but because of resistance of the more heated internal layers this process will be hampered or will not take place at all, and the surface layer will first elastically and then plastically expand. Upon returning to the initial temperature the size of the surface layer will coincide with its initial size. However, the values of residual tensile stresses in it may amount to the yield stress value.

The depth of the plastically deformed layer is determined by heating and cooling conditions, as well as by physical-mechanical properties of material of this layer, such as thermal expansion coefficient, elasticity modulus and thermal conductivity. Structural changes in the material during thermal cycling, and strengthening and weakening in particular, at different stages of cyclic deformation may cause a change in type of the hysteresis loop. If reaching the maximal cycle temperature is followed by holding till the next cooling cycle, this will cause relaxation of thermal stresses and, as a result, change in the hysteresis loop (see Figure 1). All this indicates that there is no such a stress value which can characterise thermal fatigue [4].

Repeated plastic strains, like under conditional cyclic loading, lead to formation of cracks, and simultaneously with their deepening and extension a fire crack network forms on the surface.

The purpose of this study was to investigate the effect of a sub-layer, geometric sizes of the sub-layer and a wear-resistant layer on heat resistance of the clad parts.

Investigations were carried out on steel rolls designed for hot rolling. As mentioned above, thermal fatigue of the tools used for hot deformation of metal is affected by the maximal heating temperature in a zone of contact of a tool with a heated billet, as well as by the distribution of temperature in its surface layers.

The character of distribution of temperature across a roll during rolling was determined by the calculation-experimental method at the first stage of the in-

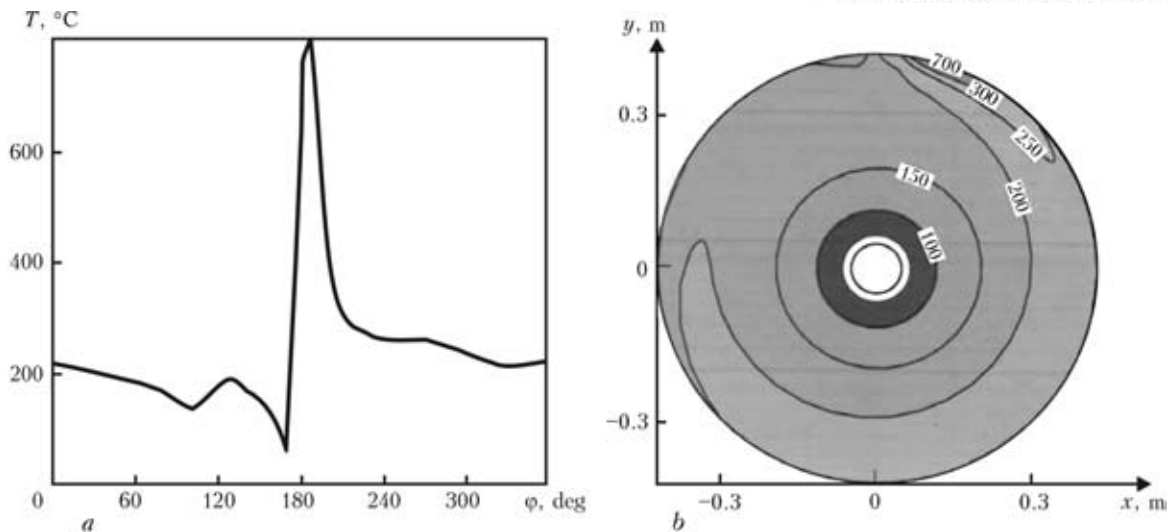


Figure 2. Distribution of temperature on the roll surface (a) and calculated isothermal lines of temperature fields across the roll section (b) during rolling

vestigations [11]. It is reported [1, 2] that in contact with the deformed billet the surface layers of the roll heat up to a maximal temperature of 700–800 °C (Figure 2, a). Then, during rotation of the roll, they intensively cool down, and their temperature dramatically decreases to 200 °C. The temperature at the roll centre is 20 °C (Figure 2, b).

As follows from these data, in operation of a forming roll the thermal cycle is of a serrated character, and holding at the maximal temperature is absent. In this connection, in calculation of the thermal fatigue it is possible to ignore the creep, which substantially decreases resistance to the thermal fatigue [3]. Thickness of the layer heated to 700 °C is 4–6 mm, and temperature of the underlying layers dramatically decreases to 300–400 °C (total thickness of the layers heated above 300 °C is 6–8 mm) and then to 200 °C.

Therefore, thickness of the working layer of the forming roll subjected to cyclic thermal loads will be 6–8 mm. A more important characteristic for materials of the layers heated below 200 °C will be fatigue strength under cyclic service force loading. So, it is a ductile sub-layer that should play an essential role in this case, as fatigue strength of the base metal of the forming roll (as a rule, these are medium- and high-carbon low-alloy steels) is low.

Geometric sizes of the sub-layer and main layer were selected on the basis of the above calculations on specimens for testing of heat resistance of the metal deposited with flux-cored wire PP-Np-25Kh5FMS, which is widely used for cladding of forming rolls, dies and other similar parts.

Cladding by the following methods was performed on billets of steel 40Kh: cladding with flux-cored wire

Table 1. Characteristics of deposited layers on experimental specimens

Specimen No.	Type of alloying of deposited metal	Quantity of deposited layers	Thickness of wear-resistant layer after grinding, mm	Hardness of deposited metal HRC
1.1	25Kh5FMS (without sub-layer)	2	3–4	45–47
1.2		4	7–8	46–47
1.3	Sv-08 + 25Kh5FMS sub-layer	2 + 2	3–4	43–45
1.4		2 + 4	7–8	44–46

Table 2. Results of layer-by-layer chemical analysis and hardness of deposited metal of the 25Kh5FMS type

Layer No.	Content of alloying elements, wt.%						HRC
	C	Si	Mn	Cr	V	Mo	
1	0.22	0.69	0.53	4.5	0.25	0.87	46–48
2	0.24	0.74	0.56	5.4	0.37	0.95	48–50
3	0.26	0.79	0.64	5.5	0.40	1.01	49–51
4	0.26	0.76	0.64	5.4	0.40	0.99	49–51
25Kh5FMS (TUU 05416923.024–97)	0.22–0.33	0.7–1.2	0.4–1.0	4.7–5.9	0.3–0.6	0.9–1.5	45–53



Table 3. Heat resistance of deposited metal specimens

Specimen No.	Quantity of heating-cooling cycles		
	To initiation of first cracks	To propagation of cracks	To formation of crack network
1.1	69	114	175
1.2	66	104	170
1.3	72	123	186
1.4	86	130	200

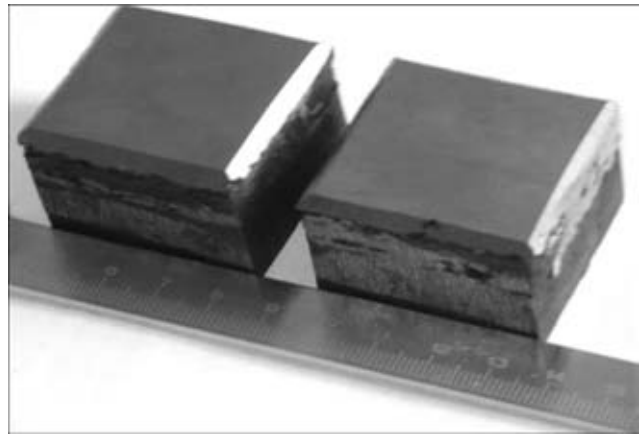


Figure 3. Appearances of clad specimens

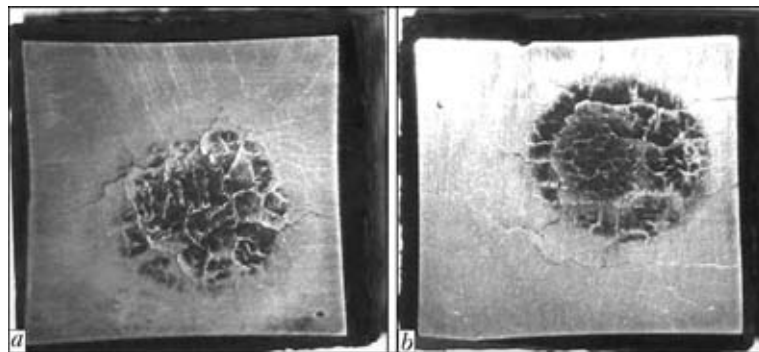


Figure 4. Appearances of the specimens clad with flux-cored wire PP-Np-25Kh5FMS without (a) and with sub-layer Sv-08 (b) after heat resistance tests

PP-Np-25Kh5FMS without a sub-layer (in two and four layers, total thickness of the deposited metal after grinding was 4 and 8 mm, respectively); deposition of the ductile sub-layer with wire Sv-08 (in two layers) and wear-resistant layers with flux-cored wire PP-Np-25Kh5FMS (in two and four layers, total thickness of the wear-resistant deposited metal after grinding being 4 and 8 mm, respectively) (Table 1).

Cladding was performed with overlapping of beads approximately to 50 % by using 2.8 mm diameter wire under the following conditions: cladding current $I_c = 350-400$ A, arc voltage $U_a = 28-30$ V, and cladding speed $v_c = 16$ m/h. After cladding the specimens were slowly cooled under a flux layer.

Layer-by-layer chemical analysis of the deposited metal, as well as standard composition of the metal deposited by using flux-cored wire PP-Np-25Kh5FMS are given in Table 2. As seen from the Table, the deposited metal corresponding in chemical composition to specification TUU 05416923.024-97 is provided already in the second layer.

Then specimens measuring $40 \times 40 \times 30$ mm for heat resistance tests were cut out from the clad billets. The clad surface of the specimens with plane sizes of 40×40 mm was subjected to grinding prior to the tests (Figure 3). Three-four specimens of each cladding variant were made and tested.

Heat resistance was studied by using a modular machine developed by the E.O. Paton Electric Welding Institute for testing different properties of the deposited metal [12].

Testing conditions were as follows: heating of the ground deposited surface of a specimen to 800°C was provided by using a gas cutter (heating spot of 15 mm, plane size of the heated surface of a specimen of 40×40 mm), and cooling of the heated surface with a water jet to 60°C . The heating-cooling cycles were repeated to formation of a fire crack network, which can be seen with the unaided eye. Heat resistance was evaluated on the basis of a number of the heating-cooling cycles to initiation of the first cracks and reaching of a certain degree of cracking, i.e. formation of the fire crack network.

The test results (average over 3-4 specimens of each type) are given in Table 3, and appearances of the specimens after the tests are shown in Figure 4.

As proved by the results obtained, deposition of the sub-layer provides heat resistance of the deposited metal of the 25Kh5FMS type, especially at a stage of formation of the fire crack network.

CONCLUSIONS

1. It was established by the calculation-experimental method that thickness of the working layer of a roughing stand forming roll, which is heated to $200-700^\circ\text{C}$ in the zone of contact with a billet formed, is 6-8 mm. For materials of the layers heated below 200°C an important characteristic is fatigue strength under cyclic service force loading. On this basis, it is recommended to use low-carbon low-alloy steels characterised by high ductility and fatigue strength for cladding of a sub-layer on the hot forming rolls.



2. It was experimentally found that deposition of a ductile sub-layer with wire Sv-08A provides an approximately 20 % increase in heat resistance of the 40Kh steel specimens clad with flux-cored wire PP-Np-25Kh5FMS.

1. Frumin, I.I. (1961) *Automatic electric arc surfacing*. Kharkov: Metallurgizdat.
2. Tylkin, M.A. (1971) *Increase in service life of metallurgical equipment parts*. Moscow: Metallurgiya.
3. Dulnev, R.A., Kotov, P.I. (1980) *Thermal fatigue of metals*. Moscow: Mashinostroenie.
4. Balandin, Yu.F. (1967) *Thermal fatigue of metals in ship and power machine building*. Leningrad: Sudostroenie.
5. Davidenkov, N.N., Likhachev, V.A. (1962) *Irreversible forming of metal in cyclic heat action*. Moscow: Mashgiz.
6. Tylkin, M.A., Yalovoj, N.I., Polukhin, P.T. (1970) *Temperature and stresses in parts of metallurgical equipment*. Moscow: Vysshaya Shkola.
7. Birger, I.A., Shorr, B.F., Demianushko, I.V. et al. (1975) *Thermal strength of machine parts*. Moscow: Mashinostroenie.
8. Artinger, I. (1982) *Tool steels and their heat treatment*. Moscow: Metallurgiya.
9. Dovnar, S.A. (1975) *Thermomechanics of strengthening and fracture of forging dies*. Moscow: Mashinostroenie.
10. Troshchenko, V.T., Shemegan, Yu.M., Sinyavsky, L.P. (1974) Study of fracture mechanisms of alloys in thermal fatigue and in combined effect by cyclic mechanical and thermal stresses. In: *Proc. of All-Union Symp. on Low-Cycle Fatigue at Higher Temperatures* (Chelyabinsk), Issue 2, 137–156.
11. Ryabtsev, I.A. (2010) *Reconditioning and strengthening of parts used under wear conditions and different types of cyclic loading by the cladding methods*: Syn. of Thesis for Dr. of Techn. Sci. Degree. Kiev.
12. Ryabtsev, I.I., Chernyak, Ya.P., Osin, V.V. (2004) Modular machine for testing of deposited metal. *Svarshchik*, 1, 18–20.

PECULIARITIES OF THERMAL SPRAYING OF COATINGS USING FLUX-CORED WIRE (Review)

B. WIELAGE, C. RUPPRECHT and H. POKHMURSKA

Institute of Materials Science, Chemnitz University of Technology, Germany

Methods for production and application of flux-cored electrode wires for flame and electric arc spraying of various-purpose coatings are considered. Possibilities of applying advanced 2.0 and 2.8 mm diameter flux-cored wires for electric arc deposition of coatings are noted. It is shown that high-speed filming can provide important information on the nature of running of the spraying process which determines the coating quality.

Keywords: *thermal spraying, coatings, flux-cored wires, designs of wires, coating methods*

The technology of thermal spraying has found wide commercial application, in particular, for deposition of wear- and corrosion-resistant coatings. As reported by Linde AG [1], flux-cored wire is one of the most widespread consumables for thermal spraying, its annual utilisation amounting to over 50,000 t. The use of such wires allowed not only the range of their application to be widened to electric arc, plasma and flame spraying, in contrast to solid wires, but also the properties of the resulting coatings to be changed as needed, this explaining the year to year increase in their production volume and choice.

Designs and materials of flux-cored wires. Flux-cored wire consists of a sheath made from metal strip (steel, nickel, cobalt etc.) and a core, which is a powder of one component or a mixture of powders of alloying components and hardening particles (ferroalloys, pure metals, carbides, borides etc.). The flux-cored wires come in several designs. In practice, the most common designs of the flux-cored wires are overlap butt, tight butt and tubular.

The main groups of flux-cored wires used for spraying of repair, corrosion- and wear-resistant coatings are given in the Table. The iron-, nickel-, cobalt- and

aluminium-base flux-cored wires are now available in the market. The main application field of the coatings deposited by flux-cored wire spraying is protection from different kinds of wear, the most-used coatings being coatings of high alloys or coatings containing hard particles, as well as pseudo-alloys.

Another important application field of the coatings deposited by using flux-cored wires is protection from corrosion, including from gas corrosion at increased temperatures, for which the use is mainly made of nickel-base alloys.

Functional coatings, e.g. for improvement of anti-friction properties of friction surfaces, are produced by spraying of flux-cored wires with solid lubricants, e.g. boron nitride, contained in their charge. Alumoceramic coatings sprayed by using tubular flux-cored wires, the charge of which consists of hard ceramic particles, have been developed lately for wear and corrosion protection of surfaces of the parts made from magnesium alloys. These coatings can also be used as anti-sliding ones.

Chemical and phase compositions of the flux-cored wire charge may vary within wide ranges, this opening up considerable opportunities for development of new systems of the coatings and, hence, for further expansion of their practical application fields [2].

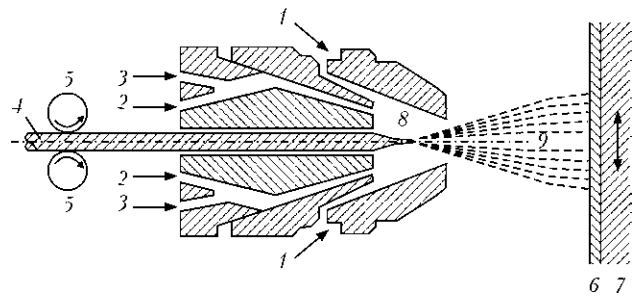


Examples of application of flux-cored wires for thermal spraying of coatings

Base	Type of alloying	Properties of coatings and application examples
Iron	FeCrNiMoSiC	Austenitic alloys for wear and corrosion protection
	FeCrAlSi	Protection from gas corrosion at increased temperatures, good machinability by cutting
	Fe + WSC / WC	Protection from abrasive wear
Nickel	NiCr NiAl	Utilisation as a sub-layer to ensure adhesion to base metal
	NiCrB NiCrBSi	Low friction coefficient. Wear protection under thermal loading, hydro- and gas-abrasive protection, chemical stability
	Ni + WSC / WC	Increased wear resistance
Cobalt	CoCrWFeCSiMn	Protection from abrasive wear, boundary friction, cavitation and corrosion
	CoCrMoFeNiSiMnC	Coatings with increased wear, heat and corrosion resistance
Other	Al + Al ₂ O ₃	Anti-sliding coatings
	Cu + BN	Coatings with dry lubrication effect

Methods for deposition of coatings using flux-cored wires. Flame spraying. Coatings of flux-cored

wires are deposited by using torches designed for solid wire spraying (Figure 1).



The process of melting of the flux-cored wires differs to some extent from that of the solid wires. With decrease in thickness of the flux-cored wire sheath, as well as with decrease in density of the wire filling, the sharpened shape of the melted wire tip changes into a shorter, rounded or truncated one (Figure 2, a, d).

Figure 1. Schematic of the flame spraying torch according to DIN EN 657 [3]: 1 – compressed air; 2 – fuel gas; 3 – oxygen; 4 – wire or rod; 5 – feeding mechanism; 6 – spray coating; 7 – substrate; 8 – melted wire tip; 9 – jet of molten particles

The compressing gas flow forming in the melting zone is characterised by turbulence, in contrast to the flow forming in melting of the solid wires (Figure 2, b, e). This leads to expansion of the jet of molten particles and, as a result, to increased heterogeneity of microstructure of the sprayed coating (Figure 2, c, f). Inclusions of coarse particles of the sheath material

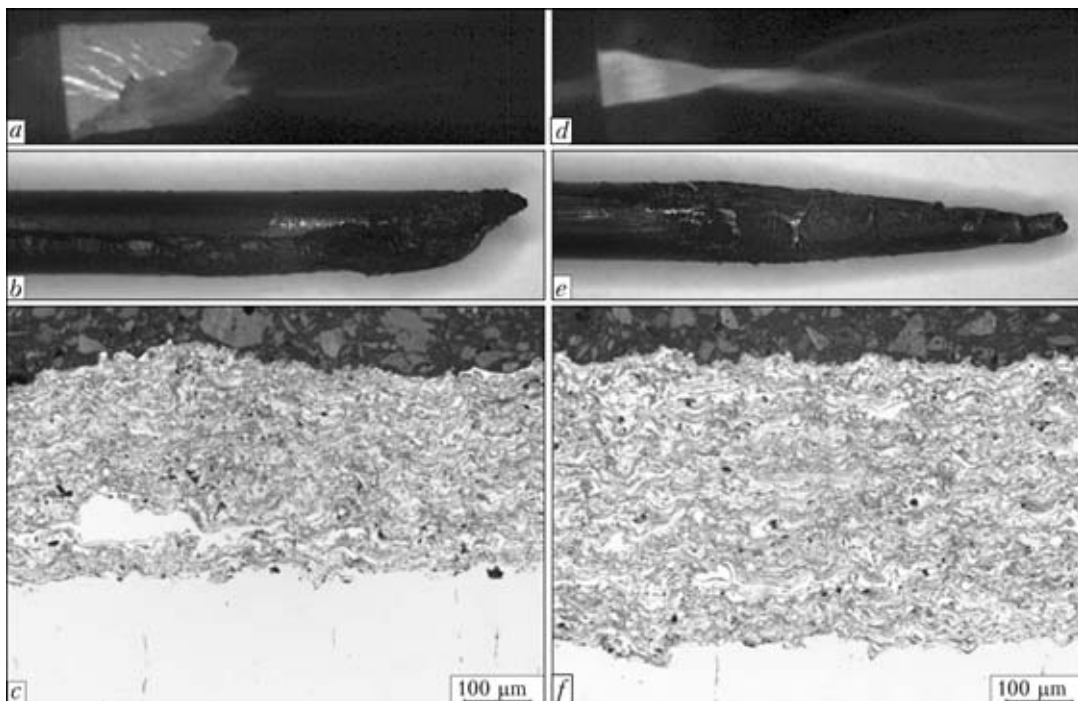


Figure 2. Fragments of high-speed filming of the HVOF spraying process with flux-cored wire AISI 316L (a) and solid wire (d), appearances of the melted wire tips (b, e) and microstructures of coatings (c, f)



(light regions in the coating), which had no time to fully fuse with the charge material in the arc during spraying, can be seen in microstructure of the HVOF coating deposited by using the flux-cored wire with a chemical composition matching that of austenitic stainless steel AISI 316L (Figure 2, c). This increase in structural heterogeneity of the coatings may have a negative effect on their service characteristics [4].

Analysis of peculiarities of the spraying process and corresponding microstructures of the coatings deposited by HVOF spraying using different designs (overlap butt, tight butt and seamless tubular) of flux-cored wires of the AISI 316L composition, as well as solid wires, is presented in study [4].

Electric arc spraying. Deposition of coatings by the electric arc flux-cored wire spraying method (electric arc metallising) is performed with the guns used for solid wire spraying. Figure 3 shows flow diagram of the electric arc spraying process.

Electric arc spraying is applicable for spraying of conducting materials. So, it can be applied for spraying of coatings using flux-cored wires with a metal sheath. An important advantage of flux-cored wire spraying, compared to solid wire spraying, is the possibility of adding arc stabilising components to a composition of the powder mixture.

Spraying of metal of the type of austenitic stainless steel AISI 316L in the form of both solid and flux-cored wires with the appropriate optimisation of parameters of the electric arc spraying process can provide coatings of a good quality with very low porosity (Figure 4).

Optimisation of electric arc spraying using large-diameter flux-cored wires. The option of flux-cored wires available now in the market for spraying of different-application coatings is very wide. Almost all

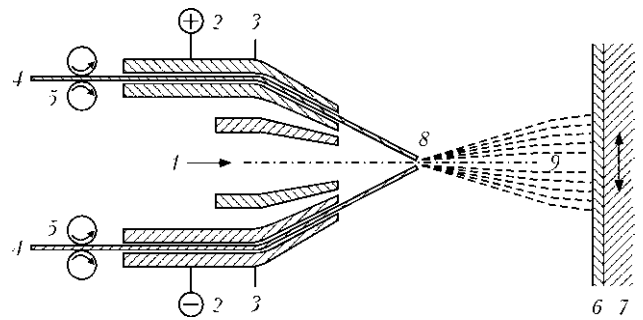


Figure 3. Flow diagram of electric arc flux-cored wire spraying using the gun according to DIN EN 657 [3]: 1 – compressed air; 2 – power supply; 3 – contact tubes; 4 – wires; 5 – feeding mechanism; 6 – spray coating; 7 – substrate; 8 – melted wire tips; 9 – jet of molten particles

wires for thermal spraying of wear-resistant coatings come in diameter of 1.6 mm (e.g. products of TAFSA, Castolin, Praxair, Sultze Metco, etc.). A comparatively low factor of filling of this diameter wires with a charge limits the possibilities of adding a higher concentration of alloying elements and hardening particles to a coating. Therefore, in terms of widening the opportunities for development of new compositions of flux-cored wires and raising the productivity of the electric arc spraying process it is of interest to investigate peculiarities of spraying of large-diameter flux-cored wires.

The effect of the operating current, spraying distance and other parameters on the process of formation of structure of a coating and oxidation of molten particles during spraying was investigated. The use was made of the iron-base 2.0 and 2.8 mm diameter flux-cored wires designed for electric arc spraying, providing the following chemical composition, wt.%: 6–7 Cr; <1 Mo; <1 V; 1 Al for the 2.0 mm diameter wire and 1–2 Al for the 2.8 mm diameter wire; <1 (1–2) Si; 1 (1–2) Mn. The 2.0 and 2.8 mm diameter

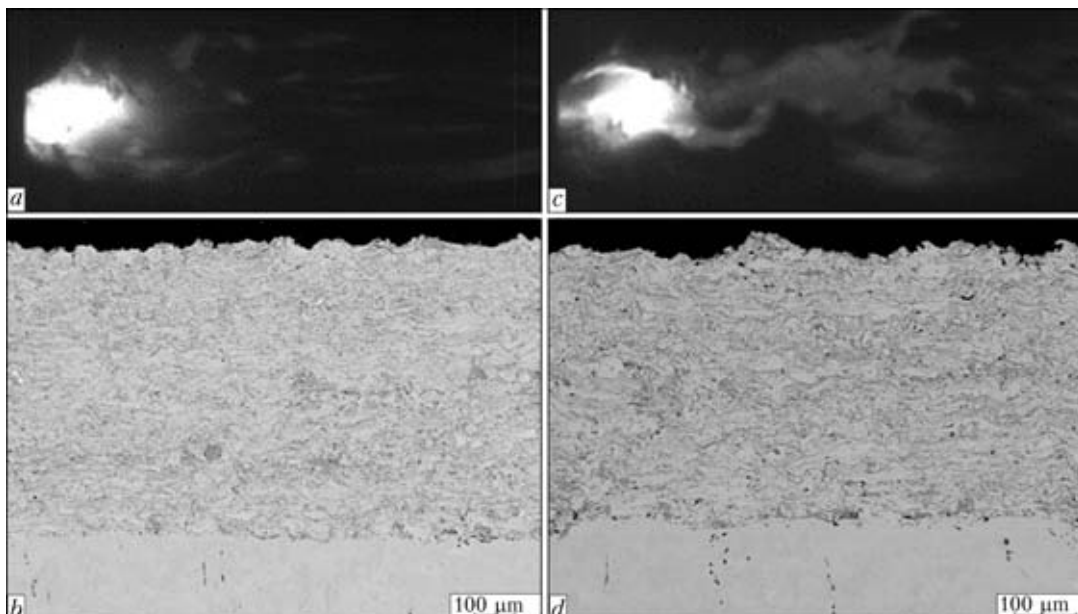


Figure 4. Fragment of high-speed filming of electric arc spraying using flux-cored wire AISI 316L (a) and solid wire (c), and microstructures of coatings (b, d)

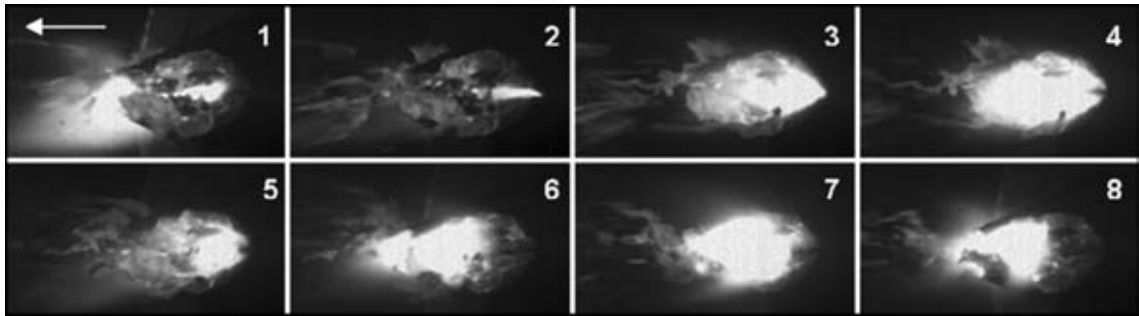


Figure 5. Sequence of frames of high-speed digital filming of the electric arc spraying process using 2.8 mm diameter flux-cored wire (arrow – spraying direction)

flux-cored wires had close chemical composition. However, the larger-diameter wire contained a small addition of flux.

The OSU gun with spraying head LD/U2 was employed for electric arc spraying. The values of the electric current and spraying distance were varied during spraying, the rest of the parameters being kept constant. Parameters of electric arc spraying of coatings using the 2.0 and 2.8 mm diameter flux-cored wires were as follows: current 100–150 A, voltage 25 V, spraying gas pressure 35 MPa, and spraying distance 80, 100 and 120 mm. The surface of the steel substrate was subjected to shot blasting prior to spraying [5]. Spraying of both types of the wires provided dense coatings with good adhesion to the substrate.

Detailed analysis of melting of the wires in the electric arc during spraying was carried out by using a high-speed digital camera. It was shown that the process of spraying of the larger-diameter flux-cored wires was of a stable character. Uniform convective stirring of the molten material with insignificant fluctua-

tions in a flow of particles was observed at the wire tips. As found owing to a high resolution of filming (10,000 frame/s), in spraying of the thick flux-cored wire the spot of the arc root was characterised by a considerable variable displacement, thus providing a uniform heating of the wire (Figure 5).

When spraying the smaller-diameter wire, the trend was to a substantial variation in the arc length, especially after detachment of coarse metal particles, which added to instability of the spraying process.

In spraying of the smaller-diameter wires a change in distance between their tips was more pronounced than in spraying of the larger-diameter wires. The smaller-diameter wires induced lesser disturbance in the spraying particle flow, which had a positive effect on divergence of the flow.

As established as a result of the investigations, the use of the larger-diameter flux-cored wires in electric arc spraying does not necessarily cause deterioration of the coating quality. Moreover, spraying of the larger-diameter flux-cored wires results in a more ho-

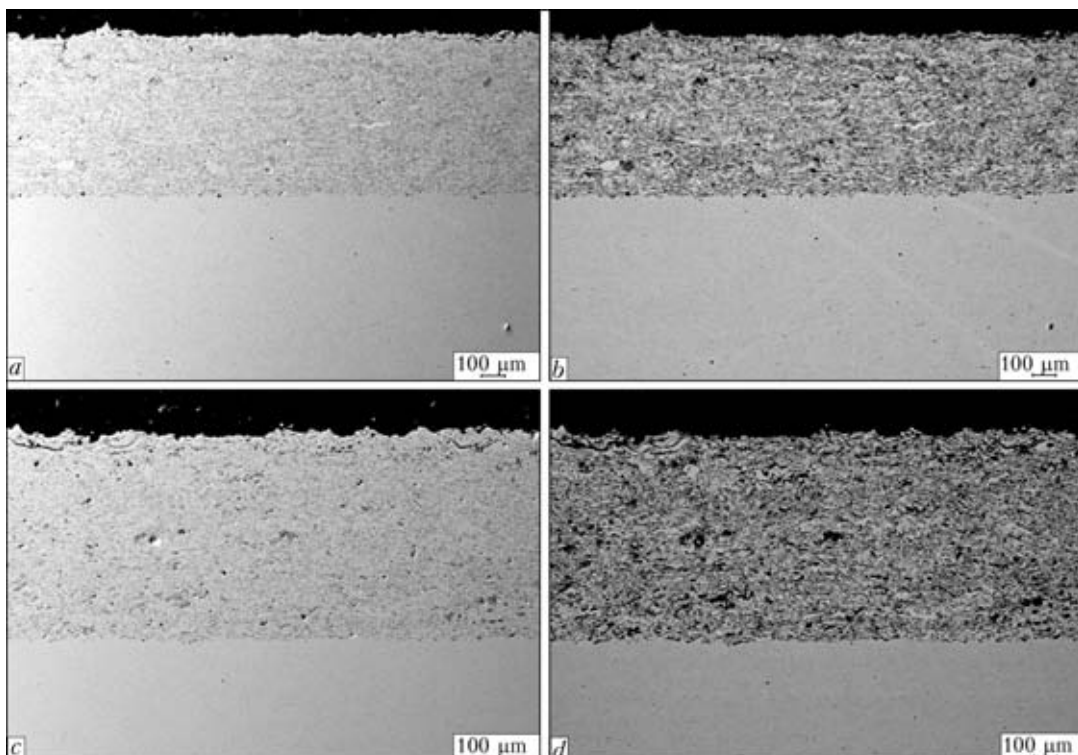


Figure 6. Microstructure of coatings deposited by electric arc spraying of the 2.0 (a, b) and 2.8 (c, d) mm diameter flux-cored wires at current of 150 A and spraying distance of 120 mm revealed by secondary (a, c) and back-scattered electron (b, d) microscopy

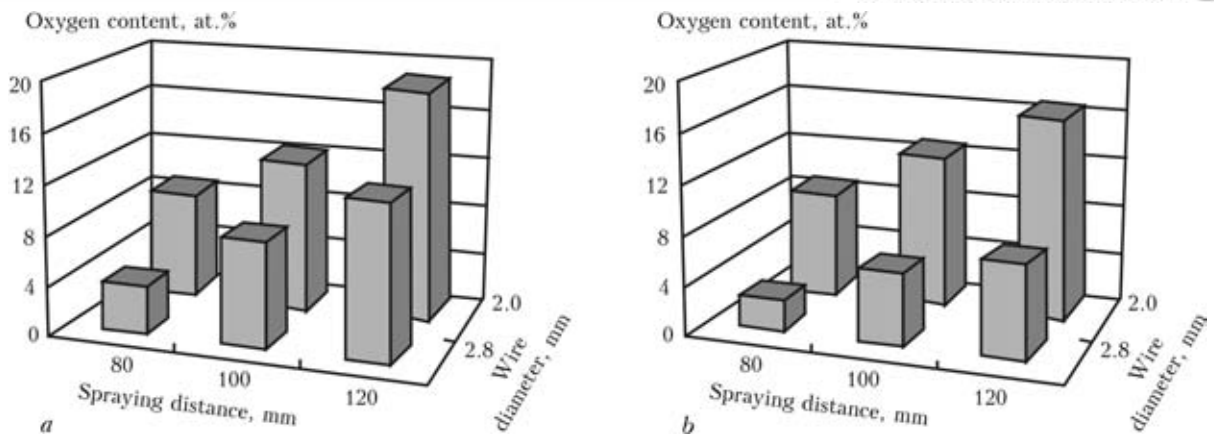


Figure 7. Effect of current (*a* – 100, *b* – 150 A) and spraying distance on oxygen content of the coatings produced by electric arc spraying using flux-cored wires of different diameters

homogeneous microstructure of the coating. Characteristic feature of spraying of the larger-diameter flux-cored wires is that the melt of the charge and sheath stays for quite a long time in a volume confined by the external ends of a wire, this providing a more complete melting of the material, homogenisation of the melt and, hence, decrease in porosity of the coatings (Figure 6).

Analysis of chemical composition of the sprayed coatings conducted by the energy-dispersive X-ray spectroscopy method reveals a clear dependence of susceptibility of the coatings produced by spraying of the flux-cored wires of both diameters to oxidation, which shows up in the oxygen content of the coatings, on the spraying parameters (Figure 7).

Increase in the spraying distance leads to a more intensive oxidation of the coatings because of increase in the time of dwelling of molten particles in the spraying flow. At the same time, the effect of increase in the current on the oxidation process was noted only

for the larger-diameter wire containing a flux addition.

It can be noted in conclusion that electric arc spraying using the larger-diameter iron-base flux-cored wires can provide the high-quality defect-free coatings with a homogeneous structure and low porosity. Peculiarities of formation of the melt during spraying were investigated, and regularities in formation of structure of the coatings were established by using high-speed digital filming.

1. Wielage, B., Bobzin, K., Rupprecht, C. et al. (2008) Thermisches Spritzen – Potenziale, Entwicklungen, Märkte. In: *Thermal Spray Bull. 1*. Duesseldorf: DVS, 30–36.
2. Lugscheider, F.-W. (2002) Handbuch der thermischen Spritztechnik, Technologien–Werkstoffe–Fertigung, Fachbuchreihe Schweißtechnik. *Ibid.*, Band 139.
3. *DIN EN 657*: Thermisches Spritzen – Begriffe, Einteilung.
4. Wielage, B., Landes, K., Rupprecht, C. et al. (2006) Einsatzmöglichkeiten des HVOF-Drahtspritzens, Tagungsband 7. In: *Proc. of HVOF Kolloq.*, 81–88.
5. *DIN EN 13507*: Thermisches Spritzen – Vorbehandlung von Oberflächen metallischer Werkstücke und Bauteile fuer das thermische Spritzen.

CURRENT CONSUMABLES AND METHODS OF FUSION ARC WELDING (Review)*

V.N. SHLEPAKOV

E.O. Paton Electric Welding Institute, NASU, Kiev, Ukraine

State-of-the-art and existing problems in the field of development of materials for welding carbon and low-alloy steels are analyzed, namely, coated electrodes, solid and flux-cored wires. Challenging technologies of their application, and also organizing and aspects of production and application of consumables are considered.

Keywords: arc welding, carbon and low-alloy steels, coated electrodes, solid wires, flux-cored wires

As a part of world economy, welding production related with manufacture of metal structures experiences significant influence of the declines and rises of financial and business activity in the recent years. The enterprises and organizations, scope of activity of which lies in manufacture and application of the electrode materials for fusion arc welding, tend to adjust to dynamically changing market requirements.

Manufacturers of welding consumables have to base on the statistical data and predictions concerning tendencies of change of the market requirements as a whole as well as regarding specifically manufactured materials with evaluation of competitiveness in each area of their application for planning and providing of stable operation of the enterprise.

Manual coated electrodes, solid and flux-cored wires make the main group of electrode materials of mass and special designation for welding and surfacing. Mechanized and automatic welding processes provide for application of additional filler and shielding materials (flux, gas), with exception of welding with flux-cored wires. Stable rise of application of the materials for mechanized and automatic (including robotic) welding is a general tendency for a change in structure of manufacture and application of the electrode materials, especially in economically developed countries of South-East Asia (Japan, South Korea, PRC), America (USA, Canada, Brazil) and Europe (Great Britain, Germany, France, Italy, Holland etc.). Such technological processes as laser welding and series of hybrid and combined processes were among developing competitive methods of fusion welding. This was possible due to rapid development of microelectronics as well as application of modern systems of automatic control.

Coated electrodes. Manual coated electrodes are the most widely used consumables being multi-purpose from point of view of welding process organizing under plant and site conditions. Arrangement of a welding station does not require large investments in equipment and expenses on electrodes relatively small.

Small melting efficiency, caused by low current density, loss of material for the stubs as well as dependence of welding quality on qualification of a welder refer to disadvantages character for process of manual electrode welding. At the same time, the possibilities of control of the welding properties through change of composition of a coating are significant that allows preserving high competitiveness of this material for mechanized processes of welding.

Leading enterprises from CIS countries made a significantly increase in a level of electrode manufacturing technologies and delivery to customers. It was advanced to global on the main indices. The issues of quality of coating deposition, starting area, marking, pre-packing and packing were solved. A range of electrodes remains relatively narrow. This is partially related to the objective reasons of behavior of consuming market. However, insufficient release of the electrodes for welding of high-strength, stainless and heat-resistant steel, nickel, aluminum and copper alloys, cast iron and for surfacing leave a part of potential market free for import purchasing.

Modern methods of analysis and investigations, in particular, computer modelling using material data base, study of sensor-based devices for welding process using statistical data processing, achievements in area of materials science, for example, experience of series of foreign companies in application of the indicator marks on coating, showing the level of humidity or temperature of baking that is important for basic coated electrodes, are not sufficiently used in electrode development.

Classification of coated electrodes approaches to international standards (ISO 2560A, EN 757, EN 1600 etc.) on main requirements and characteristics making selection of necessary type and grade of the electrodes easier for consumers. Tendencies of world market in-

* On materials of presentation made in the IV International Conference on Welding Consumables of CIS Countries «Welding Consumables. Development. Technology. Production. Quality. Competitiveness» (Krasnodar, 2011), p.193-199.



dicating the necessity of increasing of scope of information support.

Data on X-ray density, cracking resistance, base metal penetration, spattering, separability of slag, characteristics of welding fume etc. are to be presented in addition to mechanical properties indices, chemical composition, hydrogen content and data on parameters of modes for welding in different positions. Detailed information in the advertisement materials and accompanying documents raises confidence of the consumers and reduce possibility of the claims connected with lack of information.

Forms of organization of economic ties with consumers play a part in stable production of coated electrodes as well as other consumables. It is relevant to stimulate the consumers to use modern power sources with a feedback allowing a welder to perform remote adjusting of welding parameters from an electrode holder.

Solid wires. Solid wires for arc welding make more than a half of all production of welding materials in leading economically developed countries. Areas of application on a type of shielding of melting zone are divided into shielded gas welding and submerged arc welding, on level of automation they are mechanized (semi-automatic), automatic and robotic. The wires are mainly used for welding of carbon, low-alloyed and stainless steels as well as aluminum and titanium alloys dividing on classes of metal to be welded. Regulation of indices based on composition of wire as well as shielding material (monogases or mixtures, agglomerated or fused fluxes) is possible for achievement of the required service properties.

Current density in welding with solid wires is significantly higher of that with manual electrodes that allows regulating melting characteristics in a wide range, realizing synergetic and combined controllable processes in welding of different metals and objects of application. In particular, control of transfer of electrode metal in a weld can provide stable characteristics during short-circuit metal transfer, non-short-circuit drop, axial and pulse spray metal transfer or modular-regulated one on surface tension of metal drop.

Modern systems of semi-conductor and inverter type power sources with programmable characteristics of the electric parameters connected by direct and reverse adaptive control with mechanism of wire feeding in the melting zone were developed based on application of the current physical and mathematical models as well as computer modelling of process of arc fusion welding. This allows providing secure performance of a welding algorithm as well as significantly reducing energy consumption and eliminating influence of a human factor. Efficient and programmable heat input in the metal allowed achieving increase of property values of the welded joints.

Group of international standards on wires, shielding gas, flux and their combinations (EN 440, EN 439,

EN 760, EN 12072 etc.) presents a classification of solid welding wires. In this case the basic property indices correspond to ISO methodology (minimum value of yield strength and specified temperature of testing with guaranteed value of impact toughness).

There is a difference in level and range of wires, gases and fluxes with series of national standards that can result in difficulties, in particular, during product supply for export.

Only advance enterprises fulfill the requirements of the international standards as for forms of winding and packaging (requirements of European standard EN 759).

Great attention is paid to wire condition as delivered (allowances, accuracy of manufacture, winding, state and quality of surface) in the recent years. There are novel solutions for providing quality of coppered or noncopper-coated wires allowing improving indices of application in mechanized and automatic welding as well as significantly reducing gross emissions of welding fume.

Flux-cored wires. Application of the flux-cored wires requires in most cases the same equipment as for the solid wires. In the first case, however, some advantages in technological effectiveness, efficiency and metallurgical adjustment for welding of wide range of steels are present.

Flux-cored metal wire (weight fraction of non-metallic materials not more than 4 %) was for the first time implemented in the Great Britain Standard in 1974. Flux-cored welding wires are classified by European (EN 758, EN 12073) and ISO standards (ISO 17632, ISO 18276, ISO 17633) enforced in 2004–2005. There are separate national standards being adjusted to innovations, therefore, the flux-cored metal wires are often classified using standards for solid wire.

Countries of South-East Asia (Japan, South Korea, PRC) where production of flux-cored wires exceeds manufacture of manual electrodes and comes by volume to solid wires remain the leaders in production and application of the flux-cored wires in the recent years. Usage of the flux-cored wires in USA, France, Great Britain and Germany became equal with scopes of manual arc welding by coated electrodes due to development of own productions as well as admission of manufacturers from South-East Asia (Japan, South Korea) on their markets.

CIS countries significantly fall behind in this area that has promoted coming of products of Japanese, South-Korean and series of European manufacturers in this part of the market. Unfortunately, the same situation is observed in area of purchasing of equipment for mechanized and automatic welding.

Wires for gas shielded welding (rutile, basic and metal flux-cored wires) make the main portion in a structure of application of the flux-cored wires. Self-shielding wires make a separate group, allowing performance of welding process without additional gas



or flux shield. Therefore, they are the most applicable for welding-erection works.

Temporary decrease caused by the objective reasons (large diameter, excessive fume emission and insufficient level of property indices) was registered after rapid growth of consumption of the flux-cored wires (especially gas-shielded ones) in 1970–1980s. Use of flux-cored wires rises again in 2000 due to significant increase of production quality, property parameters and applicability for welding of different grade steels in the branches of industry and construction.

Concerning the flux-cored wire for submerged-arc welding, area of their application is limited by high-strength steel welding where they compete with the solid wires.

Most types of flux-cored wire provide the better technological properties (shape of the weld and joint penetration) in comparison with the solid wires.

Gas-arc welding (welding of butt joints with forced weld formation) should be outlined among the erection methods of automatic welding using flux-cored wire. It excels the competitive methods in efficiency and quality.

Flux-cored wires are divided into rolled (manufactured by means of formation of cold-rolled strip of specified size in a round profile filled by flux mixture at intermediate stage of formation) and so-called seamless obtained by filling of long-length tubular billet with agglomerated flux on special vibration tables.

Filling of tubular strip billet directly before welding of longitudinal seam carried out by laser or high-frequency currents was mastered in the recent years. Further process of manufacture includes an additional formation by rolling and drawing on a scheme similar to that used in manufacture of the solid wire with application of the intermediate anneals. Such a technology allows achieving low content of hydrogen in the wire and surfacing any types of coatings.

Realization of this technology requires significant investments in the equipment and maintenance costs. In this connection price of the product increases twice at an average in comparison with the rolled wire.

Current flux-cored wires are supplied in a ready-for-use form (on EN 759 standard) and suitable for welding using commercial equipment.

Perspective technologies for consumables application. Synergetic systems as ones among intensively developing new welding technologies have relation to all electrode materials. Such systems can solve the tasks including monitoring, sensory control, modeling and programming of the electric processes, which determine the character of arcing and transfer of electrode metal, that allows optimization of the process based on welding-processing characteristics, effective use of energy and increase of quality of the welded joints.

Improvement of service characteristics, significant reduction of influence of welder's skill, decrease of

spattering and level of emission of welding fume take place for the manual electrodes. Mechanized and automatic processes of welding by solid and flux-cored wires have wider possibilities due to simultaneous control of wire feed and electric parameters of the arc. Possibility of combining of melting characteristics and metal transfer arises at double and multiarc processes that allows regulating speed of welding and achieve better properties of a welded joint through combination of wires. Such processes are realized in automatic and robotic welding.

Combination of processes of laser welding and gas shielded flux-cored or solid wire welding is a direction being the most effectively developing among the hybrid processes. Joining of high values of penetrating capability of the laser beam and efficiency of melting of the filler material in a one weld pool allows designing shape and size of a weld which are most suitable for the welded joint. At that, high ionizing power of laser plasma increases arc discharge stability for melting of electrode wire.

Efficiency and adjustability of such a method exceed that of well-known narrow-gap welding. Increased requirements to accuracy of a joint assembly and significant costs on equipment can be referred to its disadvantages. Gas shielded tandem welding (two wires in one pool) in which mutual magnetic effect of arcs was electrically unbound due to application of two synchronized pulse power sources was successfully realized. Current miniature electromechanical drives allow making equipment for erection welding significantly lightweight and even installing wire feeder in a welding torch that is completely acceptable in using of small diameter wires.

Organizational and economic aspects of manufacture of the consumables. Manufacture of electrode materials consists of series of technological processes including (in less detail) raw preparation, manufacture of billet of product or component of billet, manufacture of marketable products, its processing and packaging, accompanied by procedures of initial (inspection), i.e. technological, and final (closing) control being part of a system of quality control.

Number of enterprises from CIS countries includes the operations which are not peculiar to basic technology of manufacture of marketable products in a structure of industrial processes. Chopping and milling of components, glass melting from a lump, treatment and initial drawing of wire from a roll, longitudinal division of strip rolls on bands etc. are referred to them, thus, transferring responsibility for risk of loss, costs of occupational safety and environment on main production.

Modern productions in developed countries work using specialization approach applying electrode, raw and auxiliary materials prepared by manufacturer requirements as well as utilities obtained based on schedule and long-term contracts with suppliers. The sup-

pliers readily sign such contracts directly or through branch enterprises (if raw finishing to required condition is necessary) according to world practice. International practice denied an opinion that the costs can be reduced during in situ processing.

Development of economic relations is effective using a futures-based designing with strict following of world market tendencies. Evolution and improvement of control for activities of enterprises using modern system of information technologies should substitute out-of-date order-supplier system.

Japanese economists related with welding engineering market of goods and services believe that a transfer of economic relations on new level through development of a stable triads manufacturer–dealer– consumer, allowing setting reasonable price and revenue sharing, is a priority. This, in particular, should be taken into account under conditions of passing of property rights and control over the plants of welding consumable manufacture to leading foreign companies on the territory of

CIS countries and significant intensification of competitiveness in all range of products.

Low level of equipment and domination of out-of-date technologies arise some alert. In this connect manufacturers of welding consumables for all methods of arc welding should be directed on application of novel achievements in technique and technology, following the situation and also stimulating transfer of consumer to current level of equipment.

Own experience, addressing to printed technical and advertisement publications should not be solely relied upon in solving of arising problems. Specialists of leading research and design-and-technological institutes can provide qualified help, especially, in such questions as choose of reasonable solution, analysis of reasons of problem appearance and searching the ways of their elimination, professional development of personnel, estimation of innovation perspectives etc. All available possibilities are to be used in the world of rapidly developing information technologies.

ELECTRON BEAM WELDING OF MEASURING CHAMBER OF MAGNETIC PNEUMATIC GAS ANALYSER

V.M. NESTERENKOV and L.A. KRAVCHUK

E.O. Paton Electric Welding Institute, NASU, Kiev, Ukraine

The selection of power and time parameters of electron beam for EBW of flat measuring chamber of magnetic pneumatic gas analyzer of stainless steel 12Kh18N10T was considered. Scheme of welding in general vacuum, welding-assembly device and conditions providing formation of overlap and circumferential welds with admissible distortions of gas channel geometric sizes and vacuum-tightness are given.

Keywords: *electron beam welding, stainless steel, overlap joint of (0.2 + 1.0) mm, heat input of welding, assembly-welding device, scheme of welding, vacuum-tightness, deformations*

In 1970 the Siemens (Germany) started the serial manufacture of magnetic-pneumatic gas analyzer of Oxymat type [1], consisting of a flat measuring chamber of stainless steel. It consists of a basement with slots in the form of a sheet 1.0 mm thick 164 × 52 mm in size, upper and lower plates of foil of thickness 0.2 mm, two exhaust pipes and two nipples (Figure 1). The design peculiarities of chamber are featured by the fact that exhaust pipes and nipples are welded-on to the upper plate by circumferential welds, and upper and lower plates are welded-on to the basement using straight-line overlap welds. During development of technology for EBW of measuring chamber of domestic gas analyzer applied for NPP it was necessary to consider that distortion of geometric sizes of gas channel in the form of ripples, sagging and buckling of upper and lower plates is admitted of not more than 0.1 mm, and drop of pressure at the level of $0.59 \cdot 10^3$ Pa for 30 min is not admitted at all.

Welding for the measuring chamber is applied for sealing the inner volume and installing of nipples and exhaust pipes. As is shown in Figure 1, longitudinal and transverse welds are produced at approximately 1 mm distance from the edge of slots. Welds pass along the whole length of the item and cross each other, thus increasing the rigidity of structure and excluding the rounding. As far as width of welds on the prototype was 0.23–0.25 mm, it can be suggested that in this case the EBW or laser welding was applied.

According to conditions of operation the measuring chamber of gas analyzer should be non-magnetic, corrosion-resistant and vacuum-tight.

Austenite Cr–Ni thin-sheet steel 12Kh18N10T (GOST 5632–72) can meet those requirements (wt.%: C < 0.12; 17–19 Cr; 9–11 Ni; 1–2 Mn). However its decreased heat conductivity and high coefficient of linear expansion predetermine the great distortion of structures and assemblies to be welded. To provide minimal postweld deformations and resistance to formation of solidification cracks, and consequently, decrease in overheating the metal of near-weld zone, it is necessary to select the conditions with the least energy input [2].

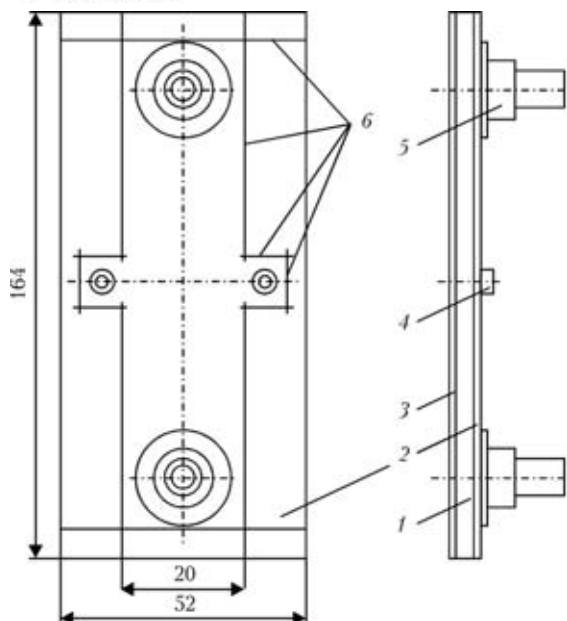


Figure 1. Scheme of measuring chamber of magnetic pneumatic gas analyzer of the Oxymat type: 1 – basement; 2 – upper plate; 3 – lower plate; 4 – nipple; 5 – exhaust pipe; 6 – overlap welds

As is shown in [3] in EBW of kovar and steel 12Kh18N10T sheets 0.3 mm thick using continuous electron beam the energy input $q/v = \eta_s U_{acc} I_b / v_w$ [J/m] (where η_s – efficiency factor of electron heating, for steel 12Kh18N10T it is equal to 0.8; U_{acc} – accelerating voltage, kV; I_b – current of electron beam, mA; v_w – welding speed, mm/s) remains constant in the range of accelerating voltage of 20–70 kV. The investigation of character of dependencies $q/v = f(v_w)$ and $B = f(v_w)$ showed that at $U_{acc} = 60$ kV the minimal heat input is achieved at $v_w = 40$ mm/s, and weld width $B = 0.25$ mm. For overlap joint the thin plate-basement of (0.2 + 1.0) mm of the steel 12Kh18N10T, the value of electron beam current on the product item penetration depth $h_{pen} = 0.3$ mm made $I_b = 2.1$ mA. The heat input at welding conditions $U_{acc} = 60$ kV, $I_b = 2.1$ mA, $v_w = 40$ mm/s was equal to $q/v = 2.52$ kJ/m.

The practicing of conditions of EBW of overlap joints of thin plate-basement of (0.2 + 1.0) mm of steel 12Kh18N10T was performed in laboratory machine OB-1803 with a modified EB column PL-102.* EB gun of triode type with a directly heated thermionic cathode of 0.27 mm diameter from tungsten-rhenium wire VR-20 together with electromagnetic adjustment system and focusing lens provide formation of a heating spot of 0.05–0.30 mm diameter and electron beam with $I_b = 0$ –15 mA [4] on the surface of item being welded. The deflection system located under focusing lens provides at its connection to the control system SU-241 [5] the deflection and movement of electron beam along the circumferential butt

* S.A. Shchyolok, manufacturing engineer of the 1st category, took part in this work.

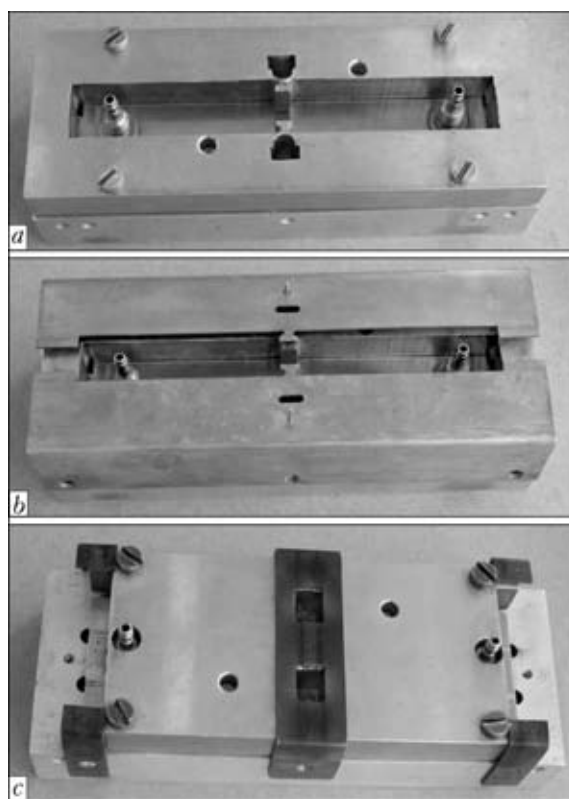


Figure 2. Welding-assembly device for EBW of measuring chamber ($\times 1.67$): a – assembly without shielding screens; b – assembly with shielding screens for performance of overlap welds respectively along the long and short (c) sides

of a fixed item (nipple or exhaust pipe) at a preset speed. Vacuum chamber with two-coordinate working table allows loading and flat welding of four measuring chambers simultaneously in welding-assembly device at rarefaction of $1.33 \cdot 10^{-2}$ Pa. The working distance is $l_{work} = 105$ mm.

The control of electron beam focusing on the surface of overlap joint of thin sheet-basement of stainless steel 12Kh18N10T was performed visually by the brightness of illumination of circular scan of 5 mm diameter and $I_b = 2$ mA on the copper massive plate located at the same level with the item to be welded and also using optical system of observation of electron-optic column PL-102 providing a clear imaging of the welding zone at (5–50)-fold magnification. Welding of overlap joint of (0.2 + 1.0) mm was performed at a sharp focusing which at $l_{work} = 105$ mm was equal to current of a coil of focusing lens $I_f = 765$ mA. Circumferential welds on flanging of nipples and exhaust pipes were produced with incomplete focusing of electron beam at $\Delta I_f = -20$ mA ($I_f = 745$ mA).

To provide a reliable heat contact along the whole length of a butt of overlap joint of (0.2 + 1.0) mm and to obtain defectless welds by analogy with the patent [6], the welding-assembly device for welding (electron beam or laser) was developed consisting of two rigid metallic bars of rectangular shape for tight clamping of measuring chamber (with two nipples and two exhaust pipes) between them, where in one of

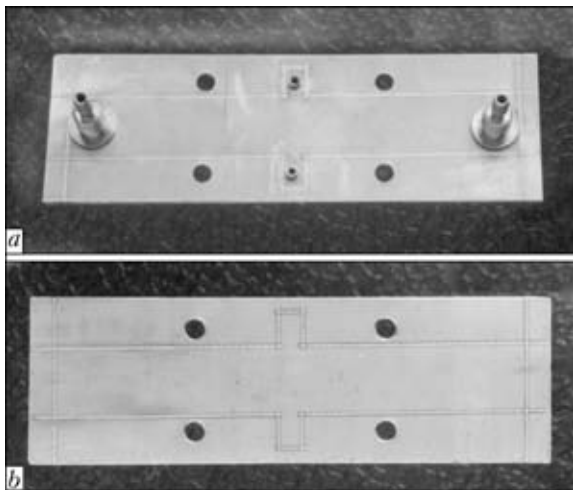


Figure 3. Measuring chamber of gas analyzer with straight-line overlap welds ($\times 1$): *a* – appearance on the side of nipples and exhaust pipes; *b* – on the side of lower plate

them the through slots are made on the side of effect of welding beam (Figure 2, *a*).

The distinctive feature of the welding-assembly device is the fact that the shielding screens with through slots of copper plate coinciding by their shape and axes with through slots in the mentioned bar are additionally installed with a gap (Figure 2, *b*). Thus, probable impact of welding electron beam on the upper pressing bar and its postweld deformation is eliminated.

During development of technological process of EBW of measuring chambers of magnetic pneumatic gas analyzer including welding-assembly device, the succession of welds performance turned to be principally important. To prevent sagging and buckling of thin plate of stainless steel 12Kh18N10T 0.2 mm thick in the area of gas channel of more than 0.1 mm, the following succession was accepted:

1) installing the nipple and exhaust pipe into the holes on thin plate of thickness 0.2 mm. The height and thickness of flanging was respectively 0.50 and 0.25 mm;

2) expansion of flanging on nipples and exhaust pipes, control of a gap between flanging and thin plate which should be not more than 0.05 mm;

3) assembly of upper thin plate with expanded two nipples and two exhaust pipes in a set with a basement and without lower thin plate in welding-assembly device (Figure 3);

4) loading of four sets of measuring chambers (nipples and exhaust pipes are directed upwards) into the vacuum chamber of the EB installation and making four straight-line overlap welds along the long side (see Figure 2, *a*, *b*);

5) evacuation of vacuum chamber and assembly of welding-assembly device with shielded screens of copper plates (Figure 2, *c*);

6) loading of four sets of measuring chambers (nipples and exhaust pipes are directed upwards) into the vacuum chamber and making four straight-line over-

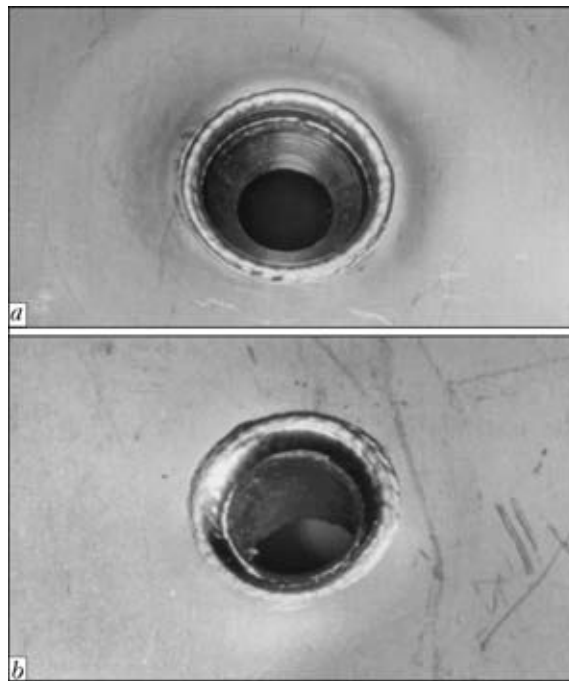


Figure 4. Appearance of circumferential welds in welding of flanging–thin plate ($\times 4$) on the exhaust pipe (*a*) and nipple (*b*)

lap welds along the short side. Observation of crossing of eight straight-line welds (Figure 3, *a*);

7) evacuation of vacuum chamber and change of position of measuring chambers in welding-assembly device without lower thin plate (nipples and exhaust pipes are directed downwards), when circumferential welds–expanded flanging–thin plate are directed towards the welding electron beam;

8) loading of four sets of measuring chambers into the vacuum chamber and performance of EBW of circumferential welds on the nipples and exhaust pipes using control system SU-241. Welding condition is as follows: $U_{acc} = 60$ kV, $I_b = 1.8$ mA, $v_w = 15$ mm/s (Figure 4);

9) evacuation of vacuum chamber and performance of visual inspection of formation of straight-line and circumferential welds for absence of defects in a form of lack of fusion and burn-outs;

10) intermediate checking of welded measuring chambers without lower thin plate for vacuum-tightness using method of excessive pressure. Drop of pressure in measuring chamber on the level of $0.59 \cdot 10^3$ Pa

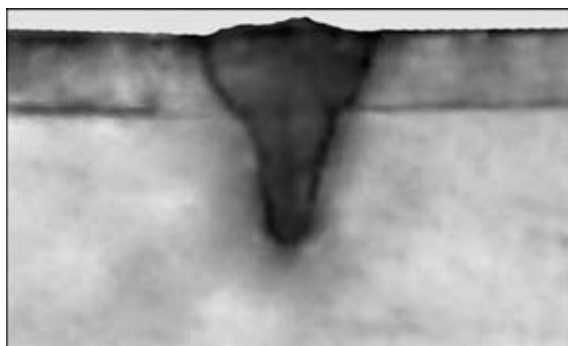


Figure 5. Transverse macrosection ($\times 60$) of overlap joint (0.2 + 1.0) mm thick of stainless steel 12Kh18N10T

determined using manometer (model 11202, GOST 6521-72) should not occur during 30 min;

11) assembly of four sets of measuring chambers in welding-assembly device with 0.2 mm lower thin plate of steel 12Kh18N10T (nipples and exhaust pipes are directed downwards), loading into vacuum chamber and making successively firstly four overlap welds along the long side and then four straight-line overlap welds along the short side (see items 4-6). Visual inspection of crossing of eight straight-line welds for absence of defects (Figure 3, *b*);

12) evacuation of vacuum chamber and performance of final testing of completely welded measuring chambers for vacuum-tightness using method of excessive pressure.

The conditions of EBW in general vacuum of measuring chamber of magnetic pneumatic gas analyzer, succession of performance of assemblies and welds, intermediate and final checking of formation of welded joints for lack of defects and vacuum-tightness allowed obtaining 100 % output of annual production. As is shown in Figure 5, the width of face bead of overlap weld was $B \approx 0.24$ mm at the depth of penetration of about 0.5 mm.

It was also established that values of residual deformations of structure of measuring chamber are in direct dependence on heat input of welding which in its turn is determined by welding conditions and depends on weld section. The measuring of postweld

deformation was performed using method of comparison with the reference sample. Sagging and buckling of thin plate of foil of thickness 0.2 mm in the area of gas channel did not exceed 0.1 mm.

CONCLUSIONS

1. EBW technology and equipment as applied to precision welding of measuring chamber of magnetic pneumatic gas analyzer of stainless steel 12Kh18N10T meet all requirements for vacuum tightness and geometric sizes of the gas channel.

2. Minimal heat input of electron beam and minimal width of the weld are achieved at $v_w \geq 40$ mm/s.

3. The given conditions of EBW of overlap and circumferential joint, succession of making assembly and welds, stage-by-stage control of quality of welding and vacuum-tightness allowed obtaining 100 % output of annual production.

1. www.sea.siemens.com/us/Products/Process-Analytics/Products.
2. Grezev, A.N., Lukianenko, V.L., Zabelin, A.M. et al. (1989) Properties of laser-welded joints of steel 08Kh18N10T. *Avtomatich. Svarka*, **12**, 63-64.
3. Kravchuk, L.A., Slutskin, M.G. (1979) Pulsed electron beam butt welding of 29NK alloy sheets of up to 1 mm thickness. *Ibid.*, **1**, 41-44.
4. Kravchuk, L.A., Nebesny, S.V., Pikulya, L.G. (1986) Electron-optical column for precision EBW. *Ibid.*, **12**, 54-57.
5. (1991) *Welding equipment*: Catalogue-Refer. Book. Kiev: Naukova Dumka.
6. Ausillo, J.S., Clemens, M. *Laser welding clamp*. Pat. 4847467 USA, Int. Cl. B23K 26/00. Publ. 11.07.89.

LIMITATION OF OVERVOLTAGES IN HIGH-VOLTAGE CIRCUITS AFTER DISCHARGES IN WELDING GUN

O.K. NAZARENKO and V.A. MATVEJCHUK

E.O. Paton Electric Welding Institute, NASU, Kiev, Ukraine

Occurrence of overvoltages in output circuits of a high-voltage power source, cable and welding gun after its discharge was studied using computer modeling. Recommendations are given on optimal parameters of elements of the overvoltage limitation circuit for the powerful power sources.

Keywords: *electron beam welding, electron gun, source of accelerating voltage, limiting resistor, natural inductance, shunting diode, high-voltage cable, discharge in gun, modeling of transition processes*

The development of abnormal non-stationary processes in welding gun, to which electric discharges refer due to the loss of vacuum seal, can result not only in violation of weld formation but also cause damage of a number of assemblies of power unit, such as a high-voltage insulator of welding gun and cable (Figure 1), and also limiting resistor. As far as mentioned assemblies can withstand test voltage twice exceeding the operating one without fracture, it can be assumed that

overvoltages exceeding operating voltage at least twice exist.

In welding gun the overvoltages were revealed after discharge as early as at the beginning of application of EBW, however the conductance of device measurements of rapidly flowing processes under high potential relatively to the earth is considerably complicated [1-4]. It partially explains the absence of publications on the problems of prevention of overvoltages after discharge in welding gun. It is managed experimentally to fix only the current overloads of sources of accelerating voltage.

The use of controlling electron pentode as a linear element prevents intense current surges in power source after discharge in welding gun. However, it

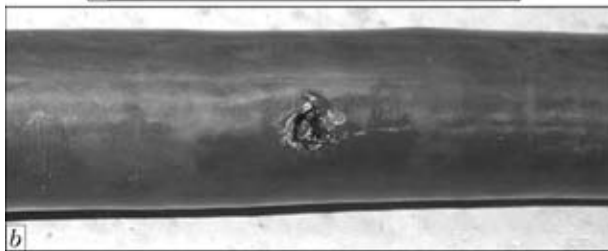
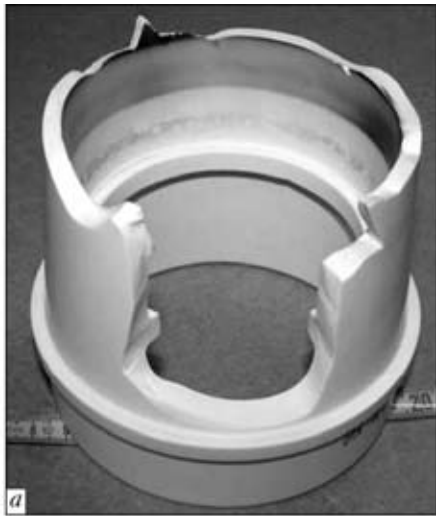


Figure 1. High-voltage insulator of high alumina ceramics (a) and high-voltage cable (b), withstood the test voltage of 120 kV but destroyed in the process of operation of standard power unit ELA-60 (rated voltage of 60 kV)

was stated that, for example, in equipment with accelerating voltage of 60 kV after discharge in the gun the voltage in controlling pentode can increase up to 130 kV which can cause almost simultaneously the discharge in controlling pentode. For this emergency case the source of accelerating voltage should be equipped with additional protective system except of maximal one. For this purpose the limiting resistors, connected in series to a load, are often used. The resistor resistance value is limited by the power, dissipated in it, and minimizing of loading characteristic of the source. Therefore, for example in work [2], it is offered in series with an output of high-voltage

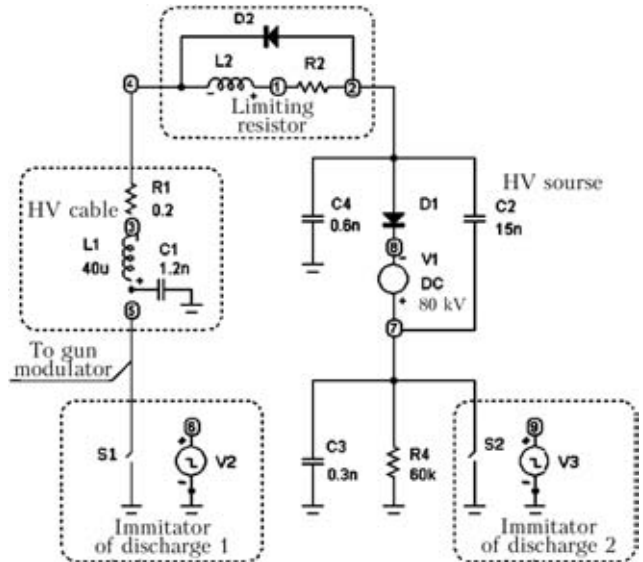


Figure 3. Diagram for modeling transition processes (for designations see the text)

power source to use high-voltage choke shunted by reverse biased diode or simply by resistor as a tool of its dynamic protection. Here, the overvoltages in the source–high-voltage cable–insulator system were not considered.

The limiting resistors as to their design can be bulk and wire-wound. The latter are characterized by noticeable natural inductance which reduces speed of power source current increment during discharge, but causes the oscillatory process in high-voltage cable and resistor itself. Earlier the optimum correlation of resistance and natural inductance was not discussed as well. Therefore this work is devoted to modeling of non-stationary and emergency situations in the source of accelerating voltage–high-voltage cable–welding gun system for selection of optimal parameters of protection from overvoltages.

Object and investigation methods. For stationary power unit ELA-60 (Figure 2) at modeling of transition processes [5] after discharge in welding gun some simplifying assumptions can be made. From the mod-

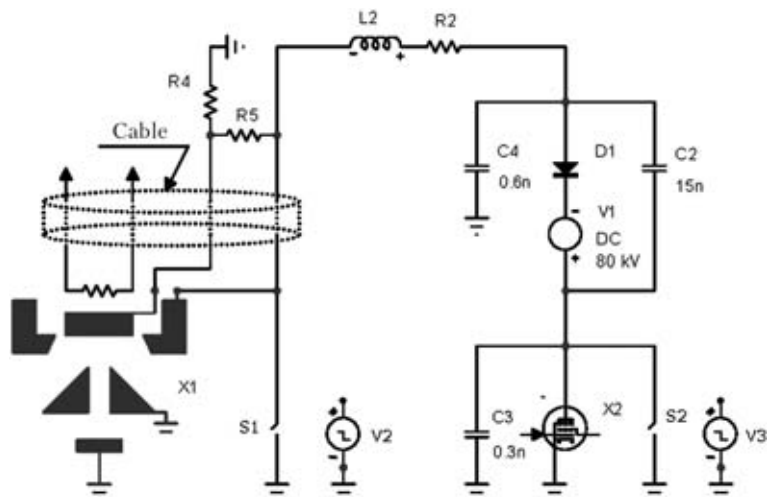


Figure 2. Simplified schematic diagram of standard power unit ELA-60 with elements for modeling transition processes (for explanations see the text)

eling scheme (Figure 3) the gun X1 itself and high-voltage cable, presented by an electric link with concentrated capacitance, inductance and resistance, are excluded. Some error of such representation affects only high-frequency components of the transition process. As was established that load current does not influence characteristics of transition processes appearing in gun discharge, it was preset arbitrary (300 mA). The source of accelerating voltage is represented by a voltage source V1 with diode D1 (capacitors C3 and C4 account for all capacitances relatively to the earth, connected to positive and negative terminals of the source). Resistor R4 = 60 kOhm, simulating the controlling electron pentode X2 in the mode of 300 mA current flow, is connected in series to the source of accelerating voltage V1 into its plus circuit. Discharges in welding gun and pentode are simulated respectively by switches S1 and S2 which

are controlled by the sources of pulse voltage V2 and V3. The resistance of contacts of breakdown imitator S1 in open state is 200 kOhm, which corresponds to the flowing of stationary current of 300 mA, the resistance of close contact S1 at imitation of discharge is 0.01 Ohm and resistance of contacts of switch S2 in open state is 100 MOhm, in close one it is 0.01 Ohm. The duration of short-circuiting is preset by a longer time (5 μ s) which corresponds to two stages of discharge: breakdown and spark [6]. As a protection the limiting resistor R2 with natural inductance L2 was used. The length of high-voltage cable is 10 m.

Results and their discussion. Time diagrams of transition processes are presented in Figure 4 where the following designations are given: $v(C1)$ – potential in the unit of cable connection to gun modulator; $v(4.2)$ – drop of voltage on the limiting resistor; $I(7.8)$ – current of accelerating voltage source;

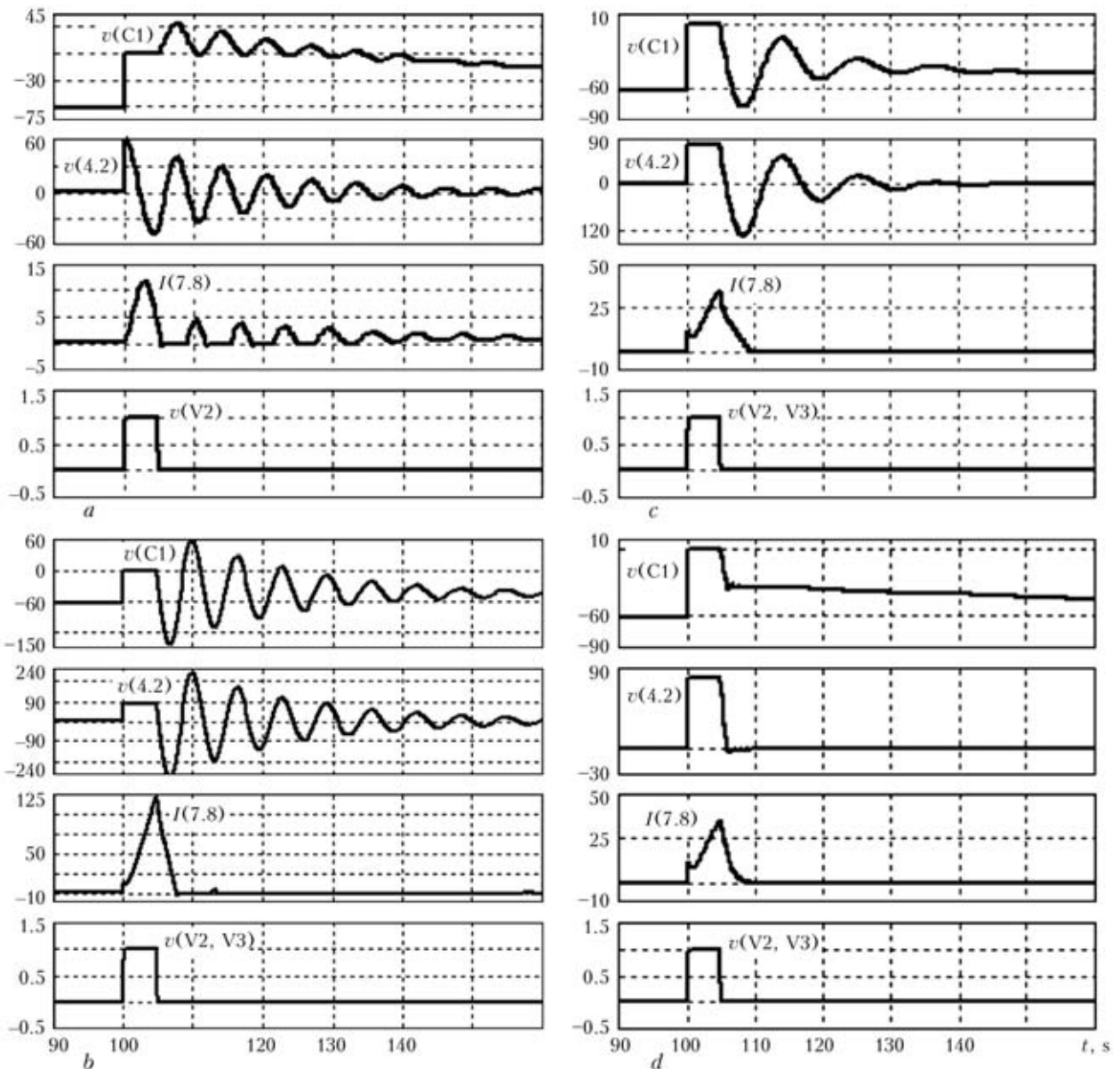


Figure 4. Time diagrams of transition processes: *a* – discharge only in gun, $R_{limit} = 200 \text{ Ohm}$, $L = 2 \text{ mH}$; *b* – successive discharge in gun and controlling pentode, $R_{limit} = 200 \text{ Ohm}$, $L = 2 \text{ mH}$; *c* – successive discharge in gun and controlling lamp, $R_{limit} = 1200 \text{ Ohm}$, $L = 6 \text{ mH}$; *d* – successive discharge in gun and controlling pentode, $R_{limit} = 1200 \text{ Ohm}$, $L = 6 \text{ mH}$, shunting diode is switched on

$v(V2)$, $v(V3)$ – presetting of time of discharge existence.

As it follows from time diagram given in Figure 4, *a*, during discharge the potential of modulator drops to zero only in the gun, and after termination of discharge the rated value of accelerating voltage is restored aperiodically without dangerous overvoltages. The amplitude of voltage oscillation in the limiting resistor is changed in the range of $\pm U_{acc}$, and amplitude of current flowing through the power source does not exceed 12 A. Such progress of events is quite acceptable and this is not an emergency situation.

However successive discharge in the gun and controlling pentode (Figure 4, *b*) has already created the emergency situation: the potential of modulator reaches -150 kV, amplitude of voltage oscillations on the limiting resistor is ± 250 kV, current of power source at the time of discharge existence succeeds in growing up to 125 A.

Therefore, to prevent this emergency situation it is necessary to increase resistance of limiting resistor up to the value acceptable regarding minimizing of load characteristics of power source, dissipation of heat evolved in oil tank and losses of net power. Naturally, this value can change for each specified source. For example, for sources with load current of about 1 A the optimal resistance is 1000–1200 Ohm. As it follows from obtained time diagrams of transition processes at simultaneous discharges in welding gun and controlling pentode using $R_{limit} = 1200$ Ohm with natural inductance $L = 6$ mH (Figure 4, *c*), after termination of discharge the overvoltage in the point of cable connection to the gun modulator decreased down to -75 kV and amplitude of current flowing through power source did not exceed 30 A. However, oscillations of potential in the circuit of limiting resistor remain significant enough (from 90 to -120 kV).

The next step in overcoming the overvoltages is shunting of limiting resistor by a diode (practically by a circuit of diodes connected in series, withstanding the drop of voltage down to $1.5U_{acc}$), as it was expected, leads to a complete suppression of oscillating process. Due to that the overvoltage in the cable is absent, drop of voltage in limiting resistor is only 80 kV (Figure 4, *d*).

Though numerous values obtained during modeling of transition processes can not be completely valid, nevertheless the general regulations of influence of parameters of protection on character of these transition processes are seemed to be convincing. The confirmation of efficiency of increase in resistance of limiting resistor and its shunting by chain of reverse biased diodes is the fact that after application of all those recommendations the breakdowns of main insu-

lation of high-voltage cables, destruction of limiting resistor and high-voltage insulators of welding guns did not occur in our practice.

The similar protection provides also an accident-free operation of powerful power units of inverter type with high-frequency transformation of mains frequency, where controlling pentode is not used. In power units of lower power the values of limiting resistor can be respectively increased, thus increasing the efficiency of protection system from overvoltages even more and decreasing the source current during gun discharge.

CONCLUSIONS

1. The system of limiting overvoltages and controlling pentode of standard power unit ELA-60 provides a safe level of overvoltages in the power source–cable–gun system after discharge in welding gun.

2. Successive discharge in gun and in controlling pentode has already created the emergency situation as the potential of modulator exceeds the level of accelerating voltage by 2.5 times and limiting resistor – by 4 times, that can lead to damage of insulator, cable and limiting resistor.

3. Maximum acceptable increase of resistance of limiting resistor by 6 times (from 200 to 1200 Ohm) does not prevent the oscillation process at successive discharge in gun and controlling pentode, but oscillation amplitude in the cable exceeds accelerating voltage only by 20 %. However the amplitude of maximal overvoltage in limiting resistor exceeds accelerating voltage twice.

4. Shunting of limiting resistor by a chain of reverse biased diodes excludes exciting of oscillating process at successive discharge in gun and controlling pentode. Due to this, the overvoltage in the cable is completely absent, drop of voltage in limiting resistor exceeds accelerating voltage only by 50 %.

5. Obtained results are acceptable for using both in sources without frequency transformation and also in inverter-type sources.

1. Nazarenko, O.K., Lanbin, V.S. (2007) Investigation of high-voltage control circuits of welding electron beam current. *The Paton Welding J.*, **5**, 17–20.
2. Shidlovskaya, N.A., Martynov, V.V. (2010) Adapting of high voltage power supply with electron beam unit. *Tekhn. Elektrodinamika*, **1**, 73–79.
3. Tkachev, L.G., Batov, N.G., Lebedev, A.F. et al. (1995) Wave processes in technological units with electron beam heating. *Elektrotehnika*, **9**, 39–41.
4. Shcherbakov, A.V., Benevolsky, E.S. (2010) Commutation processes in power supplies of electron beam guns in formation of high-voltage breakdowns. *Svaroch. Proizvodstvo*, **10**, 18–23.
5. Amelina, M.A., Amelin, S.A. (2007) *Program of circuit simulation Micro-Cap8*. Moscow: Gor. Liniya-Telekom.
6. Mesyats, G.A. (2004) *Pulsed power engineering and electronics*. Moscow: Nauka.

INFLUENCE OF PRELIMINARY CYCLIC LOADING ON EFFECTIVENESS OF WELDED JOINT STRENGTHENING BY HIGH-FREQUENCY PEENING

V.V. KNYSH, S.A. SOLOVEJ and A.Z. KUZMENKO
E.O. Paton Electric Welding Institute, NASU, Kiev, Ukraine

The paper gives the results of studying the effectiveness of application of high-frequency mechanical peening to improve the residual fatigue life of tee welded joints on low-alloyed steels with accumulated fatigue damage. It is shown that the effectiveness of strengthening welded joints by this technology can vary in a broad range, depending on operation duration and level of applied stresses during operation.

Keywords: *welded joints, fatigue, fatigue damage, high-frequency mechanical peening, cyclic fatigue life, strengthening effectiveness*

$$\sum \frac{n_i}{N_i} + \sum \frac{n_j}{N_j} \geq a,$$

Fatigue strength of welded joints is improved considerably by application of various postweld treatments, known as methods of surface plastic deformation of metal. Systematic studies conducted at the PWI of the NAS of Ukraine lead to the conclusion that high-frequency mechanical peening (HFMP) ensures the highest physico-mechanical characteristics of the strengthened metal layer and at the current stage of development of resources-saving technologies is the most efficient method of strengthening the welded structures operating under the conditions of alternating loading. Effectiveness of application of this method of welded joint treatment at the stage of structure fabrication is quite well studied, and investigation results are widely represented in literature. A number of studies are devoted to investigation of the effectiveness of strengthening welded joints in operating metal structures, i.e. after the joints have accumulated the specified damage fraction [1–5]. It is experimentally established that after HFMP of welded joints with accumulated fatigue damage (right up to the moment of formation of a surface fatigue crack) the levels of applied maximum cycle stresses in the loading block, which are much lower than the endurance limit of the strengthened welded joint, have no damaging effect. On the other hand, the data obtained in these works on improvement of cyclic fatigue life of welded joints after a certain operation period differ considerably, that is indicative of the need to perform further studies in this direction.

So, in work [1] on the influence of preliminary cyclic loading on the effectiveness of strengthening by HFMP, treatment was conducted after welded tubular connections have operated for 25–60 % of their fatigue life in as-welded condition. The authors propose to determine the fatigue life of the connections by linear summation of fatigue damage before and after strengthening:

where n_i , N_i is the number of operation cycles and cycles-to-failure at stress σ_i of as-welded joint; n_j , N_j is the number of operation cycles and cycles-to-fracture at stress σ_j of welded joint strengthened by HFMP technology in as-welded condition; a is the limit accumulated fatigue damage.

Proceeding from experimental data the authors suggest using a unity as the limit value of the sum of relative fatigue lives, i.e. the effectiveness of the increase of fatigue life of welded joints with accumulated fatigue damage by HFMP decreases with increase of the number of operation cycles before strengthening, and the maximum increase of fatigue life is achieved at strengthening right after welding.

In [2] the effectiveness of application of HFMP technology to tee welded joints of steel St3 after they have operated for 50 % of their fatigue life in as-welded condition at the load of $(0.7–0.9)\sigma_y$ was studied. Obtained fatigue curves demonstrate an increase of fatigue life of such samples by more than 2 times compared to samples strengthened by HFMP in as-welded condition. Such an increase of fatigue life in samples, pre-tested in as-welded condition before operation up to 50 % of their fatigue life, is attributed by the authors to the fact that high levels of applied stresses lead to formation of plastic strains in the stress raiser zones, and, therefore, to inducing residual compressive stresses in them. Subsequent HFMP treatment further raises the residual compressive stresses in the raiser zones. If the above formula is used for the results obtained in this work, then the limit total damage would be in the range $a = 2.5–3.1$.

In [5] treatment of welded tubular connections from steel 20 by HFMP was conducted both in as-welded condition, and after preliminary static loading at high stress levels. From the above fatigue curves it follows that strengthening after preliminary static loading is more effective (fatigue life increases by approximately 4 times), compared to strengthening

of welded joints in as-welded condition. Such an increase is attributed both by the authors of this work, and the authors of [2], to higher levels of induced residual compressive stresses in the treatment zone.

Proceeding from the results of [1, 2], prediction of the effectiveness of strengthening by HFMP technology of welded joints after certain operation period, based on linear summation of fatigue damage, apparently should take into account the levels of applied alternating stresses before and after treatment.

The purpose of this work is to establish the influence of preliminary cyclic loading on the effectiveness of strengthening tee welded joints by HFMP.

Experimental investigations were conducted on samples of tee joints of low-alloyed steels 09G2S ($\sigma_y = 370$ MPa, $\sigma_t = 540$ MPa) and 10KhSND ($\sigma_y = 450$ MPa, $\sigma_t = 570$ MPa). Blanks for samples from these steels were cut out of rolled sheets so that the long side was oriented along the rolling direction. Transverse stiffeners were fillet welded from both sides by manual electric arc welding by UONI-13/55 electrodes (Figure 1). Thickness of experimental sample is due to wide application of 12 mm thick rolled stock in welded structures, and the width of its working part was selected, proceeding from testing equipment capacity. At joint strengthening by HFMP technology surface plastic deformation was applied to a narrow zone of weld metal transition to the base metal. Fatigue testing of samples was conducted in URS 20 machine at uniaxial alternating tension with cycle asymmetry $R_\sigma = 0$. All the samples were tested to complete fracture or their withstanding $2 \cdot 10^6$ stress alternation cycles. Calculation of damage fractions of welded joints of 09G2S and 10KhSND steels in the as-welded and as-strengthened condition was performed by fatigue curves obtained earlier and given in [6, 7].

Twelve welded samples from steel 09G2S were tested in unstrengthened condition at maximum stress cycles of 180 and 260 MPa up to 50 % of fatigue life at complete fracture. After that all the samples were strengthened by HFMP technology and fatigue testing was continued at higher levels of maximum cycle stresses.

Maximum stresses initially applied to welded samples, equal to 180 MPa, were increased up to levels of 260, 278 and 296 MPa (two samples on each stress level). In six samples tested in as-welded condition at specified initial maximum cycle stresses of 260 MPa, after HFMP treatment the applied stresses were increased up to levels of 275, 290 and 305 MPa (two samples on each stress level). Selection of maximum levels of cycle stresses before and after strengthening was performed so as to cover the entire range of applied loads, characteristic for the region of high-cycle fatigue of strengthened and unstrengthened tee welded joints.

Six samples from 10KhSND steel in unstrengthened condition were tested at regular loading

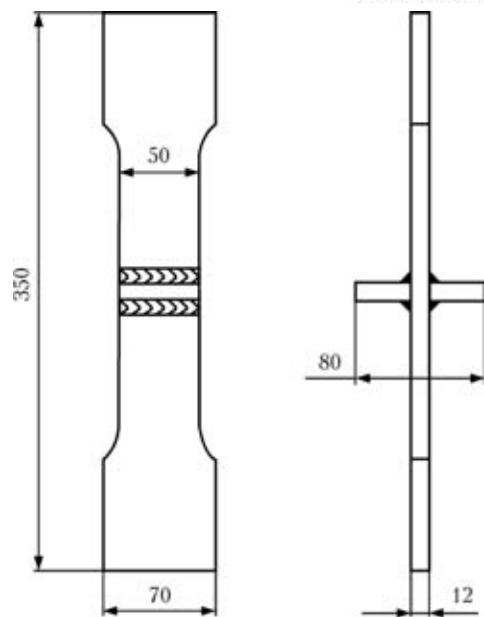


Figure 1. Schematic of an experimental sample of a tee joint of 09G2S steel

with maximum cycle stresses of 280, 290 and 300 MPa (two samples on each stress level) up to accumulation of 50 % damage. After strengthening by HFMP of welded samples from 10KhSND steel applied loads remained the same, when fatigue tests were continued.

Results of fatigue testing of welded samples of 09G2S and 10KhSND steels are given in the Table.

Limit values of the sum of relative fatigue lives obtained on six samples of tee welded joints from 09G2S steel, strengthened by HFMP after testing up to 50 % of fatigue life at maximum stresses of 180 MPa, are in the range of 0.77–1.21. Here one sample did not fail after $2 \cdot 10^6$ cycles of stress alternation in as-strengthened condition (its total damage level was equal to more than 1.80). Limit values of total damage obtained on six samples from steel 09G2S, strengthened by HFMP after testing to 50 % of fatigue life at maximum stresses of 260 MPa, are in the range of 1.51–2.13. Testing of one of the six samples was interrupted after $2 \cdot 10^6$ cycles of stress alternation in as-strengthened condition (total damage level was more than 2.37). Total damage level of tee welded joints of 10KhSND steel, tested at unchanged regular loading before and after strengthening, is in the range of 2.37–2.87. Three samples from steel 10KhSND did not fail after testing for $2 \cdot 10^6$ cycles of stress alternation in as-strengthened condition.

Obtained results are indicative of the fact that under the conditions of regular loading the limit values of the sum of relative fatigue lives of tee welded joints on low-alloyed steels, strengthened by HFMP at accumulation of 50 % of damage in unstrengthened condition, depend on the levels of alternating stresses applied to welded joints before their strengthening. This is related to the fact that the high levels of stresses applied to welded joints before strengthening can lead

Results of fatigue testing of samples of tee welded joints of 09G2S and 10KhSND steels strengthened by HFMP after testing to 50 % fatigue life in as-welded condition

Sample number	As-welded condition			Strengthened condition			$\sum \frac{n_i}{N_i}, \%$
	$\sigma_{1max}, \text{MPa}$	$n_1, \text{thou cycles}$	$n_1/N_1, \%$	$\sigma_{2max}, \text{MPa}$	$n_2, \text{thou cycles}$	$n_2/N_2, \%$	
09G2S steel							
1	180	500	50	260	798.8	51.6	101.6
2	180	500		260	>2000*	>130	>180
3	180	500		278	707.0	70.7	120.7
4	180	500		278	357.5	35.8	85.8
5	180	500		296	174.7	27.2	77.2
6	180	500		296	185.3	28.9	78.9
7	260	64		275	>2000*	>186.5	>236.5
8	260	64		275	1315.6	122.7	172.7
9	260	64		290	751.1	101.1	151.1
10	260	64		290	1011	136.1	186.1
11	260	64		305	839.5	163.2	213.2
12	260	64		305	580.8	112.9	162.9
10KhSND steel							
1	280	79.7	50	280	>2000*	>172.8	>222.8
2	280	79.7		280	>2000*	>172.8	>222.8
3	290	67.8		290	1820.3	215.5	265.5
4	290	67.8		290	>2000*	>236.9	286.9
5	300	57.7		300	1153.5**	187.3	237.3
6	300	57.7		300	1314.8	213.4	263.4

* – no failure; ** – failure in the base metal.

to partial or complete relaxation of residual tensile welding stresses across the entire sample section, and in some cases – can induce residual compressive stresses in the stress raiser zones. For an approximate determination of maximum cycle stresses σ_{max} , at which complete relaxation of residual stresses is achieved, we can proceed from $\sigma_{max} > \sigma_y / \alpha_\sigma$ inequality, where α_σ is the stress concentration factor. As is seen from the Table, such a relaxation of residual

welding stresses before performance of HFMP of welded joints with accumulated 50 % damage, increases their residual fatigue life by approximately 1.1–2.4 times, compared to fatigue life of joints strengthened in as-welded condition.

Generalizing the results of fatigue testing and results of [1, 5, 6], one may assume that the duration of testing at high levels of applied external loading before strengthening also has a significant influence on effectiveness of strengthening by HFMP. Six samples of a tee welded joint from 09G2S steel were additionally tested by the following procedure. Welded joints were tested in unstrengthened condition at maximum cycle stresses of 260 MPa up to achieving 10, 30 and 70 % fatigue life at complete fracture, two samples for each testing level, and then strengthened by HFMP technology. After sample strengthening, fatigue testing was continued at the level of maximum cycle stresses of 305 MPa.

Failure of the first sample pre-tested to 10 % fatigue life, occurred after 1,871,300 cycles of stress alternation in the base metal, i.e. welded joint fatigue life increased by more than 3.5 times, compared to as-welded condition. The second sample failed (Figure 2) in the zone of weld metal transition to non-load bear-

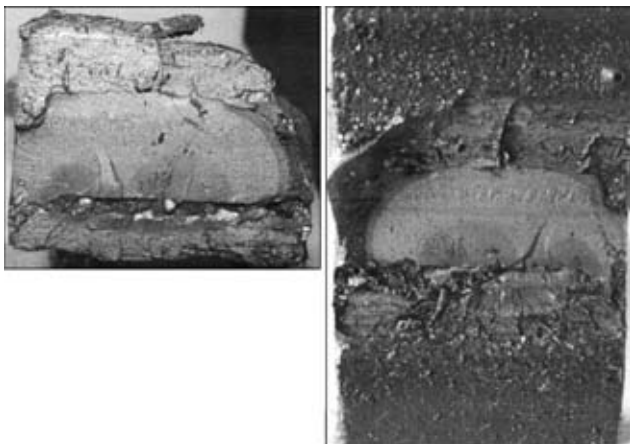


Figure 2. Fatigue fracture of a sample of 09G2S tee joint strengthened by HFMP after testing to 10 % damage level

ing stiffener after 1,614,600 cycles of stress alternation. As is seen from Figure 2, fatigue crack initiation and subsequent failure of the welded sample occurred because of incomplete penetration of one of the stiffeners joined by fillet welds.

After pre-testing of the third and fourth samples to 30 % fatigue life before strengthening at specified maximum cycle stresses of 260 MPa, they failed at 1,168,500 and 1,407,200 cycles of stress alternation, i.e. the joint fatigue life increased by 2–3 times compared to strengthening in as-welded condition.

Pre-testing to 70 % fatigue life at specified maximum cycle stresses did not lead to a noticeable increase of fatigue life. Failure of the fifth and sixth sample occurred after testing by 452,900 and 628,400 cycles of stress alternation in as-strengthened condition, respectively, i.e. residual fatigue life of joints with such test cycle numbers after strengthening by HFMP remains on the level of fatigue life of joints strengthened in as-welded condition.

Obtained experimental data are indicative of the fact that under the conditions of regular loading the effectiveness of strengthening by HFMP of welded joints with accumulated fatigue damage increases with increase of the level of applied alternating stresses before strengthening and with shortening of the duration of testing in as-welded condition. The latter can have the following explanation. High levels of applied stresses lead to relaxation of residual welding stresses in the stress raiser zones already after the first loading cycles without any significant accumulation of fatigue damage. Subsequent loading cycles (increase of testing duration) lead only to an intensive accumulation of fatigue damage. Thus, in order to increase the HFMP effectiveness, it is rational to try and reduce the duration of the impact of high stress levels before strengthening. Therefore, the maximum characteristics of fatigue strength of welded joints can be achieved at HFMP strengthening after preliminary static overloading. This is confirmed by the data of [5], where it is established that after preliminary static loading causing stresses close to the yield point in the raiser zones, the fatigue life of HFMP strengthened welded tubular connections from steel 20 rises 4 times, compared to strengthening in as-welded condition.

Thus, depending on the duration of testing and level of relaxation of residual welding stresses in the stress raiser zone in service, the effectiveness of welded joint strengthening by HFMP can vary in a broad range (limit values of the sum of relative fatigue lives $a = 0.77-4$). For approximate evaluation of the effectiveness of HFMP strengthening of welded joints which were not exposed to high loading levels in service before strengthening, a unity can be taken as the limit value of the sum of relative fatigue lives.

CONCLUSIONS

1. It is established that under the conditions of regular loading, the effectiveness of HFMP strengthening of welded joints with accumulated fatigue damage depends on the level and duration of the impact of applied loading.

2. It is shown that residual fatigue life of highly loaded tee welded joints of low-alloyed steels after HFMP strengthening at 70 % accumulated damage is not inferior to fatigue life of joints strengthened in as-welded condition. Shortening duration of testing of such joints from 70 to 10 % of their fatigue life increases the strengthening effectiveness up to 3.5 times compared to strengthening in as-welded condition.

1. Garf, E.F., Litvinenko, A.E., Smirnov, A.Kh. (2001) Assessment of fatigue life of tubular connections subjected to ultrasonic peening treatment. *The Paton Welding J.*, **2**, 12–15.
2. Knysh, V.V., Kuzmenko, A.Z., Bojtenko, O.V. (2006) Increasing fatigue resistance of welded joints by high-frequency mechanical peening. *Ibid.*, **1**, 30–33.
3. Knysh, V.V., Kuzmenko, A.Z., Solovej, S.A. (2009) Increase of cyclic fatigue life of tee welded joints with surface cracks. *Ibid.*, **1**, 29–33.
4. Knysh, V.V., Solovej, S.A., Kuzmenko, A.Z. (2010) Improvement of cyclic fatigue life of welded joints with accumulated fatigue damage by high-frequency peening. *Ibid.*, **10**, 33–36.
5. Xiaohui, Z., Dongpo, W., Lixing, H. (2011) Analysis of the S–N curves of welded joints enhanced by ultrasonic peening treatment. *Materials & Design*, **32**(1), 88–96.
6. Knysh, V.V., Solovej, S.A., Kuzmenko, A.Z. (2008) Accumulation of fatigue damage in tee welded joints of 09G2S steel in the initial condition and after strengthening by high-frequency mechanical peening. *The Paton Welding J.*, **10**, 10–15.
7. Knysh, V.V., Valteris, I.I., Kuzmenko, A.Z. et al. (2008) Corrosion fatigue resistance of welded joints strengthened by high-frequency mechanical peening. *Ibid.*, **4**, 2–4.

INFLUENCE OF WELDING POWER SOURCES ON THREE-PHASE MAINS

S.V. RYMAR, A.M. ZHERNOSEKOV and V.N. SYDORETS
E.O. Paton Electric Welding Institute, NASU, Kiev, Ukraine

Harmonic composition of three-phase electric mains at operation of welding power sources was studied. It is shown that welding sources generate higher current harmonics into the mains that impairs the quality of power. Application of higher harmonic filters is recommended to reduce the impact of welding power sources on the mains

Keywords: arc welding, power sources, three-phase mains, power quality, higher harmonics, filters

On the threshold of 1980–1990s developed countries of the world faced the problem of increasing deterioration of the quality of power in the mains, which consisted in distortion of the sinusoidal shape of voltage and current in the mains that led to increased losses and lower reliability of electrical equipment operation. It was the result of a constant increase of power consumption by equipment with non-linear loads, such as rectifiers, inverters, frequency-controlled electric drives, computers, office and other equipment. Non-linear loads generate higher current harmonics into the mains that increase losses in mains wires, equipment and loads, and also impair the electromagnetic compatibility [1–4], i.e. may lead to failure of electrical and electronic equipment, overheating of rotors and accelerated wear of bearings of electric motors and generators, failure of control systems of electric drives and explosions of electrolytic condensates in them, unreliable operation of microprocessor and computational equipment, false operation of the system of protection for electrical equipment switching off, burning of zero wires, fast ageing of the insulation, corrosion of earthing elements, burning of electric lighting instruments, etc.

Three-phase rectifiers with capacitors and different types of inverters generate powerful odd current harmonics, in particular, 5th and 7th, reaching 70–80 % of the main harmonic amplitude [1]. This brings the value of the coefficient of non-linear distortions (harmonics) of current THD_I (total harmonic current distortion) up to 80–90 % [2–4], and in a number of cases even much higher. In IEEE standards (Institute of Electrical and Electronics Engineers, Inc.) [5] acceptable THD_I levels are believed to be $THD_I \leq 5\%$ for $k_{Ik} \leq 20$, and $\leq 8\%$ for $20 < k_{Ik} \leq 50$, for mains of 0.12 to 69 kV voltage, depending on the transmission capacity of the mains and short-circuiting current (here k_{Ik} is the coefficient of short-circuiting current ratio equal to the ratio of short-circuiting current to rated current). Acceptable values of the coefficient of non-linear voltage distortions THD_U (total harmonic

voltage distortion) are regarded to be values of up to 3 % for individual nonlinear loads, and for cumulative mains loads the admissible value is equal to 5 % [5]. Local standards [6] allow the value of $THD_U = 8\%$, at which the mains quality already considerably deteriorates.

This undesirable phenomenon can be eliminated by several methods, for instance, increase of the mains power at the expense of commissioning of new power plants and power units or using higher current harmonic filters. Application of filters appears to be more cost-effective and promising.

IEEE Standard 519–1992 [5] which calls on the power users to take measures to suppress higher current harmonics, is valid in North America since 1992. In the countries of the Euro Union, International Standards EN 61000-2-2, -3-2, -6-3, -6-4 have also been introduced in the last few years, which specify the limit levels of higher current harmonics generation for diverse electrical equipment. Work on approval of similar standards is underway in Ukraine and CIS countries.

Equipment for various technologies of welding and related processes, where the electric arc is applied on a mass scale, is a non-linear load. Welding rectifiers and inverters, thyristor power sources of electric furnaces and electrolyzers and other welding equipment also are powerful generators of higher current harmonics. However, welding fabrication has traditionally paid little attention to these problems, although in fabrication of critical welded structures requirements of operation of just one power source were made, so as to eliminate the mutual interference of the power sources.

This may lead to the conclusion about the urgency of the problem of higher harmonics for welding fabrication, particularly, when the issue of promotion of local welding technologies into the developed countries is considered, that is confirmed by the experience of the Chinese experts [7].

The purpose of this paper is assessment of the influence of welding power sources operating in the standard technological mode on three-phase mains, as

well as preparing recommendations on reduction of higher current harmonics, generated by them.

A number of welding power sources were tested for this purpose. This paper gives and analyzes the data on four power sources typical for welding and related processes:

- three-phase welding rectifier VDU-305 with thyristor control, which is batch-produced by industry and is designed for coated stick electrode manual arc welding and for consumable electrode gas-shielded arc welding by rectified current of up to 300 A;
- three-phase thyristor pulsed power source I-169 developed by PWI and designed for consumable electrode gas-shielded pulsed-arc welding;
- all-purpose three-phase transistor inverter power source Trans Puls Synergic TPS 5000, commercially produced by Fronius, Austria, and designed for manual, automatic and mechanized, as well as gas-shielded pulsed-arc welding;
- single-phase installation for electroslag remelting UEShP of metals under a flux layer [8], based on R-951 installation, developed at PWI and designed for remelting of copper, nickel, titanium, tungsten and high-alloyed steel.

Chauvin Arnoux C.A. 8230 analyzer (France) of mains quality (single phase) was used as the main measuring instrument. This is an all-purpose instrument, which allows obtaining not only time dependencies of current and voltage with their characteristic values (maximum and minimum value, total, active and reactive power, etc.), but also the harmonic spectra up to maximum harmonic number $h_{max} = 50$. The analyzer has the function of recording and computer connection for further mathematical processing of the data.

Obtained experimental data are used when writing the specification in case of designing the higher harmonic filters, as filters can be used to suppress higher current harmonics and lower the influence of welding power sources on the mains. In addition to experimental data, calculation data were also used when preparing recommendations on lowering the higher harmonics level. These included the following:

Coefficients of non-linear distortions of current THD_I and voltage THD_U [4] are

$$THD_I = \sqrt{\sum_{h=2}^{h_{max}} I_{h\%}^2} ; THD_U = \sqrt{\sum_{h=2}^{h_{max}} U_{h\%}^2}$$

where h is the harmonic number; $I_{h\%}$, $U_{h\%}$ are the current and voltage values in percent of the acting current and voltage values of the 1st fundamental harmonic, taken as 100 %: $I_{h\%} = I_h / I_1$, $U_{h\%} = U_h / U_1$.

Another important parameter which determines by how many times additional losses in the electrical equipment and conductors of the mains will increase compared to the case, if only the 1st fundamental

current harmonic flowed in the equipment and mains, is K -factor, given by the following formula:

$$K = \frac{\sum_{h=1}^{h_{max}} (hI_{h\%})^2}{\sum_{h=1}^{h_{max}} I_{h\%}^2}$$

Additional losses are caused by eddy currents, flowing in the current-carrying parts and conductors of the equipment and mains. The eddy currents proper are due to magnetic leakage fluxes, passing through the current-carrying parts and conductors [9].

Obtained experimental and calculated data are summarized in the Table, which has the following designations: I , U are the acting values of current and voltage; $k_{m, I}$, $k_{m, U}$ are the coefficients of amplitude of current and voltage, equal to the ratio of amplitude values to acting values $k_{m, I} = I_m / I$, $k_{m, U} = U_m / U$; S , P , Q are the total, active and reactive power, respectively; k_p is the power factor equal to the ratio of active power to total power ($k_p = P / S$); $\cos \varphi$ is the coefficient of phase shift between current and voltage — cosine of angle φ ; $\text{tg } \varphi$ is the tangent of angle φ .

Let us consider operation with 50 Hz three-phase AC mains of VDU-305 welding rectifier with connection of power transformer windings — D/Y. Welding of stainless steel 12Kh18N10T was performed with 3 mm stick electrode OZL-8 at welding current of 90 A.

Dependencies of relative values of line current i_* (in the mains line wire) and line voltage u_* in the mains (between two phases) on time t at operation of welding rectifier are given in Figure 1, *a*. Values i_*

Principal parameters of the mains at operation welding arc power sources

Parameter	VDU-305	I-169	TPS 5000	UEShP
I_{m+} , A	27.9	27.5	47.4	149.9
U_{m+} , V	559.0	532.7	557.8	—
I_{m-} , A	-29.1	-28.1	-32.9	-148.3
U_{m-} , V	-559.3	-532.8	-560.2	—
I , A	17.6	15.9	11.2	78.1
U , V	386.6	374.7	396.5	—
S , V·A	6425.4	6175.8	4417.8	—
P , W	5043.1	3917.4	1824.1	—
Q , V·A	3981.5	4774.3	4023.6	—
k_p	0.785	0.634	0.413	—
$\cos \varphi$	0.797	0.680	0.741	—
$\text{tg } \varphi$	0.746	1.074	0.877	—
THD_I	16.966	40.709	142.321	27.385
THD_U	2.672	1.039	1.245	—
K	2.348	5.849	43.455	2.452

and u^* are referred to their largest amplitude values: $i^* = i|I_m|$ and $u^* = u|U_m|$, where $I_m = -29.1$ A, $U_m = -559.3$ V, and are shown in the Table, which gives the largest «+» and smallest «-» amplitude values of voltage and current over the period I_{m+} , I_{m-} , U_{m+} , U_{m-} , obtained in the experiment. As is seen from Figure 1, *a*, the current curve shape differs considerably from the sinusoidal curve. Only small breaks are observed on the voltage curve. These qualitative results are confirmed by quantitative results, i.e. diagram of harmonic components of current $I_{h\%}$ and voltage $U_{h\%}$ (Figure 1, *b*). In Figure 1, *b* the values of harmonic numbers are limited by the 27th to improve the visualization of the diagram. From the diagram it is seen that in the supply mains at operation of welding rectifier the following harmonics are manifested: 3rd current harmonic equal to 3 % of the 1st, 5th – 15.2, 7th and 9th – 1.6, 11th – 3.3, 13th – 1.0, 17th – 1.3 %, while the other odd current harmonics do not exceed 1 %. Odd numbers of voltage harmonics exceeding 1 % of the 1st harmonic, have the following values: 5th – 2.3, 7th – 1.1 %. Also manifested are the direct current component at 1.2 % and even current harmonics: 2nd – 4.2, 6th – 1.5 %. The direct component and even harmonics of voltage are negligible.

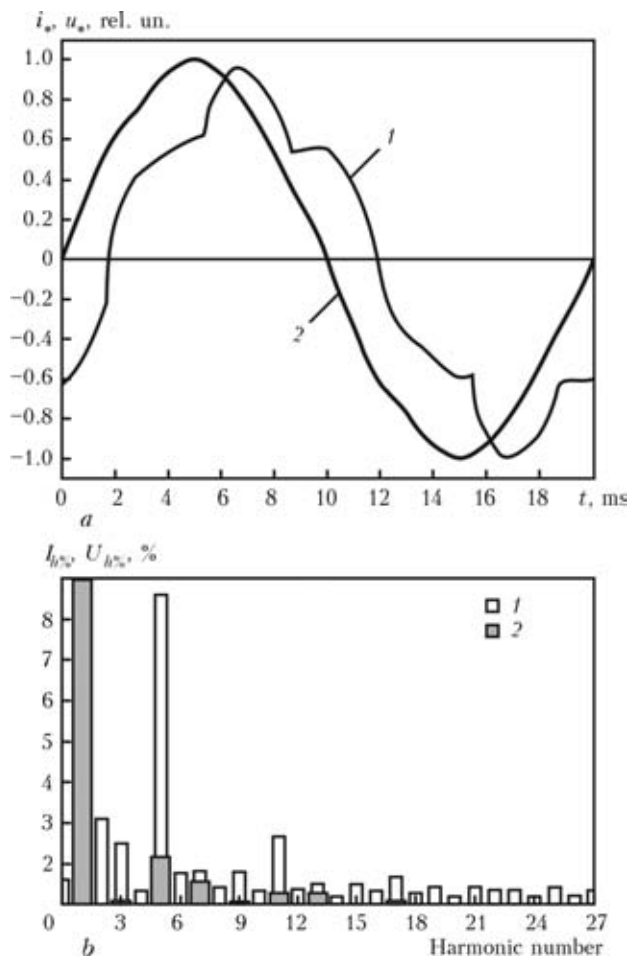


Figure 1. Dependencies of relative values of current (1) and voltage (2) on time in the mains for three-phase welding rectifier VDU-305 (a) and harmonic composition of line current (1) and line voltage (2) of the mains (b)

Coefficients of non-linear distortions of current and voltage are as follows: $THD_I = 16.9$ %, $THD_U = 2.7$ %, K -factor is equal to 2.3. Thus, additional losses in the mains and equipment at operation of the considered welding rectifier at this kind of its loading increase by more than 2 times.

The Table gives the main calculated and experimental values of welding rectifier parameters for VDU-305 at the considered kind of load. These values can change at a change of welding current, but THD_I coefficient can vary in the range of 16–25 %, and THD_U coefficient – in the range of 2.5–3.5 %.

According to the standard [5], acceptable values of THD_I coefficient are in the range of 5–8 %. The studied rectifier exceeds these values by more than 2 times. THD_U value is not exceeded, but the rectifier already can affect the operation of other equipment.

Industrial three-phase welding rectifiers VDU-504-U3 and VDU-506-U have similar characteristics.

Let us consider the influence on three-phase mains of a test sample of three-phase power source I-169 with Y/Y connection of windings of the source power transformer. Welding was performed with 1 mm wire Sv-08G2S in argon and in mixture of Ar + 18 % CO₂, at welding current of 200 A, with pulse repetition rate of 200 Hz and pulse duration of 3 ms.

Time dependencies of relative values of line current and line voltage in the mains at power source operation are given in Figure 2, *a* ($I_m = -28.1$ A, $U_m = -532.8$ V). Although the current curve differs greatly from the sinusoid, the voltage curve is almost undistorted.

From the diagram of harmonic components of acting value of current and voltage (Figure 2, *b*) it is seen that the following current harmonics are manifested in the supply mains at operation of test sample of the power source: 3rd current harmonic, equal to 10.7 % of the 1st harmonic, 5th – 36.3, 7th – 12.4, 11th – 5.7, 13th – 3.4, 17th – 3.1, 19th – 1.45, 23rd – 1.6 % with the other odd harmonics not exceeding 1 %. Voltage harmonics, exceeding 1 % of the 1st harmonic, are only slightly manifested. Even current harmonics are as follows: 2nd – 1.7, 4th – 1.4 %.

Coefficients of non-linear distortions of current and voltage for the 1st harmonics of current and voltage are $THD_I = 40.7$ %, $THD_U = 1.0$ %, and K -factor is equal to 5.8.

Welding power source has THD_I value exceeding the admissible value [5] by 5 times, THD_U level in this power source is very low, but additional losses in the mains and equipment at power source operation at this kind of its load increase by almost 6 times.

The Table gives the main parameters of power source operation for I-169 at the considered kind of load. At the change of welding mode these values change and THD_I coefficient has rise up to 49 %.

Time dependencies of the relative value of line current and line voltage in three-phase mains at operation of a transistorized inverter power source TPS

5000 are shown in Figure 3, *a*. The greatest amplitude values of currents and voltages are as follows: $I_m = 47.4$ A, $U_m = -560.2$ V.

Figure 3, *b* shows harmonic composition of line current and line voltage at the input of welding power source in welding in mixture of Ar + 18 % CO₂ with 1.2 mm wire at 150 A welding current. Current curve has two clear-cut pulses against the background of almost zero values for the rest of the half-period. The voltage curve, even though similar to a sinusoid, has an almost horizontal turn in the field of the extremes.

Practically all the odd current harmonics are manifested in the source mains, in particular 3rd current harmonic, equal to 42.6 % of the 1st harmonic, 5th – 83.3, 7th – 79.7, 9th – 23.7, 11th – 42.7, 13th – 37.1, 15th – 3.5, 17th – 14.1, 19th – 7.0, 21st – 4.9 %. Voltage harmonics are only slightly manifested. Also manifested in the direct current component at 10.8 % and practically all the even current harmonics: 2nd – 16.9, 4th – 12.1, 6th – 14.3, 8th – 13.1 %.

Coefficients of non-linear distortions of current and voltage for the 1st harmonics of current and voltage are as follows: $THD_I = 142.3$ %, $THD_U = 1.2$ %, K -factor being equal to 43.5.

The studied power source exceeds the values specified by the standard [5] for THD_I coefficient by 17.7 times, which is indicated by the current curve shape. Here an extremely wide range of harmonic components of current are generated into the mains. Values of THD_U coefficient in this source are greater than those in the previous power source, but they are quite admissible.

Additional losses in the mains and equipment at power source operation with this kind of load increase by more than 43 times.

The Table gives the main parameters of power source operation for TPS 5000 with the considered kind of load. At a change of welding mode these values will change, THD_I coefficient is in the range of 120.5–168.7 %, and THD_U coefficient is in the range of 1.7–1.8 %.

Other inverter welding power sources feature an extremely high level of higher harmonics [10].

Let us show the influence on the mains of operation of single-phase electroslag remelting installation UEShP [8], based on R-951 installation developed at PWI. The high-power installation containing two single-phase transformers TShP 10000 connected in parallel (current in the secondary circuit of one transformer is 10 kA, secondary voltage changes in the range from 42 up to 76 V, transformer rated power is 700 kV·A, maximum power is 760 kV·A, primary voltage is 380 V), thyristor block of current control and smoothing reactor, is connected to two phases of three-phase mains. Time dependencies of relative instant values of current in one of the parallel conductors of the mains powering the installation, are shown in Fi-

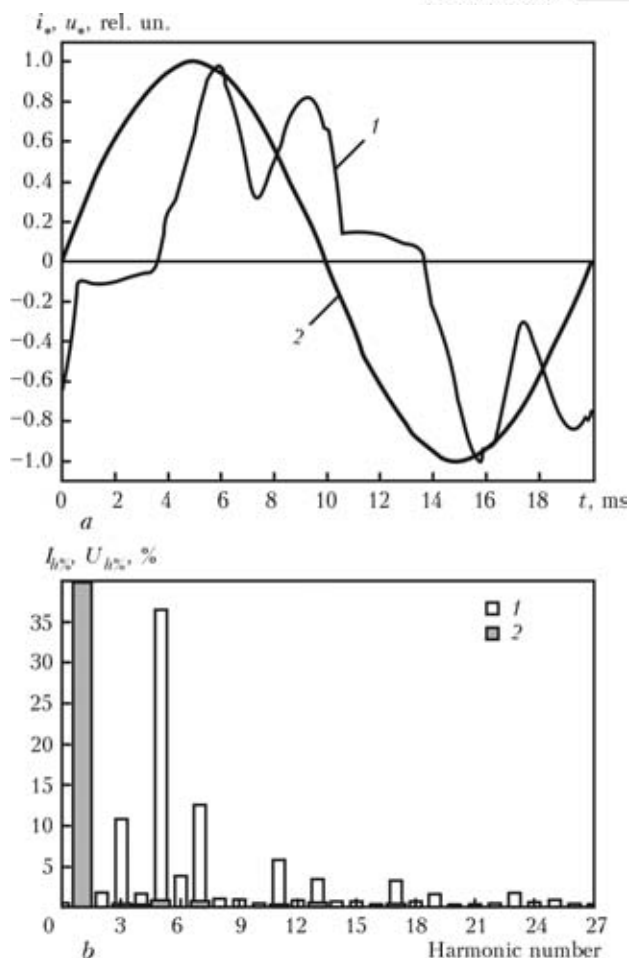


Figure 2. Dependencies of relative values of current (1) and voltage (2) on time in the mains for a test sample of three-phase thyristor pulse power source I-169 (*a*) and harmonic components of line current (1) and line voltage (2) in the mains (*b*)

gure 4, *a*. The greatest amplitude value of current is $I_m = 149.9$ A. Harmonic composition of line current at the input to the installation at electroslag remelting of metal is shown in Figure 4, *b*. Voltage on installation terminals was not measured because of the complexity of their access.

In the mains 3rd current harmonic equal to 24.5 % of the 1st harmonic, as well as 5th – 6.7, 7th – 8.9, 9th – 2.6, 11th – 2.1, 13th – 1.6, 15th – 2.6, 17th – 1.3, 23rd – 1.1 %, are manifested, and the other odd current harmonics do not exceed 1 %. Even numbers of current harmonics are practically absent. Coefficient of non-linear distortions of current for the 1st current harmonic is $THD_I = 27.4$ %, K -factor is equal to 2.4.

Values of THD_I coefficient specified by the standard [5] are exceeded in the installation by more than 3 times. Here, considerable harmonic components of current are generated into the mains. Additional losses in the mains and equipment at installation operation increase by more than 2 times.

The Table gives the main installation operation parameters for UEShP at the considered load type. These values can change at variation of the melting

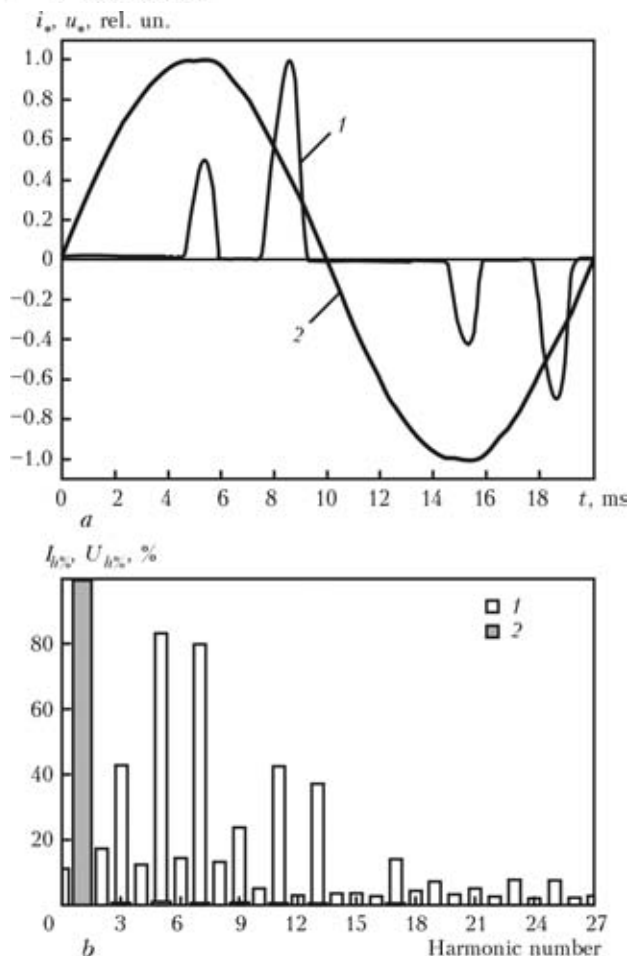


Figure 3. Dependencies of relative values of current (1) and voltage (2) on time in the mains for versatile three-phase transistor inverter power source TPS 5000 (a) and harmonic composition of line current (1) and line voltage (2) in the mains (b)

mode, while THD_I coefficient can vary in the range of 25 to 33 %.

As the installation is connected to two phases of the mains, three-phase mains is loaded non-uniformly and its subsequent balancing is recommended.

Thus, in order to improve the power quality and lower the level of higher current and voltage harmonics generated by welding equipment, it is rational, and in a number of cases, necessary to apply filters of higher current harmonics. Here, the welding power sources, in addition to providing the necessary technological parameters, will also have good electromagnetic compatibility, lower the additional losses in the mains wires and equipment connected to the mains.

It should be noted that the positive feature of most of three-phase welding power sources, unlike the single-phase sources, is the fact that they only slightly load the zero wire of the mains by higher current harmonics, that is related to practically uniformly distributed load in the three phases, and in the case of triangle connection of primary windings of the power transformer, current harmonics divisible by three, are decreased.

Lowering of the level of higher current harmonics generated by welding equipment can be performed by

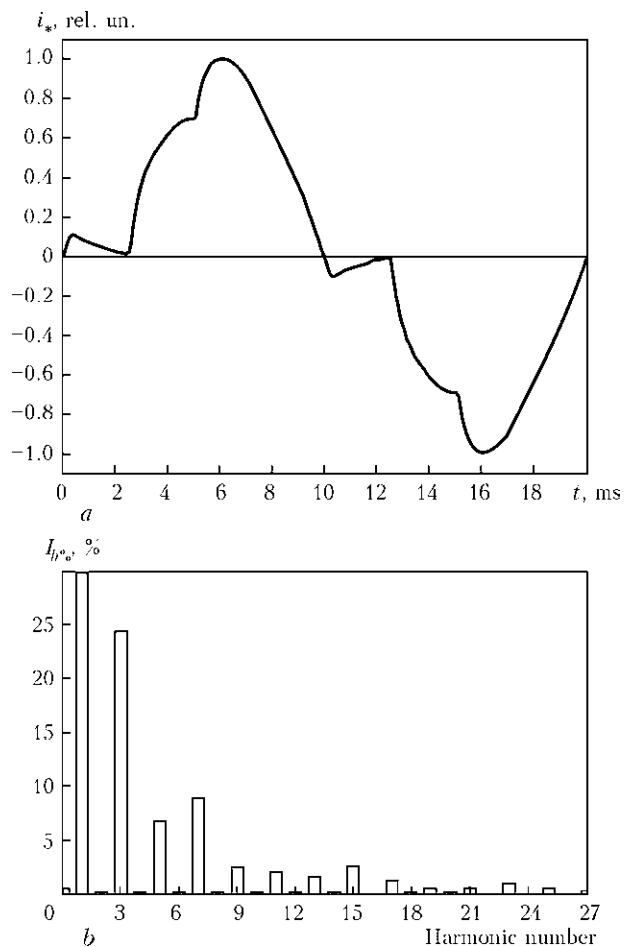


Figure 4. Time dependencies of relative values of current in the mains of UEShP (a) and harmonic composition of line current (1) and line voltage (2) in the mains (b)

the so-called active and passive filters. Active filters containing many elements of both power and microelectronics, are expensive, sophisticated and not always reliable in operation. Therefore, we focused on passive filters, which include:

- three-phase resonance L-C filters of higher current harmonics [11], connected directly at welding equipment input;
- phase-shifting transformer and autotransformer filters of higher current harmonics [1, 4, 12], which also balance the mains. They are connected at the input of a plant or building, having non-linear loads uniformly distributed by phases. Their prototype were devices for three-phase mains balancing [12, 13].

Filters minimize generation of reactive power into the mains, which has an adverse influence on mains operation, and they have a higher reliability at operation in «poor quality» mains, providing lowering of THD_I coefficient to 4–8 %, even in the mains with a high content of higher current harmonics.

The E.O. Paton Electric Welding Institute and Institute of Electrodynamics of the NAS of Ukraine have accumulated extensive experience on development of filters of higher current harmonics in supply mains. Procedures were developed for calculation of mains parameters, required at calculation of the parameters of filters of higher current harmonics and of

the procedure of development of the filters proper and their electromagnetic elements.

CONCLUSIONS

1. Value of the coefficient of non-linear current distortions, determining the level of generation of external current harmonics into the mains, at operation of the studied three-phase power sources, is in the range of 16.0–168.7 %, that is much greater than the norms specified by IEEE Standard 519–1992, and is indicative of their poor electromagnetic compatibility.

2. *K*-factor, coefficient allowing for increase of additional losses from eddy currents in equipment and in the mains, was equal to 2.35–43 %, that does not allow including the three-phase welding power sources into the category of power saving.

3. Application of filters of higher current harmonics together with three-phase welding power sources is rational, and in a number of cases necessary, as their application improves the quality of three-phase mains at welding power source operation, lowering the coefficient of non-linear current distortions to acceptable values of 4–8 %.

1. Pentegov, I.V., Volkov, I.V., Levin, M. (2002) Devices for suppression of higher current harmonics. In: *Technical elec-*

*trodynamic*s: Issue on Problems of current electrical engineering. Pt 1. Kyiv: IED.

2. Dugan, R.S., McGranaghan, M.F., Beaty, H.W. (1996) *Electrical power systems quality*. N.Y.: McGraw-Hill.
3. Waggoner, R.M. (1997) *Practical guide to quality power for sensitive electronic equipment*. Kansas: ES&M Books.
4. Paice, D.A. (1995) *Power electronic converter harmonics. Multipulse methods for clean power*. N.Y.: IEEE Press.
5. *IEEE Standard 519–1992*: IEEE recommended practices and requirements for harmonic control in electrical power systems.
6. *DSTU IES 61000-3-2:2004*: Electromagnetic compatibility. Pt 3-2: Norms. Norms for emission of current harmonics (for equipment input current of not more 16 A per phase). Kyiv: Derzhspozhyvstandart Ukrainy.
7. Zhao, W.-S., Zhao, W.-Sh. (2009) Study on electromagnetic compatibility design for inverter welding machine. *Electric Welding Machine*, 39(12), 47–50.
8. (1974) *Technology of fusion electric welding of metals and alloys*. Ed. by B.E. Paton. Moscow: Mashinostroenie.
9. Bessonov, L.A. (1964) *Theoretical principles of electrical engineering*. Moscow: Vysshaya Shkola.
10. Zhang, X.-P., Cao, T.-Q. (2009) Study on the harmonics and EMI of switching power supply for welding power source. *Electric Welding Machine*, 39(12), 59–62.
11. Volkov, I.V., Kurilchuk, M.N., Pentegov, I.V. et al. (2005) Improvement of electrical power quality in networks of industrial enterprises by means of filters of higher current harmonics. In: *Visnyk Pryazov.DTU*: Transact. on Electric Engineering. Pt 2, Issue 15, Mariupol: PDTU, 15–19.
12. Shidlovsky, A.K., Kuznetsov, V.G. (1985) *Improvement of power quality in electrical networks*. Kiev: Naukova Dumka.
13. Shidlovsky, A.K., Novsky, V.A., Kaplychny, N.N. (1989) *Stabilization of electrical power in distribution networks*. Kiev: Naukova Dumka.

ATTENTION TO SPECIALISTS!

The E.O. Paton Electric Welding Institute has published promotional-information booklet «Electron Beam Welding». It contains the generalised data on the 50-years' experience of the Institute in the field of development and manufacture of the electron beam welding equipment.

EBW is widely applied in a number of industries.

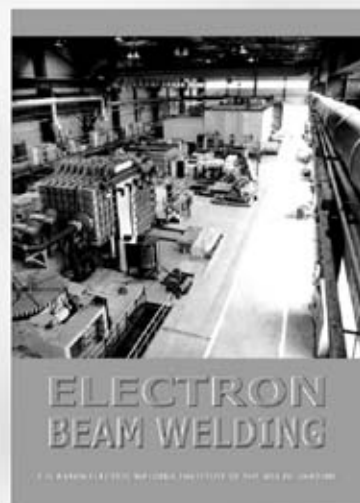
116 installations for welding units of stainless steels, nickel-base alloys, titanium, aluminium and copper alloys are in operation in **space engineering**.

Large-size installations KL-115 and KL-118 have found application in **aircraft engineering** of Russia, USA and India.

Installations UL-214 are efficiently utilised for welding large marine structures in **ship building** of Russia and Ukraine.

10 installations SV-112 / 103 are applied in **instrument making**. 56 packages of the EBW equipment, including installations with vacuum chamber capacities of up to 100 m³, have been put in operation during the last 10 years and are manufactured now.

The booklet can be ordered from the Editorial Board of «The Paton Welding Journal»



FIRST MEETING OF COUNCIL OF CHINESE-UKRAINIAN E.O. PATON WELDING INSTITUTE



Signing of Regulations about CUPWI: *left to right*: Zhan Decun – Vice-Director of Department of Science and Information of Government of Guangzhou city, Gong Guoping – Vice-Director of Department of Science and Technology of Government of Guangdong province, Academician B.E. Paton – President of the NAS of Ukraine, Qui Xianyang – Director of GGRIT

On September 9, 2011 the first meeting of the Council of the Chinese-Ukrainian E.O. Paton Welding Institute (CUPWI) was held at the E.O. Paton Electric Welding Institute of the NAS of Ukraine (PWI) (Kiev). From the Chinese side the representatives of Department of Science and Technology of Guangdong province, Government of Guangzhou city and Guangdong General Research Institute of Industrial Technologies (GGRIT) were present.

During the meeting of CUPWI Council the following problems were discussed and decisions were taken:

- on behalf of working groups on preparation of projects and organizational structure of CUPWI the reports of Dr. V.N. Korzhik, the leader of working group from the Ukrainian side, and of Dr. Yang Yongqiang, the leader of working group from the Chinese side, were presented and approved;
- Regulations and Statute of the CUPWI Council were approved;
- Qao Jianlin, Vice-Minister of Science and Technology of China, and B.E. Paton, President of the NAS of Ukraine, PWI Director, were elected as honored chairmen of the CUPWI Council;
- CUPWI Council was elected (from the Chinese side Dr. Gong Guoping, Vice-Director of Department of Science and Technology of Government of Guangdong province; Prof. Qui Xianyang, Director of GGRIT; Dr. Zhan Decun, Vice-Director of Department

of Science and Information of Government of Guangzhou city; Prof. Liu Min, GGRIT Vice-Director; Prof. Deng Weidong, Chief of Department of management technology of GGRIT; from the Ukrainian side Prof. L.M. Lobanov, Academician of NASU, PWI Deputy Director on Research Works; Prof. I.V. Krivtsun, Corr.-Member of NASU, PWI Deputy Director on Research Works; Dr. V.B. Yurlov, PWI Deputy Director on Marketing and Economy; Prof. G.S. Marinsky, Chief of PWI Department on welding and allied technologies in medicine and ecology; Prof. S.V. Akhonin, Chief of PWI Department of physical-metallurgical problems of titanium alloy welding and diffusion bonding of metallic materials.

Prof. I.V. Krivtsun was elected as the chairman of the CUPWI Council, and Dr. Gong Guoping was elected as the vice-chairman.

Secretariat of the CUPWI was elected (Council secretary – Zeng Lu, Chief of Department of Science and Technology of Guangdong province; Council vice-secretary – Zhu Dongyan, Chief of Department of Communication and Cooperation of Department of Science and Information of Government of Guangzhou city; and D.V. Kovalenko, PWI staff scientist).

Directorate of CUPWI was approved (CUPWI director from the Chinese side – Dr. Yang Yongqiang, from the Ukrainian side – Dr. V.N. Korzhik).

Results of working group work on preparation were approved and decision was taken about financing of the first group of projects (development of advanced technologies of welding in the manufacture of elements of power equipment; challenging plasma technologies and their application; development of updated technologies and equipment for flash butt welding and their application in industry; development of compositions of flux-cored wires and technology of their manufacture for shielded-gas welding of high-strength steels).

Proposals were considered and approved on the subject of the second group of projects, whose beginning of realization is planned since 2012. In particular, the projects were supported on welding of live tissues, development of advanced laser technologies and equipment, creation of new technologies and materials to improve the technical characteristics of LED-modules, as well as other projects.



NEWS

NEW INTERACTIVE ELECTRIC WELDING LABORATORY

PWI RC SKAE completed development of a new facility for welder's training during the real process. Arc welder's trainer (DTS-06) is designed for on-line analysis of the level of professional skills of arc welding specialists. Interactive electric welding laboratory allows accelerating the process of training in welding technologies (and reducing the cost, respectively), improving the quality of specialist training due to application of modern interactive technologies when learning practical skills of the welding process. Welder's trainer is a unique local development of PWI specialists.

The trainee is able to conduct preliminary trials and welding process under the instructor's guidance for familiarization with the training facility. Then test welding can be performed for assessment of welder's professional level. Various calculation procedures are used for calculation assessment for each welding process type. Welder's training and testing are performed for real processes of MMA, MIG/MAG and TIG welding.

The laboratory includes: tabletop personal computer, tabletop block of technological interface with specialized electrode holder, welding table; and welding power source.

Main functions of the trainer:

- entering the task for selected welding process (from the panel or earlier saved task file);
- measurement, processing, calculation and real-time representation of the following welding process parameters and auxiliary signals: welding current; arc voltage; arc length; welding speed; heat input; horizontal angle of electrode inclination (turning along the arm axis); vertical angle of electrode inclination (up and down movement of the wrist); deposit cross-

section; deposited metal weight; gas flow rate; electrode position on the sample; filler wire feed signal; calculation assessment of the quality of performed welding (several welding passes can be performed within one assessment);

- viewing graphs of recorded welding processes after assessment;
- preservation in the form of operating system files of tasks for assessment of various kinds of welding processes for fast setting up of the training facility for a specific process;
- preservation in the form of operating system files of resulting data of assessment for possible subsequent analysis.

The training facility can be used in training establishments, specializing in arc welders' training; large welding enterprises for certification or re-certification of welder personnel or in a specialized organization involved in supervision, training or re-training of arc welding specialists.



SUBSCRIPTION FOR «THE PATON WELDING JOURNAL»

If You are interested in making subscription directly via Editorial Board, fill, please, the coupon and send application by fax or e-mail.

The cost of annual subscription via Editorial Board is \$324.

Telephones and faxes of Editorial Board of «The Paton Welding Journal»:

Tel.: (38044) 200 82 77, 200 81 45

Fax: (38044) 200 82 77, 200 81 45.

«The Paton Welding Journal» can be also subscribed worldwide from catalogues of subscription agency EBSO.

SUBSCRIPTION COUPON	
Address for journal delivery	
Term of subscription since	20 till 20
Name, initials	
Affiliation	
Position	
Tel., Fax, E-mail	



ADVERTISEMENT IN «THE PATON WELDING JOURNAL»

External cover, fully-colored:

First page of cover (190×190 mm) – \$700
 Second page of cover (200×290 mm) – \$550
 Third page of cover (200×290 mm) – \$500
 Fourth page of cover (200×290 mm) – \$600

Internal cover, fully-colored:

First page of cover (200×290 mm) – \$350
 Second page of cover (200×290 mm) – \$350
 Third page of cover (200×290 mm) – \$350
 Fourth page of cover (200×290 mm) – \$350

Internal insert:

Fully-colored (200×290 mm) – \$300
 Fully-colored (double page A3) (400×290 mm) – \$500
 Fully-colored (200×145 mm) – \$150
 Black-and-white (170×250 mm) – \$80
 Black-and-white (170×125 mm) – \$50
 Black-and-white (80×80 mm) – \$15

- Article in the form of advertising is 50 % of the cost of advertising area
- When the sum of advertising contracts exceeds \$1000, a flexible system of discounts is envisaged

Technical requirement for the advertising materials:

- Size of journal after cutting is 200×290 mm
- In advertising layouts, the texts, logotypes and other elements should be located 5 mm from the module edge to prevent the loss of a part of information

All files in format IBM PC:

- Corell Draw, version up to 10.0
- Adobe Photoshop, version up to 7.0
- Quark, version up to 5.0
- Representations in format TIFF, color model CMYK, resolution 300 dpi
- Files should be added with a printed copy (makeups in WORD for are not accepted)